Broadband Fan Noise Generated by Small Scale Turbulence

by Stewart A.L. Glegg
Center for Acoustics and Vibration
Florida Atlantic University

Final Report on NASA Grant number NAG 1-1202

Acknowledgement

The experimental results presented in this report were provided by Ulrich Ganz and Paul Joppa of Boeing Aircraft, and the author is grateful for their help throughout the course of this project. In addition the author would like to acknowledge many helpful discussions with Don Hanson of Pratt and Whitney, Ray Chi and Bruce Morin of UTRC, who were instrumental in verifying and checking many of the codes used to carry out the calculations which are presented. Also thanks are due to Tom Brooks of NASA Langley for providing the NASA Airfoil Self Noise prediction code which has been used as part of this study.

Broadband Fan Noise Generated by Small Scale Turbulence

Summary

This report describes the development of prediction methods for broadband fan noise from aircraft engines. First, experimental evidence of the most important source mechanisms is reviewed. It is found that there are a number of competing source mechanism involved and that there is no single dominant source to which noise control procedures can be applied. Theoretical models are then developed for (i) ducted rotors and stator vanes interacting with duct wall boundary layers, (ii) ducted rotor self noise (iii) stator vanes operating in the wakes of rotors. All the turbulence parameters required for these models are based on measured quantities. Finally the theoretical models are used to predict measured fan noise levels with some success.

Broadband Fan Noise Generated by Small Scale Turbulence

Contents

List of Figures

Broadband Fan Noise Generated by Small Scale Turbulence

1. Introduction

Fan noise can be considered as the combination of tone noise which occurs at the blade passing frequency and it's harmonics, and broadband noise which has a continuous spectrum contributing to all frequencies. In the past the tone noise has been considered the dominant contributor to the subjectively important part of the aircraft noise spectrum (see figure 1.1). However in new engine designs, which have larger diameters and fewer blades, the fan tones are moved to lower frequencies which are less important subjectively. Consequently the contribution of the broadband noise has been shown to be equally important as the tone noise to the subjective measures of aircraft noise for large diameter engines (Gliebe(1996)).

In general broadband aerodynamic noise is caused by turbulence and it's interaction with rigid surfaces such as fan blades or stator vanes. The primary turbulent flows in an aircraft engine are shown in figure 1.2. In some of the earliest work on broadband fan noise the most important source mechanism was assumed to be the interaction of the rotor blades or stator vanes with *inflow* turbulence (see for example Mani (1971), Mugridge and Morfey (1972), Hanson (1973), Sevik (1974), Homicz and George (1974), Amiet (1975)). For a rotor which has no upstream stator vanes the only source of turbulence, for ideal clean inflow conditions, is the boundary layer turbulence at the duct wall (Mugridge and Morfey (1972), Moiseev et al (1978), Glegg (1993)). For stator vanes, which are located downstream of a rotor, the flow is more complicated and includes turbulence in the rotor blade wakes and the secondary flows in the hub and outer wall regions (see figure 1.2).

Prediction methodology given in the papers cited above was based on a description of the turbulence and a blade response function which coupled the turbulent flow fluctuations with the radiated sound. Various levels of sophistication were used in these studies but in general the results were limited to flows with small Mach numbers. However, very little was known about the turbulence in the engine, and so estimates always had to be made of the turbulence parameters needed for the prediction models. More recently an extensive study of the turbulent flows associated with broadband fan noise has been carried out by Ganz et al (1995). This has provide new insights into inflow noise mechanisms as will be described below. Furthermore recent wind tunnel studies by Devenport (1997) have shown that the flows downstream of a typical set of loaded fan blades include both small scale turbulence and random motion of coherent structures

associated with the secondary flow. The small scale self preserving components of the turbulence will be the focus of the fan prediction methodology presented here, while the random motion of the coherent structures, which may be described by a probabilistic flow model (Glegg and Devenport (1991), Davenport et al (1996), Dhanak et al (1997)), and may also be a source of broadband fan noise (Hanson (1973)), will not be considered in detail.

In addition to the noise associated with unsteady inflows, the fan blades and stator vanes will also generate their own turbulent boundary layer and tip leakage flows, which generate broadband noise. These source mechanisms are defined as *selfnoise* sources, and may be further categorized as trailing edge noise, caused by the blade boundary layer interacting with the sharp trailing edge of the blade, and tip flow noise caused by the leakage flow between the blade tips and the fan casing.

Trailing edge noise has been studied extensively for isolated blades (Ffowcs-Williams and Hall (1970), Chase (1972), Amiet (1976),(1978), Howe (1978), Brooks and Hodgson (1981), Kim and George (1982), Brooks et al (1989)), and has recently been extended to multi-bladed rotors (Glegg (1996),(1997)). For this source mechanism sound radiation is caused by the rapid adjustments of the turbulent boundary later fluctuations as the turbulence is convected past the blade trailing edge. Analytical solutions exist for the blade response and acoustic radiation but there is no suitable theoretical model for the turbulence. However an extensive experimental study by Brooks et al (1989) provides an empirical data base from which the trailing edge noise radiation from isolated blades can be calculated as a function of blade Reynolds number, angle of attack (up to and beyond stall), Mach number etc., and this has been extended to ducted fans (Glegg(1997)). At the present time the state of the art of turbulent flow modeling using numerical approaches cannot provide the detail and range of conditions covered by the Brooks et al(1989) data, and so their semi empirical approach appears to be the most effective procedure for obtaining estimates of blade self noise currently available. However, as numerical procedures improve it may be possible to obtain a completely theoretical trailing edge noise prediction method.

Tip leakage flow increases with the size of the gap between the rotor blade tip and the duct wall casing, and there is extensive experimental evidence (Longhouse (1978), Fukano et al (1986), Mugridge and Morfey (1972), Kameier (1997)) that fan broadband noise also increases with tip gap. The tip leakage flow and the associated secondary flow is not well understood and will also depend on the rotor loading. There are currently no theoretical or semi empirical prediction models for this broadband fan noise mechanism which is surprising considering it's relative importance. However as will be shown below,

the wake turbulence close to the duct wall is also increased when the tip gap is increased so the inflow turbulence to the stator vanes is affected by the tip gap and this may cause increased noise levels, depending on the particular rotor/stator configuration. Consequently it is not always clear that increased tip flow noise is caused by "self noise", which would occur in the absence of any downstream stators, or by "inflow noise" generated by the turbulent tip flow striking downstream stator vanes. This is a typical example of why the fan broadband noise problem is so complex because it shows that it is not always possible to isolate source mechanisms when varying experimental parameters. The recent experimental study by Ganz et al (1995) has shed some light on this issue by testing a fan in a duct both with and without stators and this will be discussed in detail in section 2.

Aircraft engines often operate under conditions where the fan tip speed approaches or exceeds sonic conditions. When the fan tip speed is in the transonic range shock cells are formed on the blade surfaces. These represent a highly unstable flow condition and a small change to the inflow can cause a large change in the location of the shock cell. For open rotors it is known that during a blade vortex interaction at transonic speeds (see for example Schmitz (1994)), shock cells move rapidly upstream on the upper surface of the blade and new cells are formed and dissipated on the lower blade surface during the passage of the vortex. This is a strongly non-linear flow regime where, in general, the mean flow cannot be considered separately from the unsteady inflow. However for small disturbances a quasi linear approach can be used to evaluate the importance of this mechanism (Glegg (1994)). This will be described in more detail in section 6.

For supersonic tip speeds detached shock waves occur upstream of the blade leading edges, and the radiated sound is dominated by "buzz saw" noise. The spectrum typically consists of tones at the shaft rotation frequency and it's harmonics, and an increase in the associated broadband noise is also observed (see for example Groeneweg et al (1994)). However the importance of the broadband component of buzz saw noise is not clear because the tones are so dominant. Furthermore the flow conditions are completely different from those in the subsonic regime, and so supersonic tip speed fans must be treated completely separately from subsonic or even transonic tip speed fans.

This report will describe procedures and methodology for predicting broadband fan noise for aircraft engines. It will start by considering experimental evidence from a recent test by Ganz et al (1995). The results of this experiment will be reviewed with the aim of identifying the important mechanisms of broadband noise at subsonic fan tip speeds. The next section will describe the theoretical background to fan noise prediction methodology. Starting with the original theory of aerodynamic sound by Lighthill (1952) this section reviews more recent advances which are particularly relevant to fan noise prediction

methods. Sections 4,5, and 6 then describe prediction methodology for inflow noise, self noise and shock associated noise, and include a description of the parametric dependency of these sources. Finally in section 7 the experimental results from the recent experimental test by Ganz et al (1995) are compared with the prediction methods developed in the previous sections, using experimentally measured values of the turbulence and flow conditions as the input to the acoustic prediction codes.

2. Experimental Evidence

2.1 Introduction

This section will describe an experimental investigation into the sources of broadband fan noise which was carried out by Ganz et al (1995) in the Boeing 2.74 m x 3.66 m (9'x12') anechoic wind tunnel facility using a 0.457 m (18") model scale fan. The novel features of this test were:

(i) Upstream duct wall boundary layer bleed could be used to reduce inflow turbulence levels to the fan.

(ii) The design of the rig enabled the model to be run with or without stators, giving rotor alone noise levels.

(iii) Rings of duct wall microphones provided the ability to obtain modal decomposition of the sound field.

(iv) Far field microphone array data was used to identify external radiated acoustic power, and by use of a shield, the upstream and downstream power could be determined separately.

(v) In duct hot wire measurements were made of turbulent flows incident on the fan and the stator vanes.

(vi) The design of the duct allowed the blade tip gap to be varied.

The measurements obtained with the stator vanes removed from the duct downstream of the fan provided data which could be used for the unambiguous identification of rotor alone noise sources. Furthermore by removing the duct wall boundary layer upstream of the fan, the rotor self noise was determined as a function of fan speed, tip clearance and blade loading. Introducing a duct wall boundary layer then demonstrated the increased levels caused by the interaction of the duct wall boundary layer with the rotor blades.

The experiment also investigated rotor stator interaction noise, by placing sets of stator vanes downstream of the rotor. Three different stators were used, with 15, 30 and 60 vanes. The 15 vane and 30 vane set had the same solidity, and for the 60 vane set the solidity was doubled. These tests provided information on the relative importance of rotor and stator broadband noise, and how it varied with speed, loading, tip gap size and the upstream duct wall boundary layer thickness. In addition, the test was complemented by extensive hot wire turbulence measurements in the fan duct and in the upstream outer wall boundary layer, and this provided further diagnostic evidence to support the conclusions from the acoustic measurements.

In the following two sections the results of this test are presented and interpreted from the viewpoint of identifying the most important sources of broadband noise. It represents only a fraction of the complete data set and more details can be found in the report by Ganz et al (1995). The acoustic measurements are given in terms of either the upstream or downstream sound power as broadband power spectra with the tonal components removed. The spectra are therefore smooth and the relative level of the broadband noise and the tone noise is not presented.

2.2 Rotor Alone Noise

The quietest possible configuration for an aircraft engine fan is obtained when there are no stators downstream of the rotor, there is a completely clean inflow and the tip gap is a minimum. The test results for this configuration are shown in figure 2.1. This is presented first because it represents the base line case to which all other sources must be added. Note that the spectra are smooth, monotonically decaying and that the downstream sound power is ~9 dB greater then the upstream sound power which was found to be typical of the entire data set. This result represents the self noise of the fan at low loading, and by either increasing the loading (figure 2.2) or the tip clearance (figure 2.3) the noise level is increased. Also note how the loading causes up to a 6dB increase for the small tip gap and a 2dB increase for the large tip gap, or alternatively the increased tip gap causes up to a 4 dB increase at low loading but has almost no effect at high loading. This indicates that these two source mechanisms can not be clearly separated for this case and both play a role in determining the overall sound power output.

When the duct wall boundary layer is introduced, the spectra take on a new feature (figure 2.4), which includes a series of broad peaks at the frequencies 9kHz,12 kHz,15kHz, 21kHz for the small tip gap and low loading cases. However for the large tip gap and high loading there is an additional set of low frequency peaks at 4.2 kHz, 6.8kHz, and 9.5 kHz, which are indicative of a rotating stall at this condition. At this fan speed the blade passing frequency is 3kHz and so the undulations in the spectra at low loading are indicative of "haystacking" of the tonal content which can be caused by long lengthscale coherent structures being ingested into the rotor(see for example Blake (1986)). Note that these structures must be related to the duct wall boundary layer flow, because they do not occur when there is 100% boundary layer bleed applied, and they are less significant when either the loading or the tip gap is increased.

The primary conclusion from these results is that there is no single dominant source mechanism responsible for rotor alone noise and all sources must be taken into consideration.

2.3 Rotor/Stator Interaction Noise

When a set of stator vanes are added downstream of the rotor, the radiated broadband sound power is increased as shown in figure 2.5. This result shows the radiated sound power in the upstream direction. It is clear that the stator contribution dominates in spite of having to propagate through the rotor. In general the sound power is seen to increase in proportion to the number of stators, although when the stator solidity is large (as is the case with 60 stators in figure 2.5) the increase is not as much as expected. Although this result shows that the stators are the most important source of broadband noise it should be noted that they are not overwhelmingly dominant, and a 6 dB reduction in the contribution from the stators would not give a similar reduction in the overall broadband sound power because of the contribution from the rotor.

To further understand the mechanism of rotor stator interaction noise it is necessary to consider the turbulent inflow to the stator vanes. Figure 2.6 shows the measured turbulence intensity in the fan duct downstream of the rotor as a function of radial and azimuthal location. The data was obtained with a single cross wire probe and the phase locked signal was extrcated to get the random component. The measurements show high turbulence intensity close to the duct walls and contributions from the turbulent wakes which are represented by the diagonal lines of high intensity. Between the wakes the turbulence levels are negligibly small, and the peak turbulence intensity in the wakes is only ~5%. In contrast the turbulence intensity in the duct wall region is in excess of 6% at all locations and sometimes as large as 8%. It would appear therefore that the contribution from the flow in the wall region could be a major contributor to the turbulent flow incident on the stator. The flow in the outer wall region is dominated by secondary flow and the interaction of blade passage vortices with the turbulent tip flow through the rotor. The tip flow will be more complex and of larger extent when the tip gap is larger and so one would expect the broadband noise from the stators to increase if the tip gap is increased. To verify this hypothesis we first consider the turbulence in the rotor wake: figure 2.7 shows the circumferentially averaged turbulence intensity as a function of radial position for both the streamwise and the transverse turbulence components. These results clearly show that the turbulence close to the outer duct wall increases in intensity as the tip gap is increased and also extends further into the fan duct. The effect this has on the radiated sound is shown in figure 2.8 which gives the broadband sound power for small and large tip gaps for a stator

with 60 vanes (for which stator noise dominates). The larger tip gap introduces a 3 dB noise increase, but the results are not conclusive because, as noted in the previous section, a larger tip gap will also generate more rotor noise. To eliminate this uncertainty, the rotor alone noise, under the same inflow conditions and loading, can be subtracted from the stator noise to give the stator alone contribution as shown in figure 2.9. These results show that the stator noise increases with rotor tip gap, independently of the increase in rotor noise. The increases are larger for high loading cases and interestingly for sound power radiated upstream through the rotor. It appears therefore that there are conditions where changes to the outer wall flow can increase the stator noise independently of any changes to the rotor noise.

Finally we will consider the effect of loading on the stator noise. Figure 2.10 shows the average turbulence intensity as a function of radial position for different fan loadings. This shows a general tendency for the turbulence levels, both in the wake regions and the tip flow regions, to increase with loading. In the duct wall regions, the high loading cases give twice the turbulence intensity of the low loading cases, but in the wake flow region the increase is closer to a 30% in the outer region. In the hub region the trend is reversed. Assuming the sound power output is directly proportional to the mean square turbulence level, one would expect the stator alone noise to increase as the loading is increased, but if wake flows dominate this increase may be small. Figure 2.11 shows the stator alone noise as a function of loading with all other parameters held constant, and it is clear that only small increases of this magnitude are observed. These results suggests that increases in radiated sound power as a function of loading are caused, to some extent, by increased turbulence in the fan duct, but in general this is not a large effect at this fan speed.

2.4 Conclusion

The experimental results presented above give a break down of the different source mechanisms of broadband fans noise. It is seen that there is no clearly dominant source to which noise reduction approaches can be applied, but rather a number of competing mechanisms exist which are more or less important depending on the particular fan design and flow conditions. Clearly rotors must be designed to minimize turbulent flow incident on the stators and the outer wall flows can be a contributor in this regard. The wake turbulence is of lower level but of greater extent and so can also be the dominant source of high frequency turbulent flow. The rotor noise is not very far below the stator noise and an interesting feature identified here is the contribution of the coherent structures in the wall

boundary layer which lead to broad peaks in the spectrum around the blade passage frequencies.

3. Theoretical Background - Fundamentals

Theoretical modeling of aerodynamic noise generation is based on the solutions to the equations which describe the motion of a compressible fluid. The first full formulation of this problem was due to Lighthill (1952) who re-arranged the Navier Stokes equations into a wave equation, including all the non-linear and viscous terms. For problems which involved moving bodies, Ffowcs-Williams and Hawkings (1969) introduced an approach based on generalized derivatives which has developed into a powerful tool for all types of aeroacoustic problems (Farassatt (1994)). The Ffowcs-Williams Hawkings equation considers a fluid which contains an arbitrary moving surface (or multiple moving surfaces) defined by the scalar function $f(\mathbf{y})=0$. The region of interest is defined where $f>0$ and the normal to the surface is $\mathbf{n}=\nabla f/|\nabla f|$ pointing into the fluid. For impermeable surfaces moving with a local velocity V_j the wave equation is formulated using the perturbation of the density as the acoustic variable and is defined as;

(3.1)

$$\frac{\partial^2 (H\rho')}{\partial \tau^2} - c_\infty^2 \nabla^2 (H\rho') = \frac{\partial^2 (HT_{ij})}{\partial y_i \partial y_j} - \frac{\partial}{\partial y_i}\left(p_{ij} \frac{\partial f}{\partial y_j} \delta(f) \right) + \frac{\partial}{\partial \tau}\left(\rho_\infty V_j \frac{\partial f}{\partial y_j} \delta(f) \right)$$

where H represents the heavyside function $H(f)$ and p_{ij} is the pressure stress tensor, ρ_∞ and c_∞ are the steady state density and speed of sound at the observer, and T_{ij} is Lighthills stress tensor. In this equation the lefthand side represents a wave equation for waves propagating in a stationary fluid while the right hand side represents the source terms. The first term on the right is of quadrupole order and describes sound radiation from sources in the fluid. The second term is of dipole order and describes sound radiation from the pressure stress tensor on the blade surface. The last term is referred to as the thickness source term which is only non zero for moving surfaces and represents sound radiation from volume displacement effects which occur when the displaced volume is in accelerated motion relative to the observer.

The interest of this study is to consider the sound radiation when blades move through a turbulent flow. In this case the source terms on the righthand side of this equation are hard to determine. Long and Watts(1987) proposed an integral equation formulation to obtain the surface pressure, in the absence of the quadrupole term and neglecting viscous effects. In other formulations (Amiet(1975), Mani(1995)) the quadrupole terms are treated separately from the dipole terms, and the surface pressure is obtained from the blade response function for an incoming upwash gust. There is however

a fundamental problem with using Lighthills formulation for sound radiation from turbulent flows because the volume source term T_{ij} also depends on the acoustic field.

The definition of T_{ij} is

(3.2)

$$T_{ij} = \rho v_i v_j + p_{ij} - \rho' c_\infty^2 \delta_{ij}$$

where v_i represents the velocity of the fluid and includes the mean flow, the turbulent flow in the absence of the blade, and the acoustic perturbation velocity which is required to satisfy the boundary conditions on the blade surface. Both Howe (1975) and Goldstein (1978) have introduced alternative formulations to the acoustic analogy which separate the "acoustic perturbation" terms from the "source term". Goldstein's equation has received more attention than Howe's equation for fan noise applications and so we will limit this review to his approach, since the physical mechanisms involved are essentially the same.

Goldstein's formulation describes the generation of sound due to the distortion of an upstream disturbance by a two dimensional potential flow around a stationary streamlined body. It is obtained from the *linearised* Euler equations, and so neglects the effect of viscosity and nonlinear interactions of the turbulent flow. The flow is specified in terms of it's steady velocity, pressure, density and entropy ($\mathbf{U}, p_o, \rho_o, S_o$) and it's unsteady parts ($\mathbf{u}, p', \rho', s'$) which are a function of time t. The unsteady velocity is then further split as $\mathbf{u}=\nabla\phi+\mathbf{u}^{(I)}$, where the velocity potential represents the acoustic field and is related to the pressure fluctuations in the flow using $p'=-\rho_o D_o\phi/Dt$ (where $D_o/D\tau=\partial/\partial t+\mathbf{U}.\nabla$ is the total time derivative based on the mean flow $\mathbf{U}$). The residual velocity $\mathbf{u}^{(I)}$ is a known function of the upstream flow and satisfies the differential equation

(3.3)

$$\frac{D_o \mathbf{u}^{(I)}}{Dt} + (\mathbf{u}^{(I)}.\nabla)\mathbf{U} = 0$$

Goldstein(1978) then formulates a wave type equation with non-constant coefficients which describes the generation and propagation of the acoustic velocity potential. The result is given as

(3.4)

$$\frac{D_o}{D\tau}\left(\frac{1}{c_o^2}\frac{D_o\phi}{D\tau}\right) - \frac{1}{\rho_o}\nabla(\rho_o\nabla\phi) = \frac{1}{\rho_o}\nabla\left(\rho_o \mathbf{u}^{(I)}\right)$$

where c_o and ρ_o are local speed of sound and density. The source term is specified in terms of a vortical gust velocity and an entropy disturbance which are imposed at the upstream boundary. The upstream disturbance is defined by the incompressible velocity perturbation $\mathbf{A}(\mathbf{x}\text{-}U_\infty t\mathbf{i})$ and an entropy disturbance $s_\infty(\mathbf{x}\text{-}U_\infty t\mathbf{i})$ where $\mathbf{i}$ is a unit vector in the direction of the upstream flow. The residual velocity is defined at any downstream location by

(3.5)

$$u_i^{(I)} = \mathbf{A}(\mathbf{X} - \mathbf{i}U_\infty t)\frac{\partial \mathbf{X}}{\partial x_i} + (2c_p)^{-1} s_\infty(\mathbf{X} - \mathbf{i}U_\infty t)\left[U_i - U_\infty \frac{\partial X_1}{\partial x_i}\right]$$

The vector $\mathbf{X}\text{-}\mathbf{i}U_\infty t=(X_1\text{-}U_\infty t,X_2,X_3)$ is defined so that $D_o(\mathbf{X}\text{-}\mathbf{i}U_\infty t)/Dt=0$ and can be characterized by the gradients of each component which for 2D potential flow are

(3.6)

$$\nabla X_1 = \frac{U_\infty}{U}\mathbf{s} \qquad \nabla X_2 = \frac{U}{U_\infty}\mathbf{n} \qquad \nabla X_3 = \mathbf{z}$$

where $\mathbf{s}$ is a unit vector in the direction of the flow $\mathbf{n}$ is a unit vector normal to the flow and $\mathbf{z}$ is a unit vector which lies out of the plane of the flow. Difficulties occur for blades with forward stagnation points because the gradient of the co-ordinate in the direction of the flow $\partial X_1/\partial x_i$ is singular when $U=0$, and so both the terms in (3.5) become very large. However if the functions X_1,X_2,X_3 are defined downstream of the stagnation point, equation (3.6) can be used to give a co-ordinate transformation valid in all parts of the flow, except along the stagnation streamline upstream of the stagnation point. We will use this transformation to provide further insight into the source terms of (3.4). However, first we note that

(3.7)

$$\frac{1}{c_o^2}\frac{D\mathbf{u}}{Dt} = -\frac{\nabla p}{\rho c_o^2} = -\frac{\nabla \rho}{\rho} - \frac{\nabla S}{c_p}$$

so for the mean components of an isentropic flow we have $\nabla\rho_o/\rho_o=(\mathbf{U}.\nabla\mathbf{U})/c_o^2$ and we can write

(3.8)

$$\frac{1}{c_o^2}\frac{D_o^2\phi}{D\tau^2}-\nabla^2\phi=\nabla.\mathbf{u}^{(I)}-\frac{D_o}{D\tau}\left(\frac{1}{c_o^2}\right)\frac{D_o\phi}{D\tau}-\frac{\mathbf{u}.(\mathbf{U}.\nabla\mathbf{U})}{c_o^2}$$

We next transform this equation into X_1,X_2,X_3 co-ordinates using the scale factors $h_1=U/U_\infty$, $h_2=U_\infty/U$ and $h_3=1$ so that for a vortical incoming gust

(3.9)

$$\frac{1}{c_o^2}\frac{D_o^2\phi}{D\tau^2}-\sum_{i=1,2,3}\frac{\partial}{\partial X_i}\left(\frac{1}{h_i^2}\frac{\partial\phi}{\partial X_i}\right)=\sum_{i=1,2,3}\frac{\partial}{\partial X_i}\left(\frac{A_i}{h_i^2}\right)-\frac{D_o}{D\tau}\left(\frac{1}{c_o^2}\right)\frac{D_o\phi}{D\tau}-\frac{\mathbf{u}.(\mathbf{U}.\nabla\mathbf{U})}{c_o^2}$$

and re-arranging this result and making use of the divergence free property of A_i gives

(3.10)

$$\frac{1}{c_o^2}\frac{D_o^2\phi}{D\tau^2}-\frac{\partial^2\phi}{\partial X_i^2}=\sum_{i=1,2,3}\frac{\partial}{\partial X_i}\left(\left(\frac{1}{h_i^2}-1\right)\left(\frac{\partial\phi}{\partial X_i}+A_i\right)\right)-\frac{D_o}{D\tau}\left(\frac{1}{c_o^2}\right)\frac{D_o\phi}{D\tau}-\frac{\mathbf{u}.(\mathbf{U}.\nabla\mathbf{U})}{c_o^2}$$

The interesting feature of this result is that the lefthand side is now defined in terms of a wave equation with constant coefficients because $D_\infty f/Dt=\partial f/\partial t+U_\infty\partial f/\partial X_1$ and the righthand side only includes terms which tend to zero when the flow returns to it's background value U_∞. It is relatively straightforward to show from equations (3.5) and (3.6) that the impermeability of the blades requires the boundary condition $\partial\phi/\partial X_2+A_2=0$ on the surface(s), and by using generalized derivatives (Farassatt (1994)), we can write this equation with surface source terms on the righthand side similar to those in equation (3.1) as

(3.11)

$$\frac{1}{c_o^2}\frac{D_o^2(H\phi)}{D\tau^2}-\frac{\partial^2(H\phi)}{\partial X_i^2}=$$

$$\sum_{i=1,2,3}\frac{\partial}{\partial X_i}\left(\left(\frac{1}{h_i^2}-1\right)\left(\frac{\partial\phi}{\partial X_i}+A_i\right)H\right)-\frac{D_o}{D\tau}\left(\frac{1}{c_o^2}\right)\frac{D_o(H\phi)}{D\tau}-\frac{H\mathbf{u}.(\mathbf{U}.\nabla\mathbf{U})}{c_o^2}$$

$$+A_2\delta(f)\,|\nabla f|-\frac{\partial}{\partial X_2}(\phi\delta(f)\,|\nabla f|)$$

The interpretation of each of the terms on the right of this equation is as follows: The first term represents the contribution from the volume sources and is weighted by the

factor $(1-h_i^{-2})$ where $h_1=U/U_\infty$ and $h_2=U_n/U$. The $i=1$ term therefore has a very large weighting function close to forward stagnation points where the steady flow tends to zero. This feature was discussed at length by Atassi and Grzedzinski (1989) who argued that, by allowing ϕ to be the sum of a component related to the pressure and a purely convected component which did not contribute to the acoustic filed, then the unsteady velocity on and parallel to the surface $\partial\phi/\partial X_1+A_1$ tended to zero. Consequently the singularity at the stagnation point caused by $(1-h_1^{-2})$ is canceled by the zero of $\partial\phi/\partial X_1+A_1$, and a finite contribution obtained from the source term in that region. The surface contributions of the first term are therefore finite, but small distances from the surface the cancellation of $\partial\phi/\partial X_i$ by A_i will not be complete and the most significant contributions can be expected from regions where U/U_∞ is either very small or very large, for example either close to the leading edge or the stagnation point, but not the trailing edge. This suggests that a rounded leading edge will reduce the contributions from this term at all frequencies. The second and third terms represent the contributions due to refraction of sound by the flow, and are small when flow Mach number is small. The fourth and fifth terms are the contributions from the surface, and represent the contribution from the zero normal velocity boundary condition (which is only non-zero when the surface is unsymetrical in X_i co-ordinates, and so must be a lifting surface), and the surface value of the velocity potential.

The limiting case of a flat plate at zero angle of attack is obtained when the flow speed is uniform and so only the surface terms in (3.7) are non-zero. Furthermore the incoming gust is undistorted by the flow, and so A_2 is identical on the upper and lower surface, and the net contribution from this term is also zero. The remaining equation is then defined as

(3.12)

$$\frac{1}{c_\infty^2}\frac{D_\infty^2(H\phi)}{D\tau^2}-\frac{\partial^2(H\phi)}{\partial X_i^2}=-\frac{\partial}{\partial X_2}\left(\Delta\phi\delta(X_2)\right)$$

This represents the flat plate approximation which was considered by Amiet (1975) for sound radiation from an airfoil in turbulent flow. However this approximation ignores a number of terms and there have been a number of studies to evaluate the accuracy of this approximation for isolated airfoils, as a function of thickness and angle of attack. Howe (1989,1990) considered lift and unsteady thickness effects and concluded that at low Mach numbers, the volume sources canceled the unsteady thickness sources (Glegg(1986)), and that the corrections for an airfoil at an angle of attack to altered the far field directionality of

the radiated field. Using the numerical solution described by Scott and Atassi (1990), the sound radiation from isolated blades and cascades has been studied extensively. Atassi, Fang and Patrick (1993), Hall & Verdon (1991), Atassi (1993) give calculations for both isolated airfoils and blade rows in non-uniform flows. Kerschen and Myers(1995) considered sound radiation from a lifting airfoil in the limit that $(1-h_i^{-2})<<1$, and showed significant increases in radiated sound power as the angle of incidence increased, especially at higher Mach numbers.

However the problem with Goldstein's formulation is that it does not apply to moving surfaces for which the potential flow around the body varies with time and so the thickness noise term in the Ffowcs-Williams Hawkings equation is not included. Furthermore the formulation is based on the linearised equations of motion and so does not include the non-linear convection of the incoming gust past the blade, which has been shown to be important for open rotor applications (Hardin and Lamkin(1984)). Alternative approaches, for example Guidati et al (1997) who used an approach based on tracking the vorticity in the flow, and Lockard and Morris (1998) who solved the full Navier Stokes equations and used a novel method to describe the incoming gust, are not limited by these approximations and may lead to more general methods of solution.

The primary difficulty in using numerical solutions to equations such as equation (3.4) for the broadband fan noise calculations is that the blades interact with small scale turbulence. Consequently the scale of the airfoil is large compared with the gust wavelength, and so the grid required for the numerical calculation has to be very detailed, especially around the leading and trailing edges. Typically we are interested in non-dimensional frequencies $\omega c/U_\infty$ which areas large as 70 and it unusual to find numerical calculations for non-dimensional frequencies in excess of 25. This makes the high frequency broadband noise problem particularly challenging and suggests that a complete solution will not be found using existing approaches. In the sections which follow we will discuss the analyses which have been used to date to evaluate broadband noise from fans and rotors, and we will discuss further the limitations imposed by the requirement to model the effects of high frequencies and small scale turbulence.

4. Inflow Noise

4.1 Introduction

As described above, recent advances (Atassi(1993), Hall & Verdon(1991)) in fan noise prediction have been based on numerical methods which evaluate both the unsteady loads and the radiated noise from a cascade of fan blades with finite thickness, angle of attack and camber. These approaches consider the response of the cascade to a harmonic input gust and combine both the surface and volume sources to give the radiated acoustic field. The application of these methods has been primarily to evaluate the sound generated by stator vanes in response to the mean velocity deficits in the rotating wakes of an upstream fan. In this case the inflow can be broken down into it's Fourier components to provide the amplitude of the harmonic inflow perturbations and the radiated field will be periodic in time with tones at blade passing frequencies. An obvious extension to this approach is to compute the broadband noise spectrum by considering a turbulent rather than a deterministic inflow to the cascade. Martinez (1997) carried out a study of this type and was able to generate predictions of broadband fan noise spectra but the computational effort required for this calculation was extensive.

Earlier work on broadband turbulence ingestion noise (Mani(1971),Homicz and George (1974), Amiet (1975)&(1977), Glegg (1993), considered each blade of the fan as isolated, and ignored the cascade effects or coupling between the response of adjacent blades. Ventres, Theobald and Mark(1982) developed a broadband noise prediction method based on a two dimensional blade response function for a cascade of blades modeled as flat plates, but did not include the effect of the spanwise variation of the incoming turbulence. However, as was illustrated in section 2 the turbulent inflow to both the rotor and the stator has a strong spanwise variation, especially close to the outer duct wall. These effects cannot be modeled using the strip theory approach of Ventres et al, especially if there is any spanwise flow or the stator vanes include sweep or lean. In this section we will derive a theoretical approach to broadband noise prediction which is based on a flat plate cascade blade response function, including all the spanwise effects. The advantage of using a flat plate model is that the primary effects are included without the necessity for extensive computation time, and so many different operating conditions can be considered without excessive computational effort. The blade response function which will be used is described in detail by Glegg(1997) and this approach is reviewed in section 4.3. Section 4.4 describes the application of this theory to the broadband noise problem, and characteristic results are discussed in section 4.5.

4.2 Modeling a Fan using a Rectilinear Cascade

All the studies described above only consider two dimensional cascades and a more accurate model of an aeroengine is given by a rotor and/or a stator in a circular duct. The unsteady loading and sound generation by a ducted rotor was considered by Namba (1977). The solution is obtained by solving an integral equation for the velocity potential using a collocation method and numerical results showed that three dimensional effects reduced the blade loading at low frequencies and non zero spanwise wavenumbers reduced the acoustic radiation at high frequencies. Kordama and Namba (1989) extended this analysis to a rotor with swept blades and Schulten(1997) introduced a alternative form for the Green's function in a circular duct to evaluate the acoustic radiation from swept stator vanes downstream of a fan. However Golubev and Atassi(1996) have shown that for a duct with swirling flow a reasonable approximation can be achieved using a rectilinear cascade to model the rotor or stator providing that the hub to tip ratio is not too large. This will be the approach taken here because it allows a full analytical solution to the inflow noise problem to be obtained, and eliminates many of the rather difficult mode coupling effects which occur in circular ducts, which are likely to be of secondary importance to the radiated sound power.

To model the sound radiation from a turbulent inflow incident on a set of blades we will use the linear cascade model developed by Goldstein(1976). The blades are modeled as flat plates aligned in the direction of the oncoming mean flow, mounted between rigid end walls (see figure 4.1). The span of the blades is b and the spacing between the leading edges of the blades is s. The linear cascade is an unwrapped analog of an annular duct and so all features of the fan and the flow will be periodic in the circumferential direction. Consequently if there are B blades in the fan the flow field will repeat itself at distances of Bs along the fan face. Furthermore the flow field must satisfy the rigid wall boundary condition at the end of each blade.

The acoustic velocity potential scattered by the cascade subjected to a incident gust of the type gust $w_o exp(-i\omega t+i\gamma_o x+i\alpha y+ivz)$ can be defined using equation (3.12) in the co-ordinate system shown in figure 4.2 as

(4.1)

$$\frac{1}{c_o^2}\frac{D^2(H\phi)}{Dt^2}-\nabla^2(H\phi)=-\frac{\partial}{\partial y}\sum_n \Delta\phi_o(x-nd)\delta(y-nh)e^{-i\omega t+in\sigma+ivz}$$

where $D\phi/D\tau=\partial\phi/\partial\tau+U\partial\phi/\partial x$ is the total time derivative in the direction of the uniform mean flow U in the duct, ω is the frequency, σ is the interblade phase angle (see below) and ν is the spanwise wavenumber of the gust. Since we have assumed that the blades are flat and aligned with the flow, the mean flow distortion caused by blade thickness camber and loading is ignored for this ideal cascade model.

To determine the acoustic field we will obtain the solution to equation (4.1) subject to the boundary condition of zero flow through the blades. This will be discussed in the next section and then applied to the broadband noise problem in section 4.4.

4.3 The Acoustic Field from a Three Dimensional Cascade

In the 1970's several studies were carried out to evaluate the acoustic field from a harmonic vortical gust incident on two dimensional sets of blades, represented by a cascade of flat plates at zero angle of attack. Kaji and Okazaki (1970a) considered sound propagation upstream through a cascade by solving for a distribution of dipole sources on the blade surfaces. In this approach the solution of the integral equation which relates the source strength to the velocity disturbance was obtained using a collocation procedure. In a subsequent paper Kaji and Okazaki (1970b) used the same approach to evaluate the sound generated by a rotor wake/stator interaction. Mani and Hovray(1970) considered the sound transmission problem for waves propagating through a blade row using an approximate solution based on the Wiener Hopf method. Although they gave an analytical result they assumed that there was no interaction between the leading and trailing edges of the blades. Koch(1971) extended the Wiener Hopf analysis of Mani and Hovray(1970) to blades with finite chord and gave the transmission and reflection coefficient for both upstream and downstream propagating acoustic waves. Koch's analytical solution is unwieldy and although in principle it can be used to calculate the unsteady lift on the blade surfaces he was unable to do so.

Koch's method provides the analytical basis for the solution to the cascade problem, but numerical solutions which are based on a similar approach to that of Kaji and Okazaki (1970) have proven to be more versatile (Fleeter(1973), Smith(1973)). For example Smith(1973) developed a code which gives the unsteady loading, the vortical field, and the acoustic field upstream or downstream of a blade row for any type of incoming gust.

The recent development of very high by-pass aeroengines which have blades with much larger chords than in previous designs, has lead to renewed interest in analytical methods for the blade response function at high frequencies. Peake (1993) has extended

Koch's(1971) analysis to give the unsteady loading on the blades caused by an incoming vortical gust, and has also developed analytical tools (Peake(1992), Peake and Kerschen(1995)) which enable rapid evaluation the functions required for the Wiener Hopf solution of Mani & Hovray (1970) and Koch (1971).

All the methods described above only apply to the two dimensional problem. For broadband noise spanwise effects are important and a fully three dimensional response function is required. This was derived by Glegg (1997) for a fully three dimensional rectilinear flat plate cascade. The analysis allowed for a skewed gust, which enabled both the spanwise wavenumber, the spanwise convection of the gust and the effect of blade sweep to be included. In this approach the solution to equation (4.1) was solved in blade based co-ordinates *(x,y,z)* (see figure 4.2) assuming a incident vortical gust $w_o exp(-i\omega t+i\gamma_o x+i\alpha y+ivz)$. An integral equation was derived which related the acoustic perturbation in the *y* direction on the blade surface to the discontinuity in the potential in the form

(4.2)

$$\frac{\partial \phi(x,0,z,t)}{\partial y} = e^{-i\omega t+ivz} \int_0^\infty \Delta\phi_o(x_o) K(x-x_o) dx_o$$

The discontinuity in the potential was then defined as the sum of four different solutions:

(4.3)

$$\Delta\phi_o = \Delta\phi_o^{(1)} + \Delta\phi_o^{(2)} + \Delta\phi_o^{(3)} + \Delta\phi_o^{(4)}$$

where each solution satisfies the integral equation

(4.4)

$$f^{(i)}(x) = \int_0^\infty \Delta\phi_o^{(i)}(x_o) K(x-x_o) dx_o$$

The interesting part of this approach is that each of the four solutions has a different physical interpretation, which represents a different degree of approximation in the complete solution. The first part of the solution ensures that the no flow boundary condition is met on the blade surface and also the wake which requires the boundary conditions

(4.5)

$$f^{(1)}(x) = \frac{\partial \phi}{\partial y} = -w_o e^{i\gamma_o x} \qquad x > 0 \qquad \Delta\phi_o^{(1)}(x) = 0 \qquad x < 0$$

The boundary conditions are defined on the half planes $x>0$ and $x<0$ and this type of problem can be solved using the Weiner Hopf method. In addition to the zero flow boundary condition the Kutta condition must also be satisfied. This is achieved by requiring the second part of the solution to satisfy the boundary conditions

(4.6)

$$f^{(2)}(x) = 0 \quad x < c \qquad \frac{\mathrm{D}(\Delta\phi_o^{(1)}(x)e^{-i\omega t+ivz} + \Delta\phi_o^{(2)}(x)e^{-i\omega t+ivz})}{Dt} = 0 \qquad x > c$$

This again can be solved using a Weiner Hopf approach because the boundary conditions are defined on the half planes $x>c$ and $x<c$. However the solution for $\Delta\phi_o^{(2)}$ is not necessarily zero upstream of the blade leading edge and so we must introduce two additional corrections which are coupled and satisfy equation (4.3) with the boundary conditions

(4.7)

$$f^{(3)}(x) = 0 \quad x > 0 \qquad \Delta\phi_o^{(2)}(x) + \Delta\phi_o^{(3)}(x) + \Delta\phi_o^{(4)}(x) = 0 \qquad x < 0$$

and

(4.8)

$$f^{(4)}(x) = 0 \quad x < c \qquad \frac{\mathrm{D}(\Delta\phi_o^{(3)}(x)e^{-i\omega t+ivz} + \Delta\phi_o^{(4)}(x)e^{-i\omega t+ivz})}{Dt} = 0 \qquad x > c$$

which are also boundary value problems suitable for solution using the Wiener Hopf method.

The sum of the four parts satisfy the boundary conditions of no flow through the blades, no discontinuity in potential upstream of the blade leading edges, and no pressure discontinuity downstream of the trailing edges (the Kutta condition). Consequently the cascade response problem which is defined by three separate boundary conditions, specified on different parts of the x-axis, has been broken down into four boundary value problems which are specified on semi-infinite parts of the x-axis for which there is a known method of solution.

This problem was solved by Glegg (1997) and a result obtained for the acoustic field as

(4.9)

$$\phi = \frac{\pm w_o}{\beta s_e} \sum_{m=-\infty}^{\infty} \left\{ \frac{\pi \zeta_m^{\pm} D(\lambda_m^{\pm})}{\sqrt{\kappa_e^2 - f_m^2}} \right\} e^{-i\omega t + i(\sigma - 2\pi m) y/h - i\lambda_m^{\pm}(x - yd/h) + i\nu z}$$

$$\kappa_e = \sqrt{\kappa^2 - (\nu/\beta)^2} \qquad f_m = (\sigma + \kappa M d - 2\pi m)/s_e$$

$$s_e = \sqrt{d^2 + (h\beta)^2} \qquad \lambda_m^{\pm} = \kappa M - f_m \sin\chi_e \pm \cos\chi_e \sqrt{\kappa_e^2 - f_m^2}$$

where $D(\lambda_m^{\pm})$ represents the Fourier transform of the velocity discontinuity for an upwash gust of unit amplitude defined as

(4.10)

$$D(\gamma) = \frac{1}{2\pi} \int_0^{\infty} \Delta\phi_o(x) e^{i\gamma x} dx$$

In addition $\sigma = \gamma_o d + \alpha h$ is the interblade phase angle, M is the flow Mach number, $\beta = (1 - M^2)^{1/2}$, $\chi_e = \tan^{-1}(h\beta/d)$ and $\zeta_m^{\pm} = \beta(\kappa_e^2 - (\lambda_m^{\pm} - \kappa M)^2)^{1/2}$. The blade spacing and stagger angle is defined in figure 4.2.

In the result given by equation (4.9) the terms in { } represent the amplitude of each mode of propagation, while the phase terms give the spatial dependence of the modes. From this expression it is also possible to obtain the upstream or downstream sound power for a harmonic gust as:

(4.11)

$$W_{\pm} = \left(\frac{w_o^2}{2} \right) \frac{\omega \rho_o B s b}{\beta s s_e} \sum_{m=-\infty}^{\infty} \mathrm{Re} \left[\frac{\left| \pi \zeta_m^{\pm} D(\lambda_m^{\pm}) \right|^2}{\sqrt{\kappa_e^2 - f_m^2}} \right]$$

In this expression $(w_o^2/2)$ represents the mean square magnitude of the harmonic upwash component incident on the cascade.

This summarizes the analytical results obtained by Glegg (1997). For broadband noise calculations we will need to generalize these results to the case where the upwash velocity is defined spatially as a stochastic random quantity, convected with the mean flow. However before considering the broadband noise problem we will discuss the characteristics of the blade response function for a harmonic gust.

First we note from equation (4.11) that each of the terms inside the summation sign represents the modal sound power, and that this will only be non-zero if $\kappa_e > f_m$. Therefore for modes to be cut-on the effective wavenumber κ_e must be exceed a certain value which is determined by the interblade phase angle, the Mach number and the mode order. The effective wavenumber increases with frequency, but also depends on the spanwise wavenumber. Gusts with significant spanwise variations will cut on at higher frequencies than gusts with no spanwise variations. In contrast, for a two dimensional model the spanwise variation of the gust is ignored giving $\kappa_e = \kappa$ and so the cut on frequency of each mode is only a function of the mode order and interblade phase angle. In broadband noise modeling the spanwise variations of the gusts are very significant and so the correct spanwise wave number dependence must be included.

It is shown in detail by Glegg(1997) that the radiation in the upstream direction is determined by the first and third terms in the expansion given in equation (4.3). The downstream radiation is determined by the second and fourth terms. The first term represents the leading edge noise, which would occur if the blades had semi infinite chord. However this must be modified to account for waves reflected back upstream from the trailing edge, and this is represented by the third term in the expansion. It would be convenient to ignore the waves reflected at the trailing edge, and this approach has been used in several studies (Mani & Hovray(1971), Peake (1995)), but it was shown by Glegg (1997) that this approximation can lead to significant errors, and for accurate results all the terms must be included.

4.4 Application of Cascade Theory to Broadband Noise

The theory described above gives the sound radiation from a cascade of blades in response to an incident harmonic vortical gust which is convected with the flow. To apply this theory to broadband noise the gust must be defined in a more general form and also required to satisfy various boundary conditions. The first modification we will impose is that the cascade is bounded by rigid end walls (see figure 4.1) and so both the acoustic field and the incoming gust must satisfy the no flow condition at these boundaries. Secondly the cascade flow represents an unwrapped version of a blade row in a circular duct, and so must be periodic in the azimuthal direction. Finally we will assume that the gust is convected with the mean flow at a uniform speed.

To develop a flow model which satisfies these conditions we will define the blades to be moving with velocity $\mathbf{V}_b$ and the turbulent gust to be convected with the mean flow

velocity $\mathbf{V}$ in the fixed frame of reference. The flow speed relative to the blade is then obtained as $\mathbf{V}\text{-}\mathbf{V}_b.=(U,0,0)$ defined in (x,y,z) co-ordinates (see figure 4.2). The gust must be periodic (repeating itself after B blade passages), and is described in moving co-ordinates $\mathbf{x}''=\mathbf{x}\text{-}(\mathbf{V}\text{-}\mathbf{V}_b)t$ as having an upwash velocity $\Sigma w(\mathbf{x}''\text{-}m\mathbf{d})$. The gust $w(\mathbf{x}'')$ is zero unless $0<y''<Bh$, and $\mathbf{d}=(Bd,Bh,0)$ where the (x'',y'',z'') co-ordinates are aligned with the (x,y,z) co-ordinates in figure 4.2. The unsteady upwash relative to the blades is then

(4.12)

$$\mathbf{n}.\mathbf{u}(\mathbf{x},t) = \sum_{m=-\infty}^{\infty} w(\mathbf{x} - m\mathbf{d} - (\mathbf{V} - \mathbf{V}_b)t)$$

It was argued by Goldstein(1976) that for a vortical gust between two parallel end walls the flow components parallel to the walls can be described by a Fourier cosine series expansion, so in general we can write

(4.13)

$$w(x'',y'',z'') = \int_{-\infty}^{\infty}\int_{-\infty}^{\infty}\sum_{n=0}^{\infty} \hat{w}_n(\gamma,\alpha)e^{-i\gamma x''-i\alpha y''}\varepsilon_n \cos(n\pi z''/b)d\gamma d\alpha$$

(where $\varepsilon_n=1,n>0,\ \varepsilon_o=1/2$). The integrand is defined as the wavenumber transform of $w(\mathbf{x}'')$ in the form

(4.14)

$$\hat{w}_n(\gamma,\alpha) = \frac{2}{(2\pi)^2 b}\int_{-R}^{R}\int_{0}^{Bh}\int_{0}^{b} w(x'',y'',z'')e^{i\gamma x''+i\alpha y''}\cos(n\pi z'/b)dx''dy''dz''$$

The upwash in blade based co-ordinates is then obtained as

(4.15)

$$\mathbf{n}.\mathbf{u}(\mathbf{x},t) = \int_{-\infty}^{\infty}\int_{-\infty}^{\infty}\sum_{n=0}^{\infty}\sum_{m=-\infty}^{\infty} \hat{w}_n(\gamma,\alpha)e^{-i\gamma(x-Ut-mBd)-i\alpha(y-mBh)}\varepsilon_n \cos(n\pi z/b)d\gamma d\alpha$$

Making use of the Poisson sum formula

(4.16)

$$\sum_{m=-\infty}^{\infty} e^{i\gamma mBd+i\alpha mBh} = 2\pi \sum_{k=-\infty}^{\infty} \delta(\gamma Bd + \alpha Bh - 2\pi k)$$

and integrating over α gives

(4.17)

$$\mathbf{n.u}(\mathbf{x},t) = \frac{2\pi}{Bh} \int_{-\infty}^{\infty} \sum_{n=0}^{\infty} \sum_{k=-\infty}^{\infty} \hat{w}_n(\gamma, \frac{2\pi k}{B} - \frac{\gamma d}{h}) e^{-i\gamma(x-Ut)-i(\frac{2\pi k}{B}-\frac{\gamma d}{h})y} \varepsilon_n \cos(n\pi z/b) d\gamma$$

If we define $\omega=-\gamma U$ and $\gamma_o=\omega/U$ then we obtain the upwash velocity at the blade as

(4.18)

$$\mathbf{n.u}(\mathbf{x},t) = \sum_{n=0}^{\infty} \sum_{k=-\infty}^{\infty} \int_{-\infty}^{\infty} w_{kn}(\omega) e^{-i\omega t+i\gamma_o(x-yd/h)-2\pi iky/Bh} \varepsilon_n \cos(n\pi z/b) d\omega$$

where

(4.19)

$$w_{kn}(\omega) = \frac{-2\pi}{BhU} \hat{w}_n(-\gamma_o, \frac{2\pi k}{B} + \frac{\gamma_o d}{h})$$
$$= \frac{-1}{\pi BhbU} \int_{-R}^{R} \int_{0}^{Bh} \int_{0}^{b} w(\mathbf{x}) e^{-i\gamma_o(x-yd/h)+2\pi iky/Bh} \cos(n\pi z/b) dx dy dz$$

Equation (4.18) gives a Fourier expansion of the incoming vortical gust which satisfies the periodicity condition and the end wall boundary conditions. Note that x-yd/h is constant at the blade leading edges and so the interblade phase angle of the gust is $\sigma = -2\pi k/B$.

To obtain the acoustic field from this gust we can combine equation (4.9) with equation (4.18) to give

(4.20)

$$\phi(\mathbf{x},t) =$$
$$\frac{\pm 1}{\beta s_e} \sum_{m=-\infty}^{\infty} \sum_{k=-\infty}^{\infty} \sum_{n=0}^{\infty} \int_{-\infty}^{\infty} T_{mn}^{(k)}(\omega) w_{kn}(\omega) e^{-i\omega t+i(\sigma-2\pi m)y/h-i\lambda_m^{\pm}(x-yd/h)} \varepsilon_n \cos(\frac{n\pi z}{b}) d\omega$$

where $$T_{mn}^{(k)}(\omega) = \frac{\pi \zeta_m^{\pm} D(\lambda_m^{\pm})}{\sqrt{\kappa_e^2 - f_m^2}}$$

where $T_{mn}^{(k)}$ is the amplitude of a mode of order m with a spanwise mode order n and an interblade phase angle $-2\pi k/B$. The computation of the triple summation in this expression can be simplified by using the property that $T_{mn}^{(k)}=T_{on}^{(k+mB)}$. Then if we introduce the integer variable $p=mB+k$ it follows that $\sigma-2\pi m=-2\pi p/B$.

It is valuable to specify equation (4.20) in observer coordinates which are aligned with the fan face as shown in figure 4.2. This is achieved by using the co-ordinate transformations

(4.21)

$$x - yd/h = x'/\cos\chi \qquad y/h = (y' + V_b t)/s - x'd/sh$$

to write (4.20) as

(4.22)

$$\phi = \frac{\pm 1}{\beta s_e} \sum_{p=-\infty}^{\infty} \sum_{n=0}^{\infty} \int_{-\infty}^{\infty} T_{0n}^{(p)}(\omega) \left\{ \sum_{m=-\infty}^{\infty} w_{p-mB,n}(\omega) \right\} e^{-i\omega_o t - 2\pi i p(y' - x'd/h)/Bs - i\lambda_m^{\pm} sx'/h} \varepsilon_n \cos(n\pi z/b) d\omega_o$$

$$\omega = \omega_o - p\Omega_b$$

with $\Omega_b=2\pi V_b/Bs$. The important features of this result are that the field is now defined in the y' direction. In an equivalent annular system the azimuthal coordinate θ is related to y' by $2\pi y'/Bs=\theta$ and so the integer p defines the mode order in the cylindrical co-ordinate system. Also note that the summation over m is only required over the gust coefficients and not over the blade response terms which simplifies the evaluation of equation (4.22).

For a stochastic input we need to calculate the sound power spectral density which is defined in a moving fluid as

(4.23)

$$S_{WW}(\omega) = \frac{-\rho_o \pi}{T} Ex\left[\int_S -i\omega\phi(\mathbf{x},\omega) \left\{ \nabla\phi(\mathbf{x},\omega) - \frac{\mathbf{U}}{c_o^2}(\mathbf{U}.\nabla\phi(\mathbf{x},\omega) - i\omega\phi(\mathbf{x},\omega) \right\}^* .\mathbf{n} dS \right]$$

where $\mathbf{n}$ is a unit vector pointing out of the surface and $\phi(\mathbf{x},\omega)$ is the Fourier transform of the velocity potential with respect to time. The evaluation of this expression follows the same procedure as is required for the evaluation of the sound power given by Glegg (1997)

in the blade fixed frame. Since the modes are orthogonal they contribute independently to the sound power giving

(4.24)

$$S_{WW}(\omega) = \frac{\rho_o BsbU}{2} \sum_{m=-\infty}^{\infty} \sum_{k=-\infty}^{\infty} \sum_{n=0}^{\infty} \varepsilon_n H_{mn}^{(k)}(\omega) E_{kn}(\omega)$$

where $$H_{mn}^{(k)}(\omega) = \frac{\omega \left| \pi \zeta_m^{\pm} D(\lambda_m^{\pm}) \right|^2}{U\beta s s_e \sqrt{\kappa_e^2 - f_m^2}}$$ and $$E_{kn}(\omega) = \frac{\pi}{T} Ex\left[\left| w_{kn}(\omega) \right|^2 \right]$$

If the blades are moving with speed V_b in the y' direction then the observed frequency in the stationary frame is given by $\omega_o = \omega + p\Omega_b$. To calculate the sound power in the stationary frame we note that the terms in { } in (4.23) are independent of the relative motion of the blades to the observer (because $D\phi/Dt$ and $\mathbf{U}.\mathbf{n}$ remain unaltered by the translation). However the frequency must be defined in the observer's frame of reference, so we can modify (4.24) for moving blades . Using $H_{mn}^{(k)} = H_{0n}^{(k+mB)}$ we find

(4.25)

$$S_{WW}(\omega_o) = \frac{\rho_o BsbU}{2} \sum_{p,n} \varepsilon_n \frac{\omega_o H_{0n}^{(p)}(\omega_o - p\Omega_b)}{\omega_o - p\Omega_b} \left\{ \sum_m E_{p-mB,n}(\omega_o - p\Omega_b) \right\}$$

The evaluation of this expression is dependent on the definition of the turbulence spectrum function $E_{kn}(\omega)$ which is obtained from the inversion integral,

(4.26)

$$w_{kn}(\omega) = \frac{1}{\pi BhbU} \int_0^{Bh} \int_0^{b} \int_{-\infty}^{\infty} w(\mathbf{x}) e^{-i\gamma_o(x - yd/h) + 2\pi i k y / Bh} \cos(n\pi z / b) dx dz dy$$

which gives,

(4.27)

$$E_{kn}(\omega) = \frac{1}{\pi (BhbU)^2 T} \int_0^{Bh} \int_0^{b} \int_0^{Bh} \int_0^{b} \int_{-R}^{R} \int_{-R}^{R} Ex\left[w(\mathbf{x}) w(\mathbf{x}_1) \right] e^{i\gamma_o(x - x_1) + i(2\pi k + \gamma_o Bd)(y - y_1)/Bh} \cos(n\pi z / b) \cos(n\pi z_1 / b) dx dx_1 dz dy dz_1 dy_1$$

where the extent of the flow in the x direction is $\pm R$ where R tends to infinity. Defining $T=RU$ and assuming a statistically stationary time series

(4.28)

$$E_{kn}(\omega)=\frac{2}{\pi(Bhb)^2}\int_0^{Bh}\int_0^{Bh}\int_0^{b}\int_0^{b}\int_{-T}^{T} R_{ww}(-U\tau,y,y_1,z,z_1)e^{i\omega\tau+i(2\pi k+\gamma_o Bd)(y-y_1)/Bh} \cos(n\pi z/b)\cos(n\pi z_1/b)d\tau dz dz_1 dy dy_1$$

where $R_{ww}(-U\tau,y,y_1,z,z_1)$ is the cross correlation coefficient between the velocity fluctuations at (x,y,z) and (x_1,y_1,z_1), assuming uniform convection in the x direction.

4.5 Turbulence Models

4.5.1 Wavenumber Spectrum Modeling

The simplest way to evaluate (4.28) is to use a homogeneous turbulence model for which

(4.29)

$$R_{ww}(-U\tau,y,y',z,z')=\int_{-\infty}^{\infty}\int_{-\infty}^{\infty}\int_{-\infty}^{\infty}\Phi_{ww}(k_x,k_y,k_z)e^{ik_xU\tau-ik_y(y-y')-ik_z(z-z')}dk_x dk_y dk_z$$

Using this expression in (4.28) gives

(4.30)

$$E_{kn}(\omega)=\frac{1}{U}\int_{-\infty}^{\infty}\int_{-\infty}^{\infty}\Phi_{ww}(-\gamma_o,k_y,k_z)|F_n(k_z)|^2\left|\frac{2\sin(\pi k+\gamma_o Bd/2-k_yBh/2)}{2\pi k+\gamma_o Bd-k_yBh}\right|^2 dk_y dk_z$$

$$F_n(k_z)=\frac{2}{b}\int_0^b e^{-ik_zz}\cos(\frac{n\pi z}{b})dz=\left(\frac{2i\sin(n\pi/2-k_zb/2)e^{in\pi/2-ik_zb/2}}{n\pi-k_zb}\right)\frac{2k_zb}{n\pi+k_zb}$$

If the integral length scale is small compared with the scale of the flow then we can use the relationship

$$\lim_{d\to\infty}\left[\frac{\sin^2(\xi d)}{(\xi d)^2}\right]\to\frac{\pi}{d}\delta(\xi)$$

so that

(4.31)

$$\lim_{b\to\infty}\left|F_n(k_z)\right|^2 = \frac{2\pi}{b}\delta(n\pi/b - k_z)$$

then we obtain

(4.32)

$$E_{kn}(\omega) = \frac{(2\pi)^2}{UBhb}\Phi_{ww}(-\gamma_o, 2\pi k/Bh + \gamma_o d/h, n\pi/b)$$

This shows that to specify the sound power output we primarily need to know the wavenumber spectrum of the incoming turbulence.

4.5.2 A Boundary Layer Model

In this case we assume the flow is restricted to a region close to the wall such that the integrals over the span need only be carried out over the range $0<z'<\delta$. Typically we can expect $n<N$ for cut on modes and that $N\pi\delta/b<<1$. Making this assumption we have

(4.33)

$$F_n(k_z) \approx \frac{2}{b}\int_0^{\delta} e^{-ik_z z}dz = \frac{2\delta}{b}\left(\frac{2\sin(k_z\delta/2)e^{-ik_z\delta/2}}{k_z\delta}\right)$$

so

(4.34)

$$\lim_{\delta\to\infty}\left|F_n(k_z)\right|^2 = \frac{2\pi\delta}{b^2}\delta(k_z)$$

which gives in the limit that the lengthscale of the turbulence is much smaller than the scale of the flow

(4.35)

$$E_{kn}(\omega) = \frac{(2\pi)^2\delta}{UBhb^2}\Phi_{ww}(-\gamma_o, 2\pi k/Bh + \gamma_o d/h, 0)$$

4.5.3 Wake models

If we consider the turbulent flow to consist of B_R independent blade wakes and the projected width of the blades wakes normal to the direction of the flow is W, then we can use the same approach as was used for the boundary layer flow to estimate the wave

number spectrum for a single wake as W/Bh times the homogeneous turbulence result. Then independently summing the contribution from each wake we obtain

(4.46)

$$E_{kn}(\omega) = \frac{(2\pi)^2}{UBhb}\left\{\left(\frac{B_R W}{Bh}\right)\Phi_{ww}(-\gamma_o, 2\pi k/Bh + \gamma_o d/h, 0)\right\}$$

However as was pointed out by Hanson (1997) the term in { } is simply the spatial average of the wavenumber spectrum for the flow, and can be evaluated from the average statistics of the turbulence convected past the stator vanes in the duct.

4.5.4 Von Karman and Liepmann Spectra

Various empirical models are available for the wavenumber spectra of the turbulent flow. The most commonly used is the Von Karman spectrum, which is defined as

(4.47)

$$\Phi_{ww}(k_x, k_y, k_z) = \left\{\frac{\overline{w}^2 55\Gamma(5/6)}{k_e^3 9\sqrt{\pi}\Gamma(1/3)}\right\}\left(\frac{(1-k_z^2/k_s^2)(k_s^2/k_e^2)}{4\pi(1+k_s^2/k_e^2)^{17/6}}\right) \qquad k_e = \frac{\sqrt{\pi}}{L}\frac{\Gamma(5/6)}{\Gamma(1/3)}$$

$$k_s^2 = k_x^2 + k_y^2 + k_z^2$$

The Liepmann spectrum which has a slower fall off with frequency is also used and is given by

(4.48)

$$\Phi_{ww}(k_x, k_y, k_z) = \left\{\frac{8\overline{w}^2}{\pi k_e^3}\right\}\left(\frac{(1-k_z^2/k_s^2)(k_s^2/k_e^2)}{4\pi(1+k_s^2/k_e^2)^3}\right) \qquad k_e = \frac{1}{L}$$

4.6 Characteristics of Inflow Noise

Equation (4.25) prescribes a procedure for calculating the sound power generated by a cascade of blades which encounters a turbulent flow. The input parameters are the observed frequency, the relative blade velocity, the number of blades, the blade chord, spacing and span; the turbulence intensity, lengthscale and the boundary layer or wake thickness. We are using a linear cascade model and so the mid span values should be used for all the parameters. In this section we will show some sample calculations which indicate the trends which we expect to find in the numerical calculations as the input parameters are varied.

First we compare the upstream and downstream radiated sound power spectra for a typical set of input parameters, using a Von Karman turbulence spectrum model for a boundary layer type flow incident on a set of stators (Figure 4.3). The input parameters are the same as for the 55% speed case given in table 6.3. The computations show that the downstream sound power exceeds the upstream by up to 7 dB which is typical of the data described in section 2 (see for example figure 2.1). The effect of the spectrum model is shown in figure 4.4. In general the Von Karman turbulence spectrum model is recognized as giving a better fit to measured turbulence spectra, and the computations here show only small differences between these two models. We will use the Von Karman spectrum for all the calculations presented below. Figure 4.5 shows the effect of fan speed on the radiated sound power with all other parameters held constant. The increased speed causes relatively minor changes in the spectral shape, and a broadband increase of ~ 8dB.

The spectral shape is most affected by the turbulence lengthscales and these can be estimated either from the boundary layer thickness or as an independent parameter. Glegg (1993) gave the relationship between the turbulence lengthscale and the boundary layer thickness as $k_e\delta=1.2$, where $k_e=3/4L$, so we can estimate $L\sim 5\delta/8$. Using this approach, changing the boundary layer thickness will also change the turbulence lengthscale. Figure 4.6 shows the characteristics of these two parameters when combined in this way. The thicker boundary layer has an increased level, and more low frequency content. To identify the effect of the turbulence lengthscale alone, the sound power calculations for a range of lengthscales and a constant boundary layer thickness is shown in figure 4.7. The larger lengthscale causes the low frequencies to increase dramatically, with an associated reduction in the high frequency part of the spectrum.

In conclusion, these results have considered the overall properties of the fan noise spectrum as a function of various input parameters and it appears that the spectral shape is most strongly affected by the turbulence lengthscale used as the input to the calculations. Unfortunately this is the most difficult of all the turbulence parameters to measure, and cannot be achieved without at least two point measurements. Alternatively it can be estimated from the spectrum of a single hot wire measurement and a spectral model. We will consider this point in more detail in section 6.

4.6 Conclusion

In this section we have reviewed existing methods for the prediction of broadband fan noise from inflow turbulence and developed a procedure for fan noise prediction based

on a linear cascade model. The model is a rectilinear approximation to a fan or stator in a cylindrical duct, but it's advantage over other methods is that it includes all spanwise coupling effects. The standard output of this approach is the upstream and downstream sound power, but modal amplitude and power calculations are also possible with minor modifications.

Numerical examples have been given and it is shown that the spectral shape of the radiated sound power is primarily controlled by the turbulence lengthscale, which is the typically the most difficult turbulence parameter to measure.

5. Self Noise

(This section is the reproduction of a paper presented at the AIAA Aeroacoustics Conference in 1997)

5.1. Introduction

Fan broadband noise is classified into two different categories: the first is self noise which specifies the sound radiated by the self generated turbulence close to the blade surfaces. The second is inflow noise which is the sound radiated by the interaction of the blades with turbulence generated at some upstream location. The self noise is the base level of the radiated sound field and is important because it represents the minimum achievable level of broadband noise from the fan. This section will consider methods for predicting fan self noise for ducted subsonic fans.

The self noise from a ducted fan can be further broken down into two different source mechanisms. First there is blade boundary layer noise which is generated by the turbulence in the blade boundary layer interacting with the trailing edge, and is sometimes referred to as trailing edge noise. Secondly there is tip flow noise which is generated by the complicated flow around the blade tips and its interaction with the duct wall boundary layer. Little is known about tip flow noise although experimental observations (Mugridge and Morfey (1972)) have shown changes in fan noise with variations in tip gap dimensions. In contrast a large amount of work has been done on trailing edge noise for unducted rotors (Ffowcs Williams and Hall (1970), Howe (1978), Chase (1972), Amiet (1976), Kim and George (1982), Brooks and Hodgson (1981), and Brooks, et al (1989)) but the application of these concepts to ducted fans does not appear to have been studied. This paper will address this issue and apply the known concepts of trailing edge noise to a ducted fan configuration, considering in particular the coupling of the trailing edge noise source to the sound field in the fan duct.

Theoretical studies of trailing edge noise (Ffowcs Williams and Hall (1970), Howe (1978), Chase (1972), Amiet (1976), Kim and George (1982)) have shown that the source mechanism of trailing edge noise is the scattering of sound at the sharp trailing edge of the blade. The sound is actually generated by the turbulence in the blade boundary layer but since this is convected subsonically it does not couple with the acoustic far field. However it does generate a strong near field which causes significant pressure fluctuations on the blade surfaces. To ensure that the flow past the trailing edge is continuous a viscous wake must be generated, and it is the interaction of the sound generated in the wake with the surface upstream of the trailing edge which causes waves

to propagate to the acoustic far field. Analytical solutions to this problem can be posed in terms of a boundary value problem in which the Kutta condition is imposed at the trailing edge of the blade. Of particular relevance is the theoretical approach developed by Amiet (1976) who gives a formulation relating the far field spectral level to the spectrum of the convected boundary layer pressure fluctuations and their spanwise correlation length scale. Both factors need to be known to predict the sound from a ducted fan, and while it is possible to measure the surface pressure spectrum using pressure transducers imbedded in the blade surface, it is very difficult to measure the spanwise correlation lengthscale. An alternative approach is to estimate the combination of these two parameters from acoustic far field measurements of an isolated airfoil in a wind tunnel. By using Amiet's (1976) relationship, measurements of the acoustic field can be inverted to obtain the components of the surface pressure spectrum which are important for sound radiation. This approach has the advantage that non radiating components of the surface pressure spectrum are correctly filtered out of the estimated surface pressure. A further advantage of this approach is that an extensive data base exists (Brooks et al (1989)) for the self noise generated by isolated blades at different flow speeds and blade angles of attack. Consequently by combining this data set with Amiet's theory we can specify the blade surface parameters needed to compute trailing edge noise.

In this study we are interested in ducted fan blades and so to predict the in duct sound levels we require the surface pressure spectrum and correlation length scales on the fan or stator blade surfaces. This information is not available but can, in the first instance be estimated from the measurements on isolated blades as described above. However ducted fan blades differ from the blades used in Brook's study in many respects. First fan blades are not isolated and so the flow may be influenced by the presence of an adjacent blade. This can have an important effect on the acoustic scattering as will be discussed below, but it's influence on the blade boundary layer properties is not clear. The second difference is the blade camber. Brook's measurements are for uncambered blades whereas typical fan designs have blades with significant camber. However it is argued by Chase (1972) that the boundary layer properties scale with the flow speed and the boundary layer momentum thickness at the blade trailing edge. Consequently Brook's results can be used in principle for ducted fan blades providing a relationship is established which ensures that the blade trailing edge boundary layer properties are the same in each case.

Since fan blades are rotating the flow speed and the angle of attack vary significantly across the span. However the spanwise correlation lengthscale of typical boundary layer flows may be assumed to be of the order of the boundary layer thickness and this is small compared with both spanwise scale of the mean flow variables and the

acoustic wavelength. This suggests that the boundary layer properties of a rotating blade may be approximated by splitting the blade into spanwise strips and assuming the boundary layer is the same as that of a blade in rectilinear motion with the same local flow speed and angle of attack (Brooks et al (1989)). However, the surface pressure spectrum which couples with the acoustic field is correlated over a spanwise distance which is the order of the acoustic wavelength and so this strip theory approach is only valid in the high frequency limit where the acoustic wavelength is small compared with the blade span. This is a significant limitation and the consequences of this approximation for the ducted fan configuration will be considered in section 2.

In section 2 of this paper a theory is developed for the sound power radiated from a ducted fan by trailing edge noise sources. The turbulent boundary layer fluctuations are assumed uncorrelated on each blade but a correction is included for acoustic scattering from adjacent blades. The blade surface pressure spectrum is based on the interpolation of Brook's measurements on isolated airfoils. The scaling of the results as a function of the blade design parameters is given in section 3.

5.2 The Evaluation of the In-Duct Sound Power for Trailing Edge Noise

5.2.1 Theory for Noise from Blades Rotating in a Duct

In deriving a theory for the noise generated by ducted fan blades we must consider the general problem of sound radiation from a unsteady flow over moving surfaces in a duct. This problem is illustrated in figure 5.1 which shows a set of fan blades in a circular duct and an observer at the location **x**. By using Lighthill's acoustic analogy the acoustic pressure at the observer can be specified as:

(5.1)

$$p(\mathbf{x},t) = \int_{-T}^{T}\int_{V} T_{ij}(\mathbf{y},\tau)\frac{\partial^2 G(\mathbf{y},\tau\,|\,\mathbf{x},t)}{\partial y_i \partial y_j}dV d\tau + \int_{-T}^{T}\int_{S} f_i(\mathbf{y},\tau)\frac{\partial G(\mathbf{y},\tau\,|\,\mathbf{x},t)}{\partial y_i}dS d\tau + \int_{-T}^{T}\int_{S} \rho_o V_n(\mathbf{y},\tau)\frac{D_o G(\mathbf{y},\tau\,|\,\mathbf{x},t)}{D\tau}dS d\tau$$

where $G(\mathbf{y},\tau|\mathbf{x},t)$ is the Green's function which applies for a source in the duct at **y** and an observer at **x** in accordance with the conventions given by Goldstein (1976). The first term on the righthand side of this equation is the quadrupole source term which represents the sound generated by the turbulent flow fluctuations. In the blade boundary

layer these sources are convected subsonically relative to both the observer and the rotor blades and there is no rapid streamwise distortion of the flow, which can be assumed uniform at the trailing edge of the blades if the Kutta condition applies. The second term represents the dipole source term where f_i is the force per unit area applied to the fluid by the blade. The last term represents the contribution from the moving volume of the blade commonly referred to as thickness noise. This term is not important for ducted fans and only contributes to the near field at the blade passage frequencies, and so will be ignored.

To evaluate the levels of trailing edge noise two different approaches have been used. Ffowcs Williams and Hall (1970) and Howe (1978) used a Greens function which satisfied the boundary conditions a semi-infinite flat plate and so were able to eliminate the dipole term in equation (5.1). In Howe's approach a vorticity distribution is shed from the trailing edge to ensure that the Kutta condition is satisfied. In contrast Amiet (1976) specified a convected pressure disturbance on the surface of the blade which was induced by the quadrupole sources in the blade boundary layer. He then assumed that the turbulence in the boundary layer was undistorted as it convected past the trailing edge and introduced a correction to the local acoustic field which ensured that there was no pressure discontinuity in the blade wake. In essence both Howe's and Amiet's wake corrections are identical the only difference being the manner in which the problem is set up. Howe specifies the flow explicitly while Amiet specifies the net contribution of the induced flow in the wake. Both theories show that the subsonically convected turbulence in the boundary layer does not radiate to the acoustic far field and no sound is radiated if the eddy convection velocity equals the free stream velocity. In the analysis given here we will use Amiet's approach and define the acoustic field in terms of the blade surface pressure, ignoring the quadrupole term since this does not couple with the acoustic field. This is equivalent to assuming the quadrupole field generated by shed vorticity in the wake is exactly canceled by the surface pressure discontinuity which would have existed on an imaginary extension of the airfoil surface. On this basis (Amiet (1976)) we need only consider the dipole term in equation (5.1).

The Green's function can be defined for the acoustic field in a hard walled circular duct with a uniform axial flow (Goldstein (1976)) as

(5.2)

$$G(\mathbf{y},\tau\,|\,\mathbf{x},t) =$$

$$\frac{i}{4\pi}\int_{-\infty}^{\infty}\sum_{j,s}\frac{U_j(\alpha_{js}r_o)}{\beta_{js}\Gamma_{js}}e^{-i\omega t+ij\phi_o-i(Mk_oz_o\pm\beta_{js}z_o)/\mu^2}\left\{U_j(\alpha_{js}r)e^{i\omega\tau-ij\phi+i(Mk_oz\pm\beta_{js}z)/\mu^2}\right\}d\omega$$

where the observer is located at r_o,ϕ_o,z_o and the source point is r,ϕ,z (z is in the direction of the flow and the ± refers to an observer in the upstream/downstream direction). The axial flow Mach number is M and $\mu^2=1-M^2$. The wavenumber k_o is defined as ω/c_o where c_o is the speed of sound, U_j represent the duct modes and the coefficients α_{js} are the solutions to $U'_j(\alpha a)= U'_j(\alpha h) =0$ where a is the duct radius and h is the hub radius. We also have that

(5.3)

$$\beta_{js} = \sqrt{k_o^2 - \mu^2\alpha_{js}^2} \qquad \Gamma_{js} = \pi\left[(r^2 - \frac{j^2}{\alpha_{js}^2})U_j^2(\alpha_{js}r)\right]_h^a$$

The terms in equation (5.2) have been arranged so that those which depend on the source co-ordinates are grouped in the { } brackets. Consequently when (5.2) is used in equation (5.1) we can carry out the integrals over the source variables separately and define a modal expansion for the acoustic field in the form

(5.4)

$$p(\mathbf{x},t) = \int_{-\infty}^{\infty} \sum_{j,s} A_{js}(\omega)U_j(\alpha_{js}r_o)e^{ij\phi_o - i(Mk_o \pm \beta_{js})z_o/\mu^2 - i\omega t}\, d\omega$$

where the coefficients $A_{js}(\omega)$ are the mode amplitudes at the frequency ω.

To obtain the mode amplitudes for the dipole term in equation (5.1) we will first assume that the thickness of the blade is small compared with the acoustic wavelength so the surface integral in (5.1) may be replaced by an integral over the blade planform and the force applied to the fluid is replaced by the pressure difference across the blade surfaces. The integral over the planform must be carried out for each blade separately so we define $\mathbf{y}_n(\mathbf{r},\tau)$ as the location (in stationary co-ordinates) of the point $\mathbf{r}$ on the n^{th} blade at time τ. In cylindrical co-ordinates $\mathbf{y}_n=(r,\phi_n(r,z,\tau),z)$ where $z_u<z<z_D$ specifies the axial extent of the blades at each radial location. If we define ξ as the chordwise location on the mean blade planform (see figure 5.1) and β as the angle which the mean blade planform makes with the direction of rotation (so that $\tan\beta=U/\Omega r$) then $z-z_u=\xi sin\beta$ and we can define

(5.5)

$$\phi_n = \Omega\tau - \frac{2\pi n}{B} - \xi\cos\beta / r - \theta(r,z)$$

where $\theta(r,z)$ defines the blade camber relative to the mean chord line.

The force applied to the fluid is in the direction normal to the blade surface and so the gradient of the Green's function in the dipole term of (5.1) must be evaluated in this direction. The normal is defined by $\mathbf{n}=\nabla g/|\nabla g|$ where $g=\phi-\phi_n$ and so if we define $F_n(r,\xi,\omega)$ as the Fourier transform with respect to time of the blade surface pressure fluctuations on the n^{th} blade, the mode amplitudes will be

(5.6)

$$A_{js}(\omega) = \frac{1}{2\beta_{js}\Gamma_{js}} \sum_{n=1}^{B} \int_h^a \int_0^c \zeta_{js}^{\pm}\, U_j(\alpha_{js}r) F_n(r,\xi,\omega - j\Omega) e^{ik_{js}^{\pm}\xi + 2\pi inj/B + ij\theta(r,\xi)}\, dr d\xi$$

where $k_{js}^{\pm} = j\cos\beta / r + (Mk_o \pm \beta_{js})\sin\beta / \mu^2$

$$\zeta_{js}^{\pm} = \frac{jn_\phi}{r} - \frac{(Mk_o \pm \beta_{js})n_z}{\mu^2} - \frac{\alpha_{js}U_j'(\alpha_{js}r)n_r}{U_j(\alpha_{js}r)}$$

Given the dimensions of the duct all the quantities in (5.6) are known apart from the blade loading distribution F_n. This result allows for blades with arbitrary shape but it is often reasonable to ignore the effect of the blade camber, sweep and lean on the amplitude terms in (5.6) by approximating the normal to the blade surface as

(5.7)

$$\mathbf{n} = (n_r, n_\phi, n_z) \approx (0, \sin\beta, \cos\beta)$$

The duct modes are useful because they can be used to calculate the in duct sound power propagating either upstream or downstream from the fan. The expression for the autospectrum of the sound power is (see Goldstein (1976))

(5.8)

$$S_{ww}^{\pm}(\omega) = \mathrm{Re}\left\{ \sum_{j,s} \frac{\omega \mu^4 \beta_{js} \Gamma_{js}}{\rho_0 (\omega \pm \beta_{js} U)^2} \frac{\pi}{T} Ex[\ |A_{js}(\omega)|^2\ ] \right\}$$

This is a relatively simple expression and allows the spectrum of the sound power to be obtained from the spectrum of the mode amplitudes. Note how no sound power is radiated when β_{js} is imaginary which eliminates the cut off modes from the calculation.

The in duct sound power generated by broadband noise sources is therefore given by the expected value of the mode amplitudes as a function of frequency. These can be defined from equation (5.6) in the form

(5.9)

$$\frac{\pi}{T} Ex\left[\left|A_{js}(\omega)\right|^2\right] = \left(\frac{1}{2\beta_{js}\Gamma_{js}}\right)^2 \sum_{n=1}^{B} \int_{h}^{a} \sum_{m=1}^{B} \int_{h}^{a} \zeta_{js}^{\pm}(r) \zeta_{js}^{\pm}(r') U_j(\alpha_{js} r) U_j(\alpha_{js} r') \int_{0}^{c} \int_{0}^{c} S_{FF}^{(n,m)}(\mathbf{y}, \mathbf{y}', \omega_j) e^{iK_{js}^{\pm}(\xi,r) - iK_{js}^{\pm}(\xi',r') + 2\pi i j (n-m)/B} dr dr' d\xi d\xi'$$

where $\omega_j = \omega - j\Omega$ and $K_{js}^{\pm} = k_{js}^{\pm}\xi + j\theta(r,\xi)$. The term $S_{FF}^{(n,m)}$ is the cross spectral density of the pressure fluctuations on blades number m and n at the locations $\mathbf{y}=(r,\xi)$ and $\mathbf{y}'=(r',\xi')$ which is defined as

(5.10)

$$S_{FF}^{(n,m)}(\mathbf{y}, \mathbf{y}', \omega_j) = \frac{\pi}{T} Ex\left[F_n(r,\xi,\omega_j) F_m^*(r',\xi',\omega_j)\right]$$

If the fluctuations on each blade are uncorrelated then only those terms for which $n=m$ need be included in the summations but in general that will not be the case because the blades are coupled by the acoustic field.

This result shows that the acoustic field depends on the cross spectrum of the blade loading distribution and this must be known with sufficient accuracy to calculate the surface integral in (5.9). Note that the integrand also includes highly oscillatory functions and the coupling of these to the cross spectrum is crucial to the accuracy of the result.

The blade loadings for broadband sources on rotating blades are not well understood. At the present time the fully coupled blade response to either an unsteady inflow or a turbulent boundary layer can only be obtained numerically (Schulten (1996), Kordama and Namba (1989)), and calculations to date have been limited to the first few blade passage harmonics. Broadband noise calculations are an order of magnitude more difficult because they require multiple frequency calculations at very high frequencies. Therefore we are limited at this time to estimating the blade response function for a rotating blade by using the blade response functions for rectilinear blades applied to incremental strips across the span. The accuracy of this approximation depends on the spanwise extent of the blade response to a local excitation. In broadband noise calculations it is often argued that the spanwise correlation lengthscale of the incident fluctuations is small and so each spanwise strip of the blade can be considered uncorrelated (Amiet (1976)). However this argument only applies to the flow exciting the blade and does not consider the blade response which may effectively spread the influence of a local gust across the blade span. In the following sections we will examine this approximation for trailing edge noise sources on a rotating blade.

5.2.2 The Blade Surface Pressure

The theory for trailing edge noise from an isolated blade is given by Amiet (1976) who shows that the acoustic radiation depends on both the turbulent boundary layer pressure fluctuations and the blade response function. In fan noise applications the blade response function also depends on the acoustic scattering by adjacent blades. This problem was studied for a linear cascade model by Glegg (1996) and significant blade to blade interactions were identified. In this section we will review the results of Glegg (1996) so that they may be used for the evaluation of equation (5.9).

It will be assumed that the pressure fluctuations generated by the blade boundary layer far upstream of the trailing edge of the n^{th} blade can be represented by

$$P_n(y,x,\tau) = \int_{-\infty}^{\infty}\int_{-\infty}^{\infty} P_n(\omega_j,\nu)e^{i\nu y - i\omega\tau + i\gamma_o x}\,d\nu\,d\omega_j \tag{5.11}$$

(note this formulation differs from that given by Amiet (1976) in as much that the response is allowed to be a function of span). The blade loading on a rotor blade will depend on both the boundary layer fluctuations on the excited blade as well as those on the adjacent blades and so in the presence of the trailing edge the loading can be written in the form

$$F_n(y,x,\omega_j) = \sum_{k=1}^{B}\int_{-\infty}^{\infty} g_{n-k}(x,\nu,\omega_j)P_k(\omega_j,\nu)e^{i\nu y}\,d\nu \tag{5.12}$$

where x is in the direction of the flow and y is along the span. The function g_{n-k} is the blade response function of the n^{th} blade to a boundary layer on the k^{th} blade. The cross spectrum of the surface pressure required in (5.9) will therefore depend on $Ex[P_n(\omega_j,\nu)P_m^*(\omega_j,\nu')]$ which can be evaluated for a homogeneous turbulent boundary layer which is uncorrelated from blade to blade, but has the same average properties, as

$$\frac{\pi}{T}Ex[P_n(\omega_j,\nu)P_m^*(\omega_j,\nu')] = \frac{\ell S_{PP}(\omega_j)}{\pi}\delta(\nu-\nu')\delta_{mn} \tag{5.13}$$

where $S_{PP}(\omega_j)$ is the spectrum of the surface pressure fluctuations at a point. The parameter l is the spanwise lengthscale as defined by Amiet (1976), which is a function of the spanwise wavenumber. It is often argued that the dependence of l on the spanwise wavenumber can be ignored because it is only important when $\nu\delta > 1$, where δ is a lengthscale which is of the order of the boundary layer thickness, but we will not make this approximation until a later stage. We then obtain the cross spectrum of the blade loadings as

(5.14)

$$S_{FF}^{(n,m)}(y,y',\omega_j)=\frac{S_{PP}(\omega_j)}{\pi}\sum_{k=1}^{B}\int_{-\infty}^{\infty}\ell g_{n-k}(x,v,\omega_j)g_{m-k}{}^{*}(x',v,\omega_j)e^{iv(y-y')}dv$$

The result given by (5.14) provides the cross spectrum of the loadings for a linear cascade which has uniform spanwise properties. By using strip theory we can use this result as an input to equation (5.9) to obtain the amplitude of the duct modes in terms of the surface pressure spectrum S_{PP}.

5.2.3 The Duct Mode Amplitudes obtained from Strip Theory

The mode amplitudes defined by (5.9) can only be evaluated if the cross spectrum of the loadings are known and, as stated above we will estimate these from the cross spectrum of the loadings on a linear cascade of semi-infinite flat plates with uniform flow at all spanwise locations. This is at best a high frequency approximation since the properties of the boundary layer on the rotating blade will vary significantly across the span and we must therefore use broadband strip theory to relate the linear cascade blade response to the rotating blade response. The assumption required is that $S_{FF}^{(n,m)}$ will tend to zero when the spanwise displacement r-r' is greater than some distance L over which the flow conditions may be assumed constant. The blade response extends the influence of any locally excited region over a blade surface area which scales with the acoustic wavelength. Consequently strip theory only applies when $kL>>1$. On this basis we can carry out a local expansion of the Bessel function terms in (5.9) which retains the phase variation of the Green's function across the span but relates all amplitude variations which depend on r' to their value at r. The expansion takes the form

(5.15)

$$\zeta_{js}^{\pm}(r')U_j(\alpha_{js}r')\approx\frac{\zeta_{js}^{\pm}(r)}{2}X_{js}H_j^{(1)}(\alpha_{js}r)e^{iv_1(r-r')}+\frac{\zeta_{js}^{\pm}(r)}{2}Y_{js}H_j^{(2)}(\alpha_{js}r)e^{-iv_1(r-r')}$$

where

$$U_j(\alpha_{js}r)=\frac{1}{2}X_{js}H_j^{(1)}(\alpha_{js}r)+\frac{1}{2}Y_{js}H_j^{(2)}(\alpha_{js}r)$$

This allows an approximation of the integrand of equation (5.9) in the vicinity of r so that it may be written (assuming uncambered blades aligned with the flow)

(5.16)

$$\frac{\pi}{T}Ex\left[\left|A_{js}(\omega)\right|^2\right]=\left(\frac{1}{2\beta_{js}\Gamma_{js}}\right)^2$$
$$\int_h^a\int_{r-L}^{r+L}\left[\zeta_{js}^{\pm}(r)\right]^2\frac{U_j(\alpha_{js}r)}{2}\left\{X_{js}H_j^{(1)}(\alpha_{js}r)e^{iv_1(r'-r)}+Y_{js}H_j^{(2)}(\alpha_{js}r)e^{-iv_1(r'-r)}\right\}$$
$$\sum_{n=1}^{B}\sum_{m=1}^{B}\int_0^c\int_0^c S_{FF}^{(n,m)}(\mathrm{y},\mathrm{y}',\omega_j)e^{ik_{js}^{\pm}(\xi-\xi')+2\pi ij(n-m)/B}drdr'\,d\xi d\xi'$$

In approximating equation (5.9) using (5.16) we have introduced an important simplification of the broadband noise problem from rotating blades because it allows us to substitute from for S_{FF} from (5.14) directly using the local flow conditions at the spanwise station r. Evaluating the integrals using (5.14) with $y\text{-}y'=r\text{-}r'$ and $x=\xi\text{-}c$ in the strip theory limit $kL>>1$ gives

(5.17)

$$\frac{\pi}{T}Ex\left[\left|A_{js}(\omega)\right|^2\right]=\left(\frac{1}{2\beta_{js}\Gamma_{js}}\right)^2 B\int_h^a\left[\zeta_{js}^{\pm}(r)U_j(\alpha_{js}r)\right]^2 2\ell S_{PP}(\omega_j,r)\left|\Psi(\omega_j,v_1,k_{js}^{\pm})\right|^2 dr$$

where

$$\Psi(\omega_j,v_1,k_{js}^{\pm})=\sum_{n=1}^{B}\int_0^c g_n(\xi-c,v_1,\omega_j)e^{ik_{js}^{\pm}\xi+2\pi ijn/B}d\xi$$

Note that we have used the property $g_{-n}=g_{B-n}$ and given S_{PP} a dependence on r to indicate that it is a function of spanwise location. Also we have taken g_n to be an even function of the spanwise wavenumber which is to be expected in the uniform flow approximation. This result shows how the duct mode amplitudes are dependent on the surface pressure spectrum S_{PP} , the blade response function Ψ and the spanwise lengthscale l. The blade response function can be defined analytically but the surface pressure and the spanwise lengthscale are features of the flow which are hard to predict or determine from computations of the flow. Typically we are interested in blades which are operating close to stall and so the flow is very unstable and non-linear interactions are important. At this time we are limited to estimating the surface pressure from experiments on isolated

blades and interpolating the results to the conditions of interest. This approach will be described in section 5.2.6.

5.2.4 The Phase Approximation

To obtain the result given by (5.17) it was necessary to make use of the local expansion (5.15) and in this section we will evaluate the value of the phase function v_1 . First consider a Taylor series expansion of the Hankel function in (5.15). This may be written in the form

(5.18)

$$H_j^{(1)}(\alpha r') = \exp\left[\ln(H_j^{(1)}(\alpha r) + (r'-r)\frac{\partial}{\partial r}\left(\ln(H_j^{(1)}(\alpha r)\right)\right]$$

so that we can define the phase function as

(5.19)

$$v_1 = -i\frac{\partial}{\partial r}\left(\ln(H_j^{(1)}(\alpha r)\right) = \frac{-i\alpha H_j'^{(1)}(\alpha r)}{H_j^{(1)}(\alpha r)}$$

For large values of the argument we can approximate the Hankel function as

(5.20)

$$H_j^{(1)}(\alpha r) = \sqrt{\frac{2}{\pi\alpha r}}e^{i(\alpha r+\frac{4j^2-1}{8\alpha r}-j\pi/2-\pi/4)}$$

so that

(5.21)

$$v_1 = \alpha\ -\frac{4j^2-1}{8\alpha r^2}+\frac{i}{2r}$$

We see therefore that the real part of the phase function depends on the radius, and although this dependence is weak well above cut-off, there is an implicit radial dependence.

One of the problems with using a flat plate blade response function to represent a blade rotating in a cylindrical duct is the matching of the blade response functions at frequencies where the duct modes cut on. At the cut-on frequency $\beta_{js}=0$ and so considering (5.8) and (5.9) we see that the sound power of each mode is singular at cut-on. However for a rectilinear cascade it can be shown (Goldstein (1976)) that the blade response function tends to zero at the cut on frequency and so the sound power remains finite. It is therefore important that, when modeling the response of the rotating blade by an equivalent rectilinear blade over a finite strip (however small), that the behavior at cut on is correct. This is especially significant for broadband noise calculations because at high frequencies the modal density in any bandwidth of practical interest is high, and so there will be several modes which cut on within any band. The singular behavior of the expressions for the sound power and the mode amplitudes can cause large errors unless it is accounted for correctly.

To address this problem consider the dispersion relationship for acoustic waves in cylindrical co-ordinates. For a wave field in a duct with uniform flow in the axial direction the acoustic pressure is given by $p=AU_j(\alpha_{js}r)exp(-i\omega t+ij\phi+i\gamma z)$. The dispersion relationship which determines γ is given by

(5.22)

$$\gamma^2+\alpha_{js}^2=(\omega-\gamma U)^2/c_o^2$$

In contrast the acoustic field in rectilinear co-ordinates with a uniform flow in the z direction is defined as $p=Aexp(-i\omega t+i\nu y+i\beta x+i\gamma z)$ and satisfies the dispersion relationship

(5.23)

$$\gamma^2+\beta^2+\nu^2=(\omega-\gamma U)^2/c_o^2$$

If the x axis is aligned with the azimuthal direction so that $x=\phi r$, the periodicity of the wavefield requires that $\beta=j/r$. Consequently the dispersion relationships will be identical if

(5.24)

$$\nu^2 = \alpha_{js}^2 - \frac{j^2}{r^2}$$

To first order we can expand this relationship to give

(5.25)

$$\nu = \alpha_{js} - \frac{j^2}{2\alpha_{js} r^2}$$

which is a good approximation to the Taylor series expansion given by equation (5.21).

In conclusion, when aligning the wavenumbers in rectilinear co-ordinates with the wavenumbers in cylindrical co-ordinates it is important that the dispersion relationships are preserved so that the cut on frequencies for each mode are the same in both cases. For this reason we must chose the spanwise wavenumber given by (5.24) in the rectilinear expansion and this gives a good approximation for the local expansion of the Bessel functions.

5.2.5 The Blade Response Function

The blade response function for pressure fields convected past the trailing edges of a linear cascade of blades was investigated by Glegg (1996) where it was shown that, for an incident pressure field of the type given by (5.11),

(5.26)

$$g_n(x,\nu,\omega_j) = \int_{-\infty}^{\infty} e^{-i\gamma(x-nd)} \sum_{p=-\infty}^{\infty} A_p(\gamma,\nu) e^{-2\pi i p n / B} d\gamma$$

where the function A_p is defined by equation (5.23) of Glegg (1996) (with $Qexp(i\xi_o/y_o/)=1/2$ to account for pressure doubling on the surface) and the trailing edge of each blade lies at $x=nd$. It then follows that the function required in (5.17) is given by

(5.27)

$$\Psi(\omega_j,\nu,\gamma) = 2\pi B e^{i\gamma c} \sum_{p=-\infty}^{\infty} A_{j-pB}(\gamma,\nu)$$

and by combining equation (5.23),(5.26) and (5.28) of Glegg (1996) we find that

(5.28)

$$\Psi(\omega_j, v, \gamma) = \frac{i\zeta_c e^{i\gamma x}}{4\pi i(\gamma + \gamma_c) J_+^{(j)}(-\gamma_c) J_-^{(j)}(\gamma)}$$

where $\zeta_c=(1-M_e^2)^{1/2}(\kappa_e^2-(\gamma_c+\kappa M_e)^2)^{1/2}$, $\kappa_e^2=\kappa^2-v^2/(1-M_e^2)$, M_e is the flow Mach number relative to the blade, $\kappa=\omega/c_o(1-M_e^2)$, $\gamma_c=\omega/U_c$, U_c is the gust convection velocity and the functions $J_\pm$ are defined in Glegg (1996). This result is only valid for calculating the sound field in the region downstream of the blade trailing edges because the model used is for a cascade of blades with semi-infinite chord. For the sound which propagates in the upstream direction the sound field is trapped in the blade passages and then radiates from the inflow plane of the fan. A complete theory for the propagation of waves through the blade passages, their reflection and subsequent radiation is not yet available but current indications are that there is very little energy reflected back downstream from the fan leading edge.

To interpret the results it is shown in Glegg (1996) that a reasonable approximation is given for (5.17) in the form

(5.29)

$$\Psi(\omega_j, v, \gamma) = \frac{(1-e^{2i\zeta h_o})e^{i\gamma x}}{i(\gamma+\gamma_c)} \sqrt{\frac{\kappa_e+\gamma_c+\kappa M_e}{\kappa_e-\gamma+\kappa M_e}}$$

where $\zeta=(1-M_e^2)^{1/2}(\kappa_e^2-(\gamma-\kappa M_e)^2)^{1/2}$ and h_o is the blade spacing normal to the direction of the flow. Two features are important about this result: first we the term $(1-\exp(2i\zeta h_o))$ represents the reflection of waves by adjacent blades and is typical of an interference effect. The response function therefore has zeroes at frequencies where $\zeta h_o=\pi$ and these will be apparent in the computation of the sound power spectra to be discussed in section 5.3. Secondly the function given in (5.29) reduces to the blade response function for an isolated blade in the limit that h_o tends to infinity since ζ has a small positive imaginary part so $(1-\exp(2i\zeta h_o))\sim 1$.

5.2.6 The Surface Pressure Spectrum

To evaluate the spectrum of the blade boundary layer pressure fluctuations we will consider measurements of the acoustic field from an isolated blade. It is shown in Amiet (1976) that the far field pressure spectrum from an isolated blade in a uniform flow is given in terms of the cross spectrum of the blade pressure fluctuations. To evaluate (5.17) we need to specify $2lS_{pp}$ and this can be determined from the measurement of the pressure spectrum in the acoustic far field as

(5.30)

$$2\ell S_{PP}(\omega_j) = \frac{S_{pp}(\mathbf{x}_0, \omega_j)}{\left(\frac{\omega_j z_o}{4\pi c_o r_e^2}\right)^2 b\left|\Psi_I(\omega_j, 0, \kappa M_e)\right|^2}$$

where Ψ_I is the blade response function of an isolated blade and we have specified the observer to be located at $x_o=y_o=0$. It is therefore relatively simple to obtain the pressure spectrum required for (5.17) from measurements of the acoustic field from an isolated blade. The accuracy of this estimate is determined by the knowledge of the blade response function, but this is specified theoretically, and the primary assumption is that scattering by the leading edge of the blade is ignored.

5.2.7 Numerical Implementation

The theory described above has been implemented by carrying out five separate tasks based on the input parameters of a particular fan design. Each step is described below:

(1) The self noise source spectra are calculated using the blade self noise prediction code provided by Brooks et al (1989). This calculation is carried out for each blade station and gives spectral levels between 200 Hz and 40,000 Hz in blade based co-ordinates.

(2) The duct mode eigen values and eigenfunctions are calculated for each frequency at each radial station with sufficient resolution for the radial integration required in equation (5.17).

(3) The blade response function and source level are calculated for all cut on modes at ~10 radial stations across the blade span.

(4) The radial integration is carried out numerically. The mode functions are highly oscillatory and so a small step size is required in the integration to define these

correctly. Accurate results are obtained by using at least 30 steps across the span for the lower order modes and by increasing this to $(a-h)/(5s_{max})$ for large radial mode orders where s_{max} is the largest value of s for all propagating modes at a given frequency. However relatively few source points are defined in (5.3) but they tend to vary smoothly so linear interpolation can be used to specify these functions at the small increments required for the mode functions.

(5) The sound power is evaluated for each frequency and each mode using equation (5.17).

Numerical checks have been carried out on the radial integration by comparing the results with known theoretical solutions. Further checks on the number of radial stations required in (5.3) above have shown that 10 radial stations gives a converged solution. The codes for the blade response function have been checked using the two alternate methods of calculation.

5.3. Results and Discussion

5.3.1 Numerical Examples

In this section we will illustrate the application of the self noise model described above to a ducted fan. We will limit consideration to a fan in a duct of radius 0.2286m with 20 blades and a hub to tip ratio of 0.44. The results will be presented in terms of the spectrum level of the sound power obtained from equation (5.8) and corrected for the bandwidth used in the frequency analysis by multiplying by $2\Delta\omega$ with $\Delta\omega=2\pi$ rad/sec. Unless otherwise stated the tip Mach number will be 0.7, the tip inflow angle $\beta=\tan^{-1}(U/\Omega a)=23^\circ$ and the blade chord 0.081m. Two different distributions of blade angle of attack will be considered: a constant angle of attack of 7° at all spanwise locations and a varying angle of attack in which there is a linear reduction of blade angle from 8° at the hub to 4° at the tip.

5.3.2 Self Noise Source Levels

The self noise source levels are obtained from the non-dimensionalised measured spectra given by Brooks et al (1989), for a series of NACA 0012 airfoils with different chords and at different angle of attack. The measured spectra scale with the fifth power of the inflow velocity and significant increases in the low frequency part of the spectrum were observed at high angles of attack when flow separation and/or stall occurred. Flow separation was significantly altered by the use of boundary layer trips indicating that there may be significant scale effects present.

This study is concerned with high solidity fans in which the local flow in a blade passage may vary significantly from a flow with the same Reynolds number over an isolated blade. In particular the influence of adjacent blades on flow separation and boundary layer development may be significant. Furthermore the airfoils used in Brook's study were uncambered whereas ducted fan blades usually include a significant amount of camber. The relationship between the angle of attack of an isolated blade and the equivalent angle of attack of the blades in a high solidity fan is yet to be determined and will require an extensive experimental study. However results to date suggest that the blade incidence angles are equivalent between these two cases, but further work needs to be done to confirm this preliminary conclusion.

Figure 5.2 shows the isolated blade self noise spectra for each radial station of the constant angle of attack case (Case A) described above. Note how the highest levels occur near the blade tip where the blade relative velocity is highest, and how the spectral peak occurs at ~ 9000 Hz. At inboard stations the peak moves to lower frequencies and the levels are reduced as the fifth power of the blade relative velocity.

For the case when the blade angle of attack varies across the span (Case B, Figure 5.3) a different characteristic is observed. The increase in angle of attack on the inboard stations of the blade causes the level of the spectral peak to remain constant in spite of the reduction in blade relative velocity. This characteristic is caused by the flow over the blade approaching separation and will be affected by the details of the fan design. In general we can conclude that separated flow will result in significant increases in low frequency self noise from the fan.

5.3.3 In Duct Sound Power

To demonstrate the effect of the two different variations of blade angle of attack on the radiated power levels figure 5.4 shows the downstream sound power for the blade

source levels given in figures 5.2 and 5.3. Note how the constant angle of attack case has higher levels, especially at high frequencies. The high frequency characteristic is explained by the higher angle of attack close to the blade tip for case A. In contrast the high angle of attack close to the hub causes blade stall for case B and this results in higher low frequency levels, as expected from Figure 5.3.

An interesting feature is the noticeable dips in the spectra at ~8kHz. This is caused by the interference effect discussed in section 5.2.5, and is a direct consequence of the cascade blade response function having a null in this frequency band.

The scaling with Mach number is shown in Figure 5.5 for case A giving results for blade tip Mach numbers of 0.5,0.6,0.7,0.8 and 0.9. To obtain these curves the fan speed was varied while maintaining the same inflow angle and angles of attack. An increase in the spectral level is observed with greater increases at higher frequencies. To determine the scaling of self noise with Mach number figure 5.6 shows the total sound power as a function of blade tip Mach number obtained by integrating the spectra. For Mach numbers less than 0.5 the scaling is proportional to the fifth power of the Mach number as expected from the source levels. At higher Mach numbers a greater sensitivity is observed and the scaling is closer to the sixth power of the Mach number or greater. Note that at Mach numbers greater than 0.7 the complete spectra could not be calculated and so the levels are obtained by integrating the available data shown in figures 5.5.

The scaling with angle of attack is shown in Figure 5.7 for case A with nominal angle of attack changes of -2°,-1°,0°,+1°,+2° relative to the base level. Note here how the spectral shape changes significantly at low frequencies when blade stall occurs. In Figure 5.8 the total sound power between 1kHz and 20kHz is shown as a function of angle of attack for both cases A and B and it is seen that this increases as ~2.4 dB per degree for case B which has a twisted blade for which only the hub stalls in this range of parameters. Case A which has a constant angle of attack across the span shows more sensitivity because both the tip and the hub region stall at incidence angles greater than 7°.

5.3.4 Modal Power Distribution

One of the interesting features of the approach given here is that the distribution of sound power in each mode as a function of frequency can be displayed as shown in Figure 5.9 for the constant angle of attack case (Case A). In this plot the sound power is presented for all the azimuthal modes (x-axis), against frequency (y-axis), and the contour height (z-axis) represents the sound power which is the sum of the levels in the radial modes. The plot shows a clear tendency for there to be more sound power in the

positive (co-rotating) modes at high frequencies, and at low frequencies there is more sound power in the negative (counter-rotating) modes. Figure 5.9 also highlights valleys in the modal power distribution which are caused by the blade to blade interference effects discussed in section 5.2.5.

To further investigate why the modal power is concentrated in the co-rotating modes we note that the frequency dependent factors which affect the mode strength given by equation (5.17) are the wavenumbers β_{js} and $k_{js}^{\pm}$ the source spectrum $2lS_{PP}$ and the blade response function Ψ. The source spectrum and the blade response function are both functions of $\omega_j=\omega-j\Omega$. which represents the blade based frequency and accounts for the Doppler shift of the moving blades by coupling different source frequencies into different duct modes. The interference effects due to blade to blade interactions which cause the valleys in Figure 5.9 make it hard to separate out the source spectrum scaling for each mode and so calculations were carried out using a blade response function which eliminated adjacent blade interference. This was achieved by letting h_o tend to infinity in equation (5.29). The sound power spectra for the modes $j=0,10$ and 20 are shown in figure 5.10(a). The spectral peak occurs at higher frequencies for the higher order modes, but when plotted against the blade based frequency (figure 5.10(b)) all the spectral peaks line up showing that the sound power is primarily a function of the blade based frequency. The match is not perfect at the lower frequencies because of the influence of the blade response function close to cut on, and this is even more pronounced for negative mode orders, for which the spectral peak of the zero order mode is "cut off" but the high frequency parts of the spectra line up as a function of the blade based frequency.

5.4. Conclusions

A theoretical prediction method for the broadband self noise from ducted fans has been developed. The source mechanism is assumed to be the interaction of the turbulent boundary layer with the trailing edges of the blades and the source levels are obtained from the measurements of self noise from isolated blades by Brooks, Pope and Marcolini (1989).

It was shown that strip theory must be used to apply these results to a rotating blade, and this is only a valid approximation in the high frequency limit where the acoustic wavelength is much smaller than the duct radius. A method was introduced for coupling the modes in a circular duct to the modes of a linear cascade. This is achieved

by matching the dispersion relationship of the acoustic field in each case, and if this is not done correctly then the incorrect behavior of the blade response function is obtained close to cut off. This is important due to the singular nature of the expression for the sound power at the cut off frequency.

It has been found (Glegg (1996)) that for a high solidity ducted fan the blade surface pressures are not uncorrelated on each blade and corrections must be included for the scattering from the trailing edges of adjacent blades. This is achieved by using a blade response function which assumes blades of semi infinite chord arranged as a linear cascade, and this function has the correct behavior to properly calculate the modes close to cut off which is not the case for approximate methods which do not include the effect of the spanwise wavenumber. However a correction needs to be added to account for the propagation of trailing edge noise through the blade passages and into the duct upstream of the fan.

Numerical results show that the in duct sound power scales with the fifth power of the fan speed at low Mach numbers, but this changes to the sixth power or greater at high Mach numbers. The angle of attack of the blade increases the self noise as 2.4 dB per degree and significant increases in low frequency self noise occur if blade stall occurs. For blades with a linear variation of angle of attack stall effects occur primarily in the hub region and this does not give as large increases as stall effects which occur in the tip region of the fan. Scale effects have also been considered and are found to be dependent on Reynolds number. It is also shown that the sound power is concentrated in the co-rotating modes because of the Doppler shift introduced by the fan.

The advantage of the approach given here is that it based on an experimental data base and so includes the effects of nonlinear source mechanisms and viscosity in high Reynolds number flows. Given the limitation that the flow is modeled as being the same as that of an isolated blade, the method makes a first order attempt to account for the self noise from blades at high angles of attack where separated flow and blade stall takes place over different sections of the blade. Clearly more work is required, both experimentally and numerically, to evaluate the turbulent boundary layer close to the trailing edge of fan blades which, in contrast to the blades used here, may be highly cambered and influenced by the presence of adjacent blades. However the method described here should give a first order estimate of the trailing edge noise from a ducted fan.

6. Predictions of the Boeing Broadband Fan Noise Data Set

6.1 Introduction

This section will consider the application of the theoretical results presented in this report by carrying out detailed comparisons with the measurements on the Boeing fan rig described in section 2.

6.2 Rotor Alone Self Noise

The self noise prediction method described in section 5 gives an absolute method for predicting self noise levels from a fan. The method only gives the downstream sound power because the propagation of the trailing edge noise through the blade passages is not included. Consequently we will only consider measurements in the downstream direction. As was stated in section 2, the rotor self noise will be the base level of Broadband fan noise and is most likely to be the dominant source when there are no stators, the upstream duct wall boundary layer is removed, and the tip gap is a minimum. The flow conditions and input parameters for these operating conditions are presented in Table 6.1. Of particular importance here is the detail given for the angle of attack across the span of the blade. The predicted noise spectra for the four cases considered is shown in figure 6.1, and encouraging agreement is obtained. Note that at the lower speed the level for the high loading case is 6dB higher than for the low loading case, and the prediction method accurately follows this trend. At the higher fan speed with high loading the self noise is over predicted at high frequencies, and it is not immediately clear why this is the case. The prediction methodology is based on isolated blade measurements at low Mach number, and the high speed/high loading case represents the greatest departure from these conditions. The tip Mach number in this case is 0.87 and it is unlikely that the input data is valid at this speed since shock cells are almost certainly present on the blade surfaces.

The predicted self noise spectra show a clearly identifiable dip at ~8kHz which can be attributed to blade to blade acoustic interference. This effect is not apparent in the measurements, and the prediction methodology may be over emphasizing this effect. The theory does not allow for acoustic reflection of the noise generated at the blade trailing edges by the leading edges of the blades and this may reduce the apparent null in the spectra which can be seen in figure 6.1.

Finally it should be noted that predictions of stator self noise showed that the stator self noise levels were not significant.

6.3 Rotor Alone Inflow Noise

When there is a duct wall boundary layer the rotor alone noise is increased, and the inflow noise prediction method described in section 4 should predict this change. A true comparison is only valid however if the predicted boundary layer (BL) noise is added to the rotor alone levels without the boundary layer present. Figures 6.2 through 6.5 show the predicted spectra in the upstream and downstream directions for the four different subsonic operating conditions. The overall predicted level is the sum of the measured data without the BL present and the predicted level. In general excellent agreement is obtained, however there is a trend to over predict at low frequencies in the upstream direction.

The rotor causes significant flow turning and so to partially account for this the downstream sound power has been evaluated assuming the blades are aligned with the flow in the downstream region, while the predictions in the upstream direction are based on the flow conditions upstream of the fan. At the very least this ensures that the acoustic modes downstream and upstream of the fan have the nominally correct cut on frequencies.

To obtain these predictions the boundary layer thickness and the turbulence length scale and intensity have to be specified. The boundary layer thickness was estimated from performance calculations (see figure 6.6) the turbulence intensity was obtained from hot wire measurements (see figure 6.7). However estimating the turbulence lengthscale was more difficult. To obtain a reasonable value, the turbulence spectra at 6mm(0.25") from the wall were considered (see figure 6.8). Note that the 10 dB down point for the streamwise component occurs at 6.5 kHz, while for the transverse component it occurs at 30 kHz. The spectral shape of the Von Karman spectrum for a gust in the direction of the flow is given by $(1+(\omega/k_e U)^2)^{-5/6}$ and for a transverse gust is given by $(3+8(\omega/k_e U)^2)/(1+(\omega/k_e U)^2)^{-11/6}$. By identifying the frequency where spectrum is 10dB below the level at zero frequency, we can estimate the lengthscales L_u for the streamwise gust, and L_v for the transverse gust, as

(6.1)

$$L_u = \frac{14.2U}{8\pi f_u} \qquad\qquad L_v = \frac{21U}{8\pi f_v}$$

where f_u and f_v are the frequencies of the 10dB down points respectively. Using these formulae, the lengthscales can be estimated for each component as 6.2 mm and 2.6mm (and similarly for the higher speed case). Using the smaller of these two lengthscales gives the best fit to the data, but the reason for this is not entirely clear. A possible explanation is that the lower frequency part of the streamwise turbulence spectra are dominated by coherent structures which do not fit the Von Karman model.

6.4 Rotor/Stator interaction Noise

To predict stator noise two different types of inflow turbulence must be considered. First there is the wall flow which is dominated by the wall boundary layer and the influence of the tip leakage vortex. Secondly there is the wake flow, which is of lower level, but of greater spanwise extent. To estimate the contributions from the wall flow, the BL thickness and intensity must be estimated. The lengthscales are obtained from the turbulence spectra and equation (6.1). Similarly for the wake flow, only in this case only the average turbulence intensity and lengthscale is required.

For this study the turbulent spectra in the wake were only available for the large tip gap, low loading case at the 55% operating condition (see figure 6.9). Calculations were therefore carried out for this case, and extended to the 70% operating condition for the same tip gap. Using the spectra shown in figure 6.9, the lengthscales in the outer wall region and wake region were estimated as 7.6mm and 3.4 mm respectively for the low loading case. For the high loading case the outer wall turbulence lengthscale was increased in proportion to the BL thickness. The boundary layer thickness and all the turbulence intensities were taken from figure 2.10. All the parameters used in the calculations are given in Table 6.3. Note that for the 70% operating condition the same values for the turbulence intensities and lengthscales were used as for the lower speed.

The results are presented in figures 6.10 through 6.13, and give the measured rotor alone noise, the predicted wall boundary layer noise, the predicted wake noise, the sum of these three components, and the measured stator noise. By adding the rotor alone noise to the predictions for the other sources proper account is taken of the rotor self noise, and the predictions provide the incremental increase due to the presence of the stators. In general the predictions are good, with a tendency to over predict in the low frequency, upstream direction, as was found for the rotor alone cases. The trends in the data with both speed and loading are accurately followed by the prediction methodology. Furthermore it appears that in all cases the wake flow is a greater contributor than the outer wall flow in all cases. This conclusion is consistent with the results presented in figure 2.11, with the exception of the high speed high loading case. However since no measurements of the stator inflow were made for this condition, and the prediction is based on estimated parameters, no conclusions can be drawn about this particular case.

6.5 Conclusion

In this section the prediction methodology has been compared with the broadband noise measurements obtained from the Boeing fan rig. Predictions of rotor self noise were compared with rotor alone data obtained with a clean inflow. The results showed the

compared with rotor alone data obtained with a clean inflow. The results showed the correct trends with loading, but tended to over predict at high fan speeds, where the blade tip speed is in the transonic range and the input data is most likely inapplicable. The increase of the rotor alone noise caused by the presence of a turbulent duct wall boundary was then evaluated using measured values to define the turbulence parameters. Again the results showed the correct trends with increases of speed and loading, however, the best predictions were obtained if only the smallest observed lengthscales were used in the prediction method. Finally the predicted levels of stator noise were considered, using measured values for the turbulence parameters. The measured levels were predicted well and the trends with flow speed and loading were identified. At the low speed condition, wake turbulence was evaluated as more important than wall turbulence, which is consistent with the results in section 2.

7. Conclusions

This report describes the development of prediction methods for broadband fan noise from aircraft engines. First experimental evidence of the most important source mechanisms is reviewed. Then theoretical models are developed for each source mechanism. Finally the theories are used to predict measured levels with some success.

The experimental evidence presented in this report are the results of a test carried out on the Boeing 17" model fan rig. The results give a break down of the different source mechanisms of broadband fan noise. It was found that there is no clearly dominant source mechanism to which noise reduction approaches can be applied, but rather a number of competing mechanisms exist which are more or less important depending on the particular fan design and flow conditions. It was shown that noise levels always increased when stator vanes were present downstream of the rotor. In general, fans should be designed to minimize turbulent flow incident on the stators and the outer wall flows can be a contributor in this regard. The wake turbulence is of lower level but of greater extent and so, in some cases, may be the dominant source of high frequency turbulent flow. However the rotor noise is not very far below the stator noise and good predicted levels cannot be obtained unless the rotor alone noise levels are known.

The primary difficulty in developing theoretical models for broadband fan noise is that the scale of the airfoil is large compared with the gust wavelength, and so numerical approaches have difficulty in modeling the flow, especially around the blade leading and trailing edges. Typically, predictions are required at non-dimensional frequencies, $\omega c/U_\infty$, of up to 70, and it unusual to find numerical calculations for non-dimensional frequencies in excess of 25. This makes the high frequency broadband noise problem particularly challenging and suggests that a complete solution will not be found using existing approaches. For this reason semi analytical approaches were used here to model the interaction of the turbulent flow with the fan blades and stator vanes, and measured data were used to define the properties of the turbulence. At the present time this appears the only realistic alternative, but in the future as computational methods improve, a fully non-linear viscous calculation of the stochastic compressible/turbulent flow in the fan duct and around the stator vanes, would be an enormous improvement on the approach taken here.

In section 3 the existing methods for the prediction of broadband fan noise from inflow turbulence were reviewed and a procedure was developed for fan noise prediction based on a linear cascade model. The model uses a rectilinear approximation for a fan or stator in a cylindrical duct, but it's advantage over other methods is that it includes all

spanwise coupling effects. The standard output of this method is the upstream and downstream sound power, but modal amplitude and power calculations are also possible with minor modifications. Numerical examples were given and it was shown that the spectral shape of the radiated sound power is primarily controlled by the turbulence lengthscale, which is the typically the most difficult turbulence parameter to measure.

A theoretical prediction method for the broadband self noise from ducted fans was also developed. The source mechanism is assumed to be the interaction of the turbulent boundary layer with the trailing edges of the blades and the source levels are obtained from the measurements of self noise from isolated blades by Brooks, Pope and Marcolini (1989). It was shown that strip theory must be used to apply these results to a rotating blade, and this is only a valid approximation in the high frequency limit where the acoustic wavelength is much smaller than the duct radius. A method was introduced for coupling the modes in a circular duct to the modes of a linear cascade. This is achieved by matching the dispersion relationship of the acoustic field in each case, and if this is not done correctly then the incorrect behavior of the blade response function is obtained close to cut off. This is important due to the singular nature of the expression for the sound power at the cut off frequency. For a high solidity ducted fan the blade surface pressures are not uncorrelated on each blade and corrections must be included for the scattering from the trailing edges of adjacent blades. This is achieved by using a blade response function which assumes blades of semi infinite chord arranged as a linear cascade, and this function has the correct behavior to properly calculate the modes close to cut off which is not the case for approximate methods which do not include the effect of the spanwise wavenumber. However a correction needs to be added to account for the propagation of trailing edge noise through the blade passages and into the duct upstream of the fan. Numerical results show that the in duct sound power scales with the fifth power of the fan speed at low Mach numbers, but this changes to the sixth power or greater at high Mach numbers. The angle of attack of the blade increases the self noise as 2.4 dB per degree and significant increases in low frequency self noise occur if blade stall occurs. For blades with a linear variation of angle of attack stall effects occur primarily in the hub region and this does not give as large increases as stall effects which occur in the tip region of the fan. Scale effects have also been considered and are found to be dependent on Reynolds number. It is also shown that the sound power is concentrated in the co-rotating modes because of the Doppler shift introduced by the fan.

Finally the prediction methodology was compared with the broadband noise measurements obtained from the Boeing fan rig. Predictions of rotor self noise were compared with rotor alone data obtained with a clean inflow. The results showed the

correct trends with loading, but tended to over predict at high fan speeds, where the blade tip speed is in the transonic range and the input data is most likely inapplicable. The increase of the rotor alone noise caused by the presence of a turbulent duct wall boundary was evaluated using measured values to define the turbulence parameters. Again the results showed the correct trends with increases of speed and loading, however, the best predictions were obtained if only the smallest observed lengthscales were used in the prediction method. Finally the predicted levels of stator noise was considered, using measured values for the turbulence parameters. The broadband fan noise levels were predicted well using this approach and the trends with flow speed and loading were identified. At the low speed condition, wake turbulence was evaluated as more important than wall turbulence, which is consistent with the results in section 2 for this fan design.

References

Amiet R. K., 1975, "Acoustic Radiation from an Airfoil in a Turbulent Stream" Journal of Sound and Vibration, 41(4), 407-420.

Amiet, R. K., 1976, "Noise Due to Turbulent Flow Past a Trailing Edge," Journal of Sound and Vibration, Vol. 47, pp. 387-393.

Amiet, R., 1977, "Noise produced by turbulent flow into a propeller or helicopter rotor", AIAA J. J. 15, 307-308.

Amiet, R. K., 1978, "Effect of the Incident Surface Pressure Field on Noise due to Turbulent Flow Past a Trailing Edge," Journal of Sound and Vibration, Vol. 57, pp. 305-306.

Atassi H. M., and Grzedzinski, 1989, "Unsteady Disturbances of Streaming Motions Around Bodies" J. Fluid Mech. 209, pp. 385-403.

Atassi H. M., 1993, "Unsteady Aerodynamics of Vortical Flows: Early and Recent Developments" Symposium on Aerodynamics and Aeroacoustics on the Occasion of the 80th Birthday of William R. Sears, Tucson, Arizona.

Atassi H. M., Fang, and Patrick, S., 1993, "Direct Calculation of Sound Radiated from Bodies in Nonuniform Flows" Jnl. of Fluids Engineering.115, pp. 573-579.

Atassi, H.M., 1994, "Unsteady Aerodynamics of Vortical Flows: Early and Recent Developments", in Aerodynamics and Aeroacoustics, Ed. by K-Y. Fung, World Scientific.

Atassi, H.M. and G. Hamad, October 1981, "Sound Generated in a Cascade by Three Dimensional Disturbances Convected in a Subsonic Flow", AIAA paper no. 81-2046, presented at the7th AIAA Aeroacoustics Conference.

Blake, W.K., 1986, "Mechanics of Flow Induced Sound and Vibration: Volume II", Academic Press.

Brooks T.M., and Marcolini M.A., 1983, "Airfoil Self Noise-The effect of Scale", AIAA paper 83-0785, presented at the 8th AIAA Aeroacoustics Conference.

Brooks, T.M. and Hodgson, T.H., 1981, "Trailing Edge Noise Prediction from Measured Surface Pressures," Journal of Sound and Vibration, Vol. 78(1), pp. 69-117.

Brooks, T.M., Pope D.S., and Macolini, M.A., 1989, "Airfoil Self Noise and Prediction," NASA RP 1218.

Chase, D. M., 1972, "Sound Radiated by Turbulent Flow Off a Rigid Half-Plane as Obtained From a Wavevector Spectrum of Hydrodynamic Pressure," Journal of the Acoustical Society of America, Vol. 52, pp. 1011-1023.

Devenport, W. 1997 "Results form the VT cascade rig", Limited access Web page

Dhanak M., Dowling A., and Si C., 1997, "Coherent Vortex model for surface pressure fluctuations induced by the wall region of a turbulent boundary layer", Physics of Fluids, Vol 9, No 9, September 1997, pp2716-2731

Envia, E. and E.J. Kerschen, July 1986, "Noise Generated by Convected Gusts Interacting with Swept Airfoil Cascades", AIAA paper no. 86-1872, presented at the 10th Aeroacoustics Conference, Seattle.

Ffowcs Williams, J. E. and Hawkings, D. H., 1969, "Sound Generated by Turbulence and Surfaces in Arbitrary Motion," Philosphical Transactions of the Royal Society, Vol.264A, pp321-342.

Ffowcs Williams, J. E. and Hall, L. H., 1970,"Aerodynamic Sound Generation by Turbulent Flow in the Vicinity of a Scattering Half Plane," Journal of Fluid Mechanics, Vol. 40, pp. 657-670.

Fleeter, S., 1973," Fluctuating Lift and Moment Coefficients for Cascaded Airfoils in a Non-Uniform Compressible Flow", AIAA Journal 10, pp93-98.

Farassat F., 1994 "Introduction to Generalized Functions with applications to Aerodynamics and Aeroacoustic" ,NASA TP 3428, 1994

Fukano, T. Takamatsu, Y., and Kodama Y., 1986, "The Effect of the Tip Clearance on the Noise of Low Pressure Axial and Mixed Flow Fans" Jnl. of Sound and Vibration Vol 105, pp. 291-308.

Ganz U., Joppa P., Patten T. and Reed D., 1995 "Preliminary Report 1995 Fan Broadband Noise Fan Rig Test", Preliminary Boeing Report, August 1995

Glegg S. A. L. and Devenport W.J., 1991, "The Application of Experimental Data to Blade Wake Interaction Noise Prediction" , Unsteady Aerodynamics, Aeroacoustics and Aeroelasticity of Turbomachines and Propellers, Ed H.M. Atassi, Springer Verlag.

Glegg S. A. L., 1993, "Broadband Noise from Ducted Prop Fans" AIAA 93-4402, 15th AIAA Aeroacoustics Conference, Long Beach, CA.

Glegg, S.A.L., May, 1996, "Airfoil Self Noise Generated in a Cascade" AIAA paper no 96-1739, presented at the 2nd AIAA/CEAS Aeroacoustics Conference.

Glegg, S.A.L., July, 1997, "The response of a swept blade row to a three dimensional gust" FAU report.

Gliebe, P.R., September, 1996, "Fan broadband noise -The Floor to High Bypass Engine Noise Reduction", Noise Con 96, Seattle Washington.

Goldstein M. E., 1976, "Aeroacoustics", McGraw-Hill Inc.

Goldstein M.E. 1978, "Unsteady Vortical and Entropic Distortions of Potential flows Around Arbitrary Obsticals" J. Fluid Mech. 89 pt 3, pp433-468.

Golubev V.V., and Atassi, H.M., 1996, "Sound Propagation in an Annular Duct with Mean Potential Swirling Flow" Jnl. of Sound and Vibration Vol 198, pp. 601-616.

Guidati, R. Bareiss, S.Wagner, T.Dassen, and R.Parchen, 1997, "Simulation and Measurement of Inflow Turbulence Noise on Airfoils", 3rd CEAS-AIAA Aeroacoustics Conference Proceedings, May 1997

Hall, K.C. and J.M. Verdon, 1991, "Gust Response Analysis for Cascades Operating in Non-Uniform Mean Flows", AIAA Jnl. 29(9), p 1463

Hanson D. B, 1973, "A Unified Analysis of Fan Stator Noise", Journal of the Acoustical Society of America, 54(6), pp 1571-1591.

Hanson D. B, 1997, "Quantifation of Inflow Turbulence for Prediction of Cascade Broadband Noise", Fifth International Congress on Sound and Vibration, Adelaide, Australia.

Hardin J.C and Lamkin S.L, 1984, "Aeroacoustic Interaction of a Distributed Vortex with a Lifting Joukowski Airfoil", AIAA Paper no 84-2287, Oct 1984

Homicz, G.F., and George, A.R., 1974, "Broadband and discrete frequency radiation from subsonic rotors" J. Sound Vib. 36, 151-177.

Howe, M. S., 1975, "Contributions to the theory of aerodynamic sound, with application to excess jet noise and the theory of the flute", J. Fluid Mech. Vol 71 (4), pp625-673

Howe, M. S., 1978, "A Review of the Theory of Trailing Edge Noise," Journal of Sound and Vibration, Vol. 61, pp. 437-465.

Howe, M.S. 1989, "On unsteady surface forces, and sound produced by the normal chopping of a rectilinear vortex", J. Fluid Mech. Vol 206, pp131-153,

Howe, M. S., 1990, "Correlation of Lift and Thickness Noise Sources due to a Vortex Airfoil Interaction," Journal of Sound and Vibration, Vol 137(1), p1.

Kaji, S. and Okazaki, 1970a, "Propagation of Sound Waves through a Blade Row II: Analysis based on the Acceleration Potential Method", Jnl. Sound and Vib. 11(3), pp355-375.

Kaji, S. and Okazaki, 1970b, " Generation of Sound by a Rotor Stator Interaction", Jnl. Sound and Vib. 13(3), pp 281-307.

Kameier, F., and Neise, W, 1997, " Experimental Study of Tip Clearance Losses and Noise in Axial Turbomachines and their Reduction", Transactions of the ASME Vol. 119, pp 460-471.

Kim, Y. N. and George, A. R., 1982, "Trailing-Edge Noise from Hovering Rotors," AIAA Journal, Vol. 20(9), pp. 1167-1174.
Koch, W. 1971, "On Transmission of Sound through a Blade Row", Jnl. Sound and Vib. 18(1), p111-128.
Kordama, H. and Namba, M., June 1989, "Unsteady Lifting Surface Theory for a Rotating Cascade of Swept Blades", ASME paper no 89-GT-306.
Lighthill M.J., 1952, Proc. Roy. Soc. A 211, 564
Lockard , D.P., and Morris, P.J., 1998, "The Radiated Noise from Airfoils in Realistic Mean Flows", to be published in AIAA Jnl.
Long, L. and Watts, G.A. 1987, "Arbitrary Motion Aerodynamics Using an Aeroacoustics Approach," AIAA Journal, Vol. 25(11), pp. 1442-1448.
Longhouse, R.E., 1978, "Control of Tip-Vortex Noise of Axial Flow Fans by Rotating Shrouds", Jnl. Sound and Vib. 58, pp 201-214.
Mani, R., 1971, "Noise due to interaction of inlet turbulence with isolated stators and rotors". J. Sound Vib. 17, 251-260.
Mani, R. & G. Hovray, 1970, " Sound Transmission through Blade Rows", Jnl. Sound and Vib. 12(1), pp59-83.
Mani, R., 1995, presentation at the AST workshop, Clevland, OH, Dec. 1995.
Martinez R. and Rudzinsky J., 1997 "Predictions of Diffraction of Broadband Noise by an Engine Nacelle; Part1: Calculation of a stator cascades near and far field radiations from the ingestion of rapidly distorting turbulence", CEAS/AIAA paper 97-1963, Third Joint CEAS/AIAA Aeroacoustics Conference,Atlanta,GA, May 1997.
Moiseev, N., Lakshminarayana, B. And Thompson, D.E., 1978, Noise due to interaction of boundary-layer turbulence with a compressor rotor. J. Aircr. 15, 53-61.
Mugridge, B.D. and Morfey C.L., 1972, "Sources of Noise in Axial Flow Fans", Journal of the Acoustical Society of America, Vol. 51(5) Part 1.
Myers, M.R. and Kerschen E.J., 1995, "Influence of Incidence angle on Sound Generation by Airfoils Interacting with High Frequency Gusts" J. Fluid Mech. 292, pp. 271-304.
Namba, M., 1977, "Three Dimensional Analysis of Blade force and Sound Generation for an Annular Cascade in Distorted Flows", Jnl. Sound and Vib. 50(4), pp479-508.
Peake, N. 1993, "The scattering of Vorticity Waves by an Infinite Cascade of Flat Plates in Subsonic Flow", Wave Motion 18, pp255-271.
Peake, N., 1992, "The interaction between a High Frequency Gust and a Blade Row", J. Fluid Mech. 241, pp261-289.
Peake, N. and E.J. Kerschen, 1995, "Uniform Asymptotic Approximation for High Frequency Unsteady Cascade Flow", Proc. Royal Soc. 449 pp177-186.
Ribner H. S., March 1987, "Spectra of Noise and Amplified Turbulence Emanating from Shock-Turbulence Interaction" AIAA Journal, Vol. 25, pp. 436-441.
Schulten, J.B.H.M., June 1997, "Vane Sweep Effects on Rotor/Stator Interaction Noise", AIAA Journal Vol. 35 no 6, pp 945-951
Scott J.R. and Atassi, J.M., 1990, "A Finite Difference , Frequency-Domain Numerical Scheme for the Solution of the Linearized Unsteady Euler Equations," Computational Fluid Dynamics Symposium on Aeropropulsion, NASA Conference Publication 3078, pp 55-104
Sevik, M., 1974, "Sound radiation from a subsonic rotor subjected to turbulence", Int. Symp. Fluid Mechanical Engineering. Des. Turbomach., pennsylvania State Univ., University Park; NASA {Spec. Pub.] SP NASA Sp-304, Part II.
Smith, S.N., 1973, "Discrete Frequency Sound Generation in Axial Flow Machines", Aeronautical Council R&M 3709.
Ventres, C.S., Theobald M.A. and Mark W.D., July, 1982, "Turbofan Noise Generation:Vol(1) Analysis" NASA CR-167952.

Tables

Table 6.1: Input for Boeing Fan Rotor Alone Self Noise Calculations

Minimum Frequency		1000 Hz
Maximum Frequency		25000Hz
Number of Frequency points		25
Analysis Bandwidth		15.6Hz
Duct Radius		0.2286 m
Hub Radius		0.1m
Blade Chord		0.081m
Number of Blades		20
RPM:	55%	9156 rpm
	70%	11663 rpm
Axial Flow	55%	84 m/s Low
		77 m/s Hi
	70%	110 m/s Low
		100m/s Hi

Blade Chord

(r-h)/(a-h)	c
0.0500	0.0718
0.1500	0.0736
0.2500	0.0758
0.3500	0.0768
0.4500	0.0769
0.5500	0.0769
0.6500	0.0768
0.7500	0.0770
0.8500	0.0784
0.9500	0.0801

Angle of Attack (rotor incidence)

r/a	55% Low	55% Hi	70% Low	70% Hi
0.05	8.3	11	8	10.8
0.15	7.5	10	7.5	10
0.25	6.6	9.1	6.2	8.8
0.35	5.7	8.1	5.2	7.7
0.45	5	7.2	4.6	6.8
0.55	4.7	6.8	4.3	6.4
0.65	4.5	6.6	3.9	5.9
0.75	4.4	6.4	3.9	5.7
0.85	4.4	6.1	3.9	5.7
0.95	4.4	6.1	3.9	5.7

Table 6.2: Input for Boeing Fan Rotor Alone Inflow Noise Calculations

Boeing Test Input Data (Inflow Noise)

Analysis Bandwidth	15.6Hz
Duct Radius	0.2286 m
Hub Radius	0.1m
Rotor Blade Chord	0.081m
Number of Rotor Blades	20
Number of Stator Vanes	30
Stator Chord	0.044m
Duct radius at stator	0.2286m
hub radius at stator	0.1m

	55% Low	55% Hi	70% Low	70% Hi
Rotor upstream				
U (rotor)	94 m/s	94m/s	123m/s	123m/s
V (rotor)	0	0	0	0
rpm	9156	9156	11663	11663
BL thickness	8.9mm	8.9mm	7.6mm	7.6mm
Lengthscale	2.6mm	2.6mm	2.8mm	2.8mm
Turb. Int.	2%	2%	2%	2%
Run No	759	762	766	763C
100%bleed	782	779	783C	786
Rotor downstream				
U (rotor)	94 m/s	94m/s	123m/s	123m/s
V (rotor)	50 m/s	50 m/s	61 m/s	61 m/s
rpm	9156	9156	11663	11663
BL thickness	8.9mm	8.9mm	7.6mm	7.6mm
Lengthscale	2.6mm	2.6mm	2.8mm	2.8mm
Turb. Int.	2%	2%	2%	2%
Run No	760	761D	765C	764
100%bleed	781D	780D	784	785C

Table 6.3: Input for Boeing Fan Stator Noise Calculations

Stator upstream				
U	123 m/s	123m/s	157m/s	157m/s
V	50 m/s	50 m/s	61 m/s	61 m/s
BL thickness (tip clear 0.05",fig H31)	14.9mm	22.86mm		
BL Len. Sc (estimated from spectra 10dB down pt of 8kHz fig H21)	7.6mm	11mm		
Turb. Int.	5.5%	6%		
Wake Int	3%	4%		
Wake Len Sc (estimated from spectra 10dB down pt of 18kHz fig H21)	3.4mm	3.4mm		
Run No.	1001D	1004	1008	1005
Rotor alone	717	720	724	721
Stator downstream				
U	123 m/s	123m/s	157m/s	157m/s
V	50 m/s	50 m/s	61 m/s	61 m/s
BL thickness (tip clear 0.05",fig H31)	14.9mm	22.86mm		
BL Len. Sc (estimated from spectra 10dB down pt of 8kHz fig H21)	7.6mm	11mm		
Turb. Int.	5.5%	6%		
Wake Int	3%	4%		
Wake Len Sc (estimated from spectra 10dB down pt of 18kHz fig H21)	3.4mm	3.4mm		
Run No.	1002	1003D	1007	1006
Rotor alone	718D	719D	723C	722

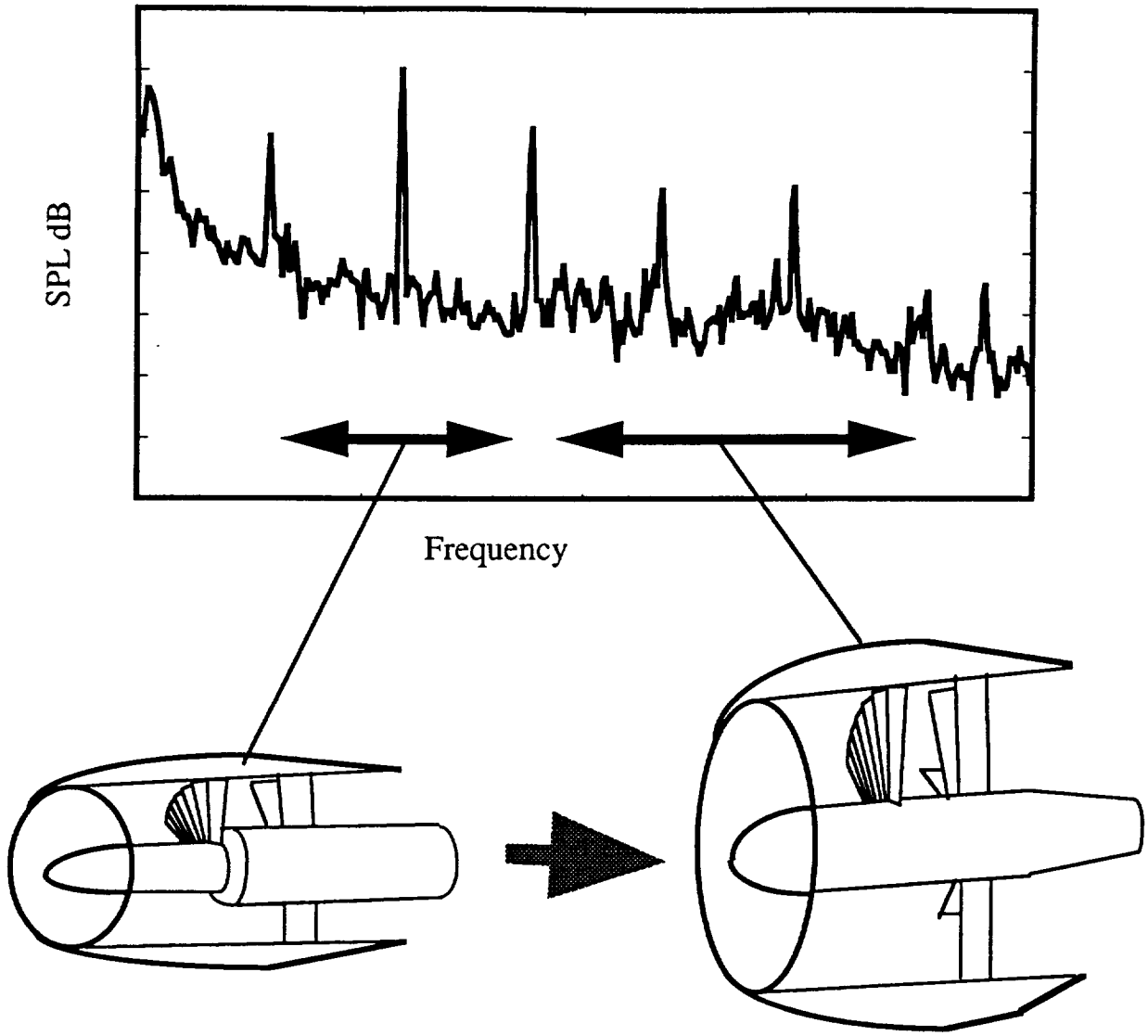

Figure 1.1: Typical fan noise spectrum showing the subjectively important regions for large and small diameter engines.

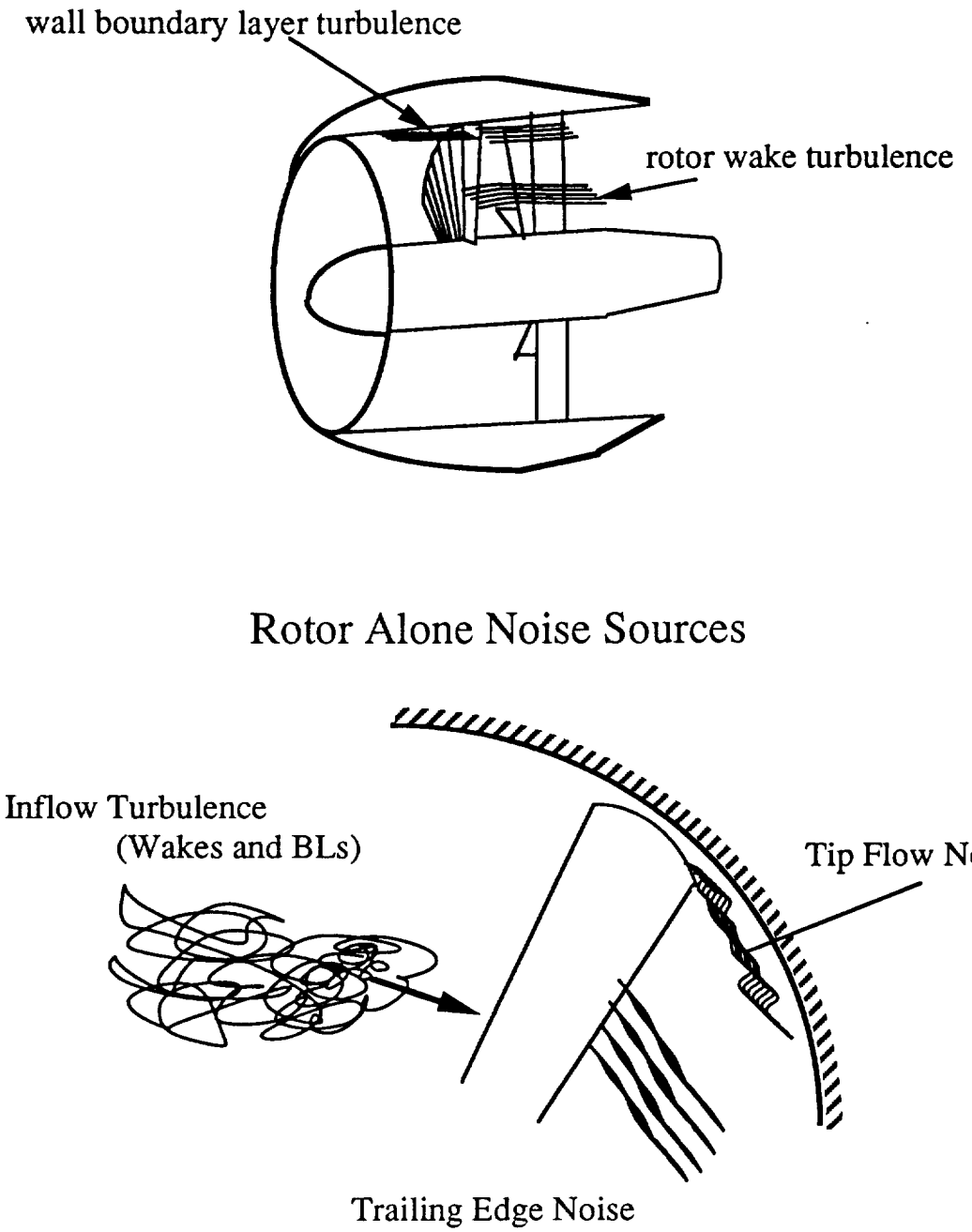

Figure 1.2 Internal Turbulent Flows in an aircraft engine

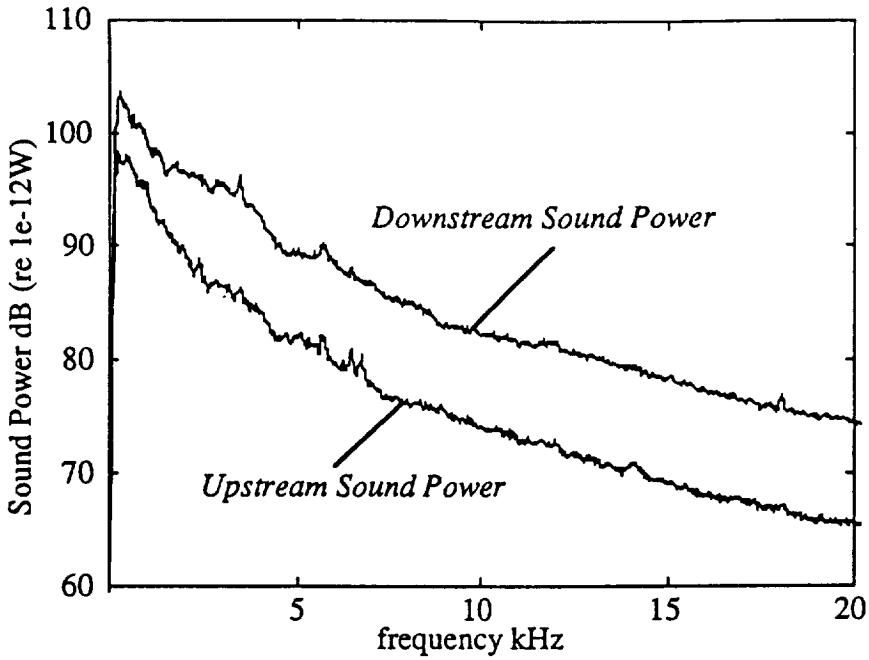

Figure 2.1: Broadband noise power spectra in the upstream and downstream directions for the rotor alone case with 100% boundary layer bleed on the outer duct wall upstream of the rotor. (55% speed, low loading, tip gap 0.02")

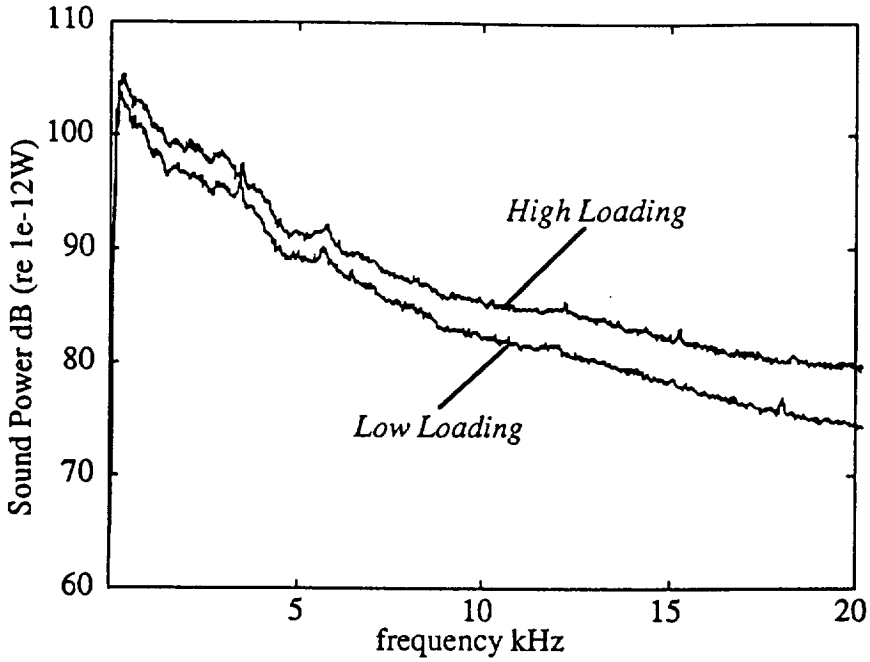

Figure 2.2: Broadband noise power spectra in the downstream direction for the rotor alone case with 100% boundary layer bleed on the outer duct wall upstream of the rotor, showing the effect of loading. (55% speed, tip gap 0.02")

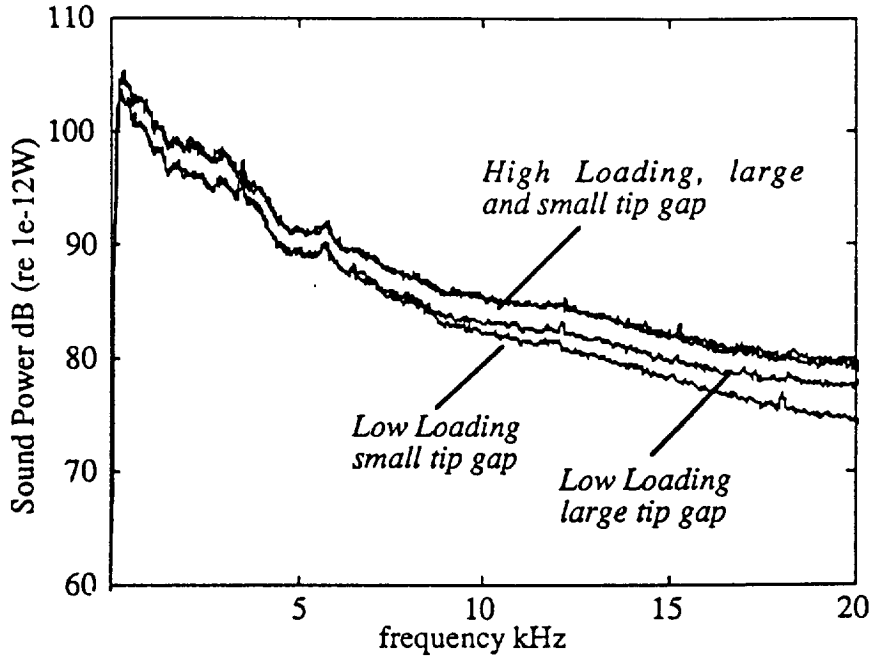

Figure 2.3: Broadband noise power spectra in the downstream direction for the rotor alone case with 100% boundary layer bleed on the outer duct wall upstream of the rotor, showing the effect of tip gap and loading. (55% speed)

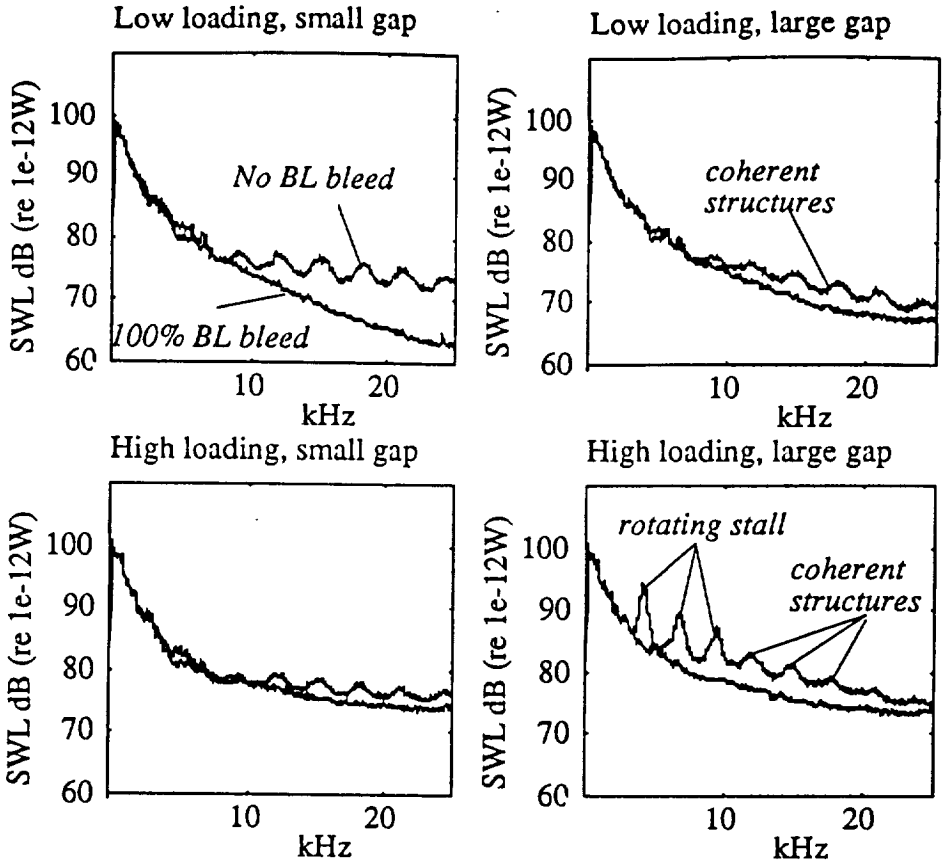

Figure 2.4: Broadband noise power spectra in the upstream direction for the rotor alone case with no boundary layer bleed on the outer duct wall upstream of the rotor. (55% speed)

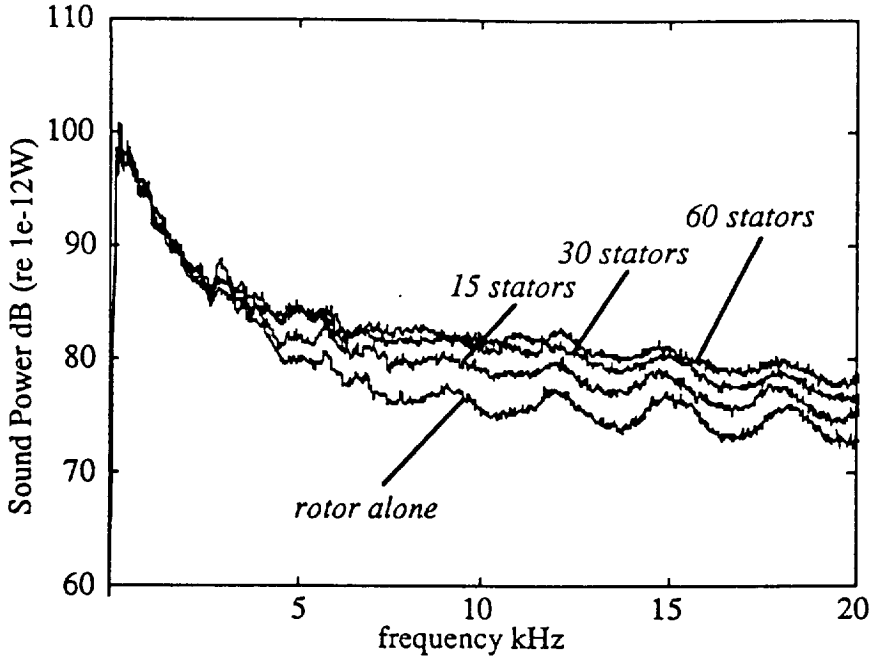

Figure 2.5: Broadband noise power spectra in the upstream direction showing the relative importance of rotor and stator noise. (55% speed, no boundary layer bleed and 0.02" tip gap)

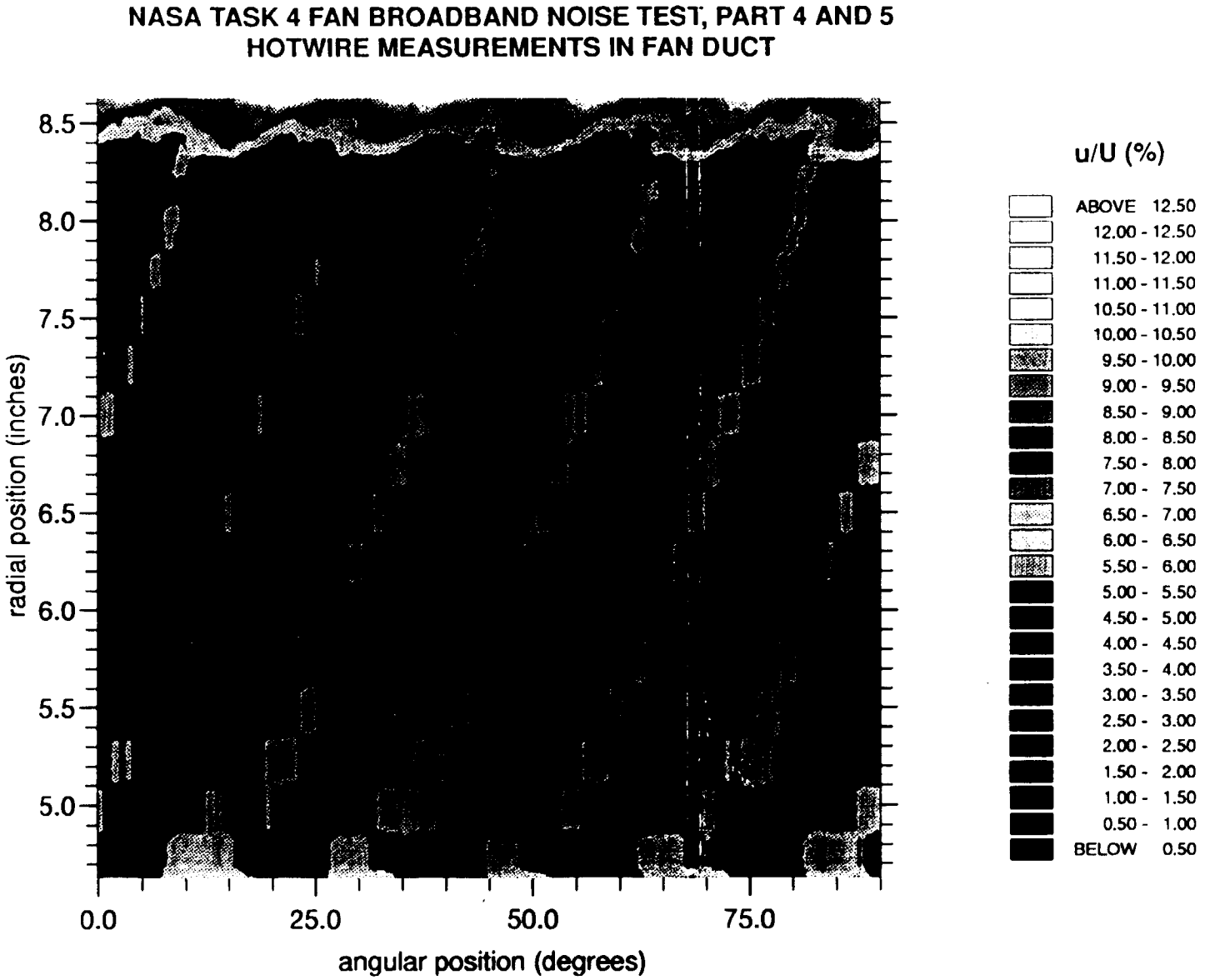

Figure 2.6: The measured turbulence intensity in the fan duct at 55% speed with no boundary layer bleed.

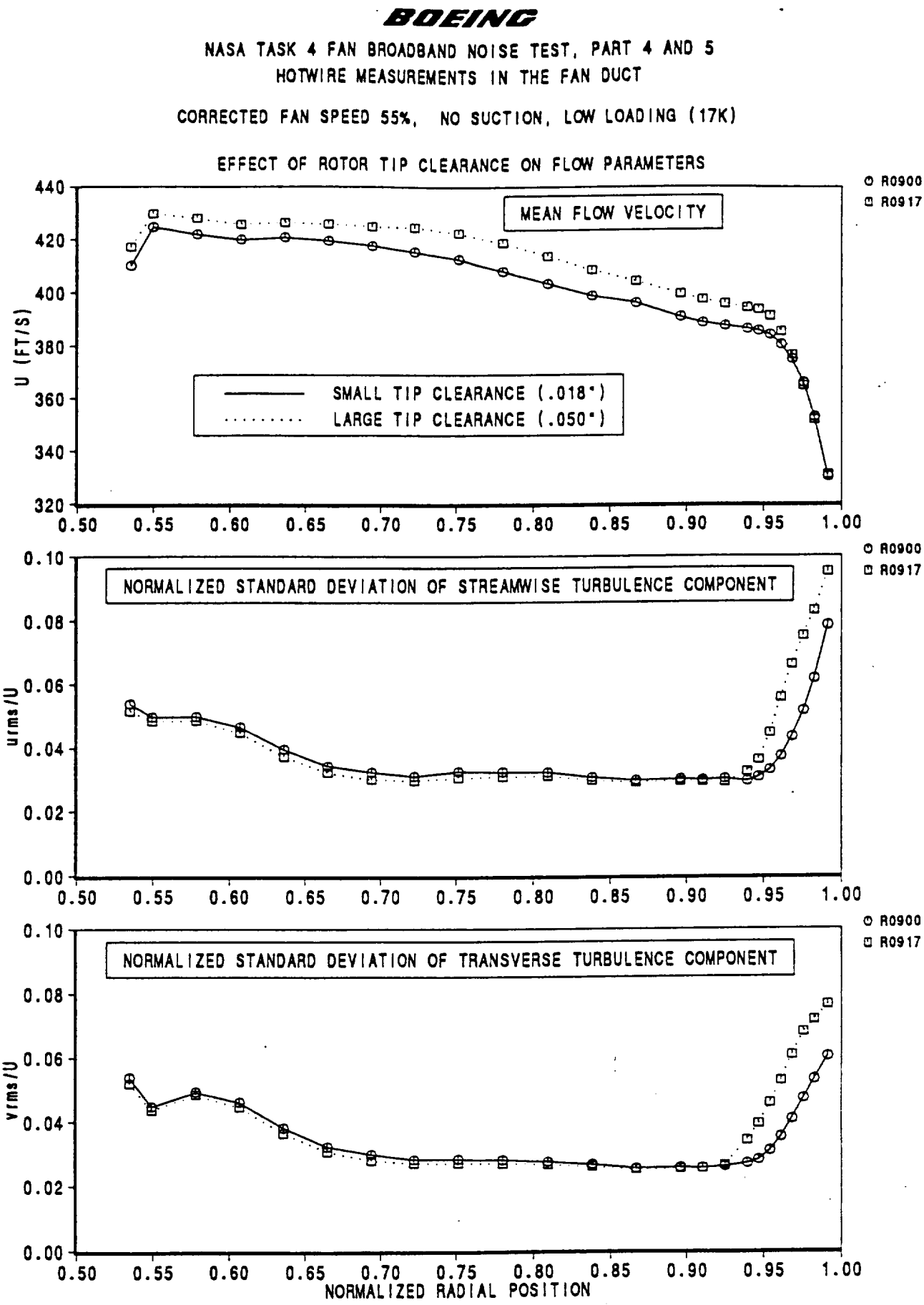

Figure 2.7: The effect of rotor tip gap size average turbulence intensity levels downstream of the rotor at 55% speed as a function of radial position for both streamwise and transverse turbulence components. Also shown is the mean flow.

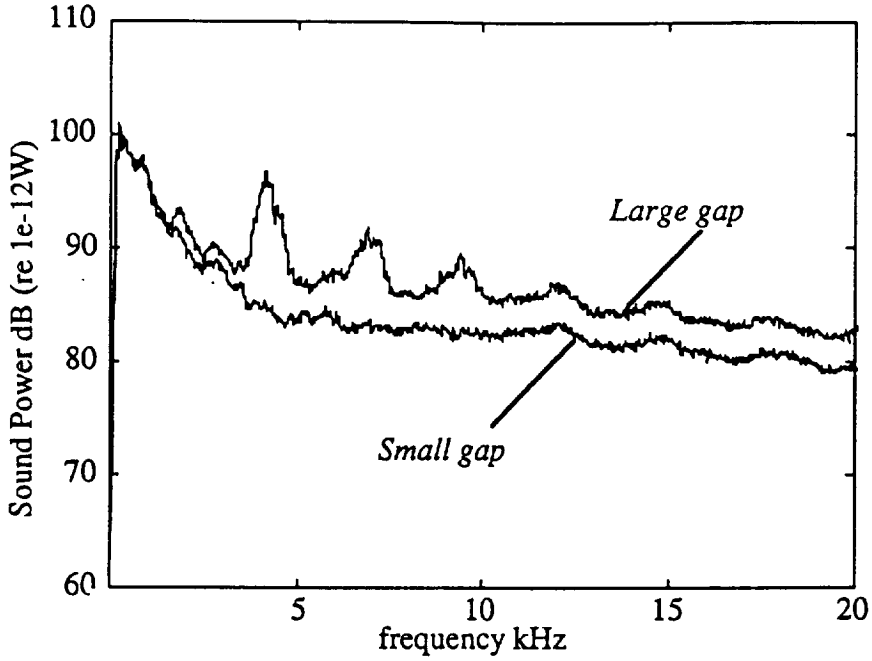

Figure 2.8: Broadband noise power spectra in the upstream direction showing the effect of rotor tip gap size on stator noise. (55% speed, no boundary layer bleed, 60 stators)

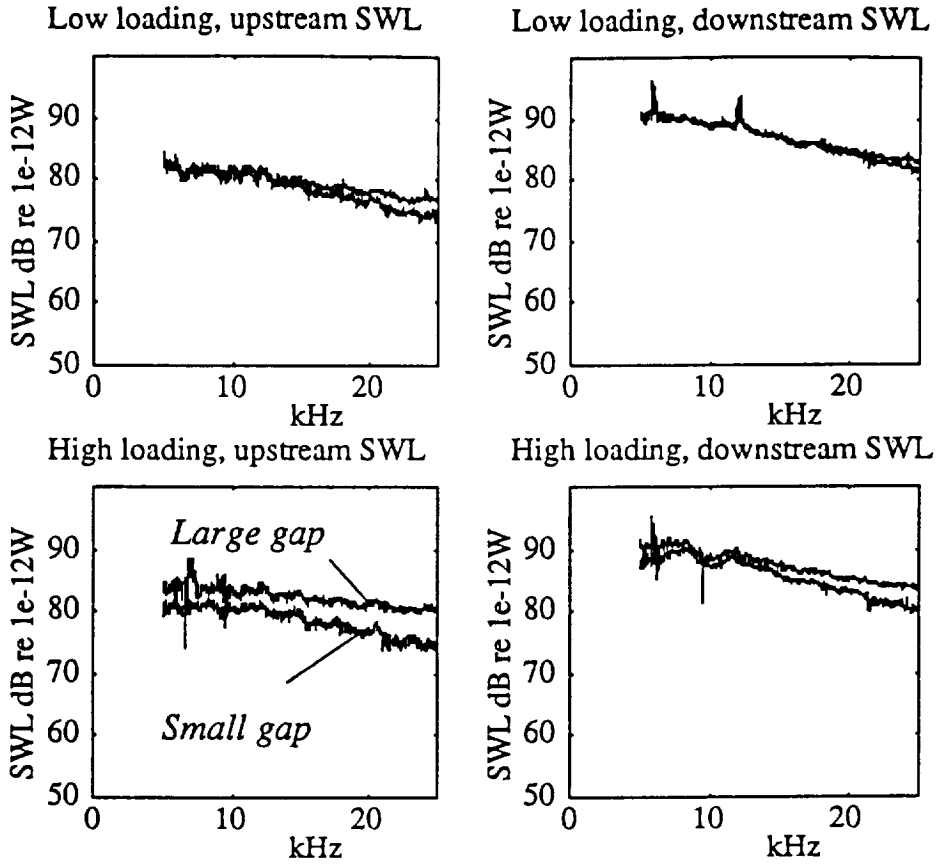

Figure 2.9: Broadband noise power spectra with rotor alone noise subtracted showing the effect of rotor tip gap size on stator noise. (55% speed, no boundary layer bleed,60 stators)

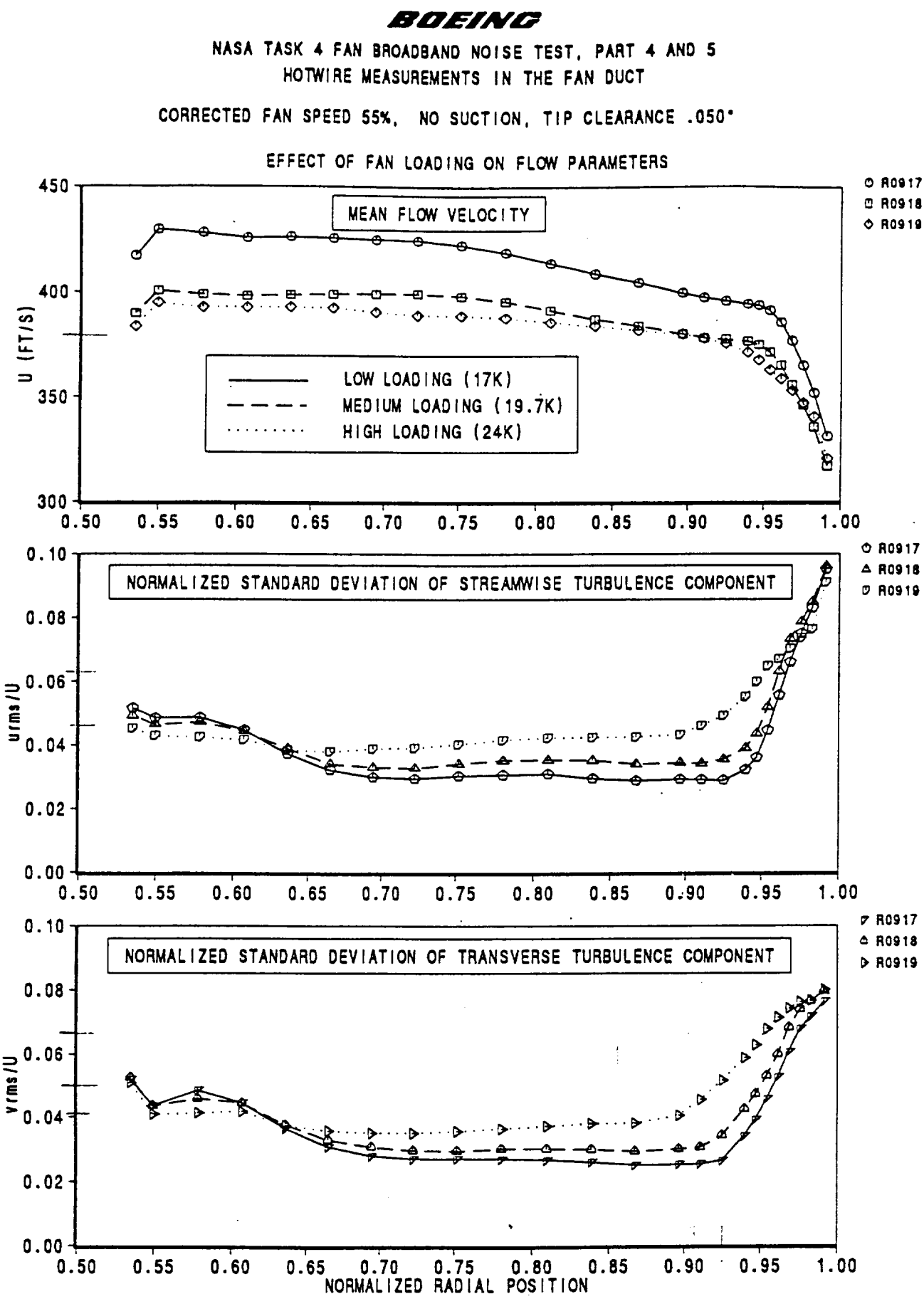

Figure 2.10: The effect of fan loading on the average turbulence intensity levels downstream of the rotor at 55% speed as a function of radial position for both streamwise and transverse turbulence components. Also shown is the mean flow.

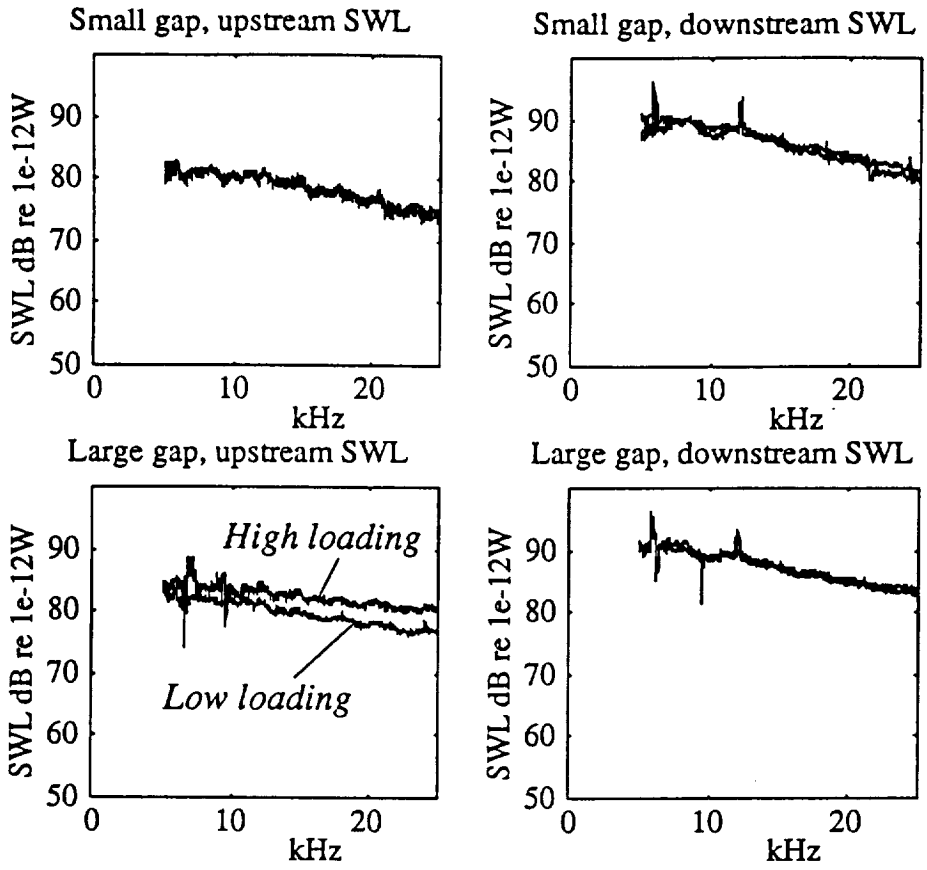

Figure 2.11: Broadband noise power spectra with rotor alone noise subtracted showing the effect of rotor loading on stator noise. (55% speed, no boundary layer bleed,60 stators)

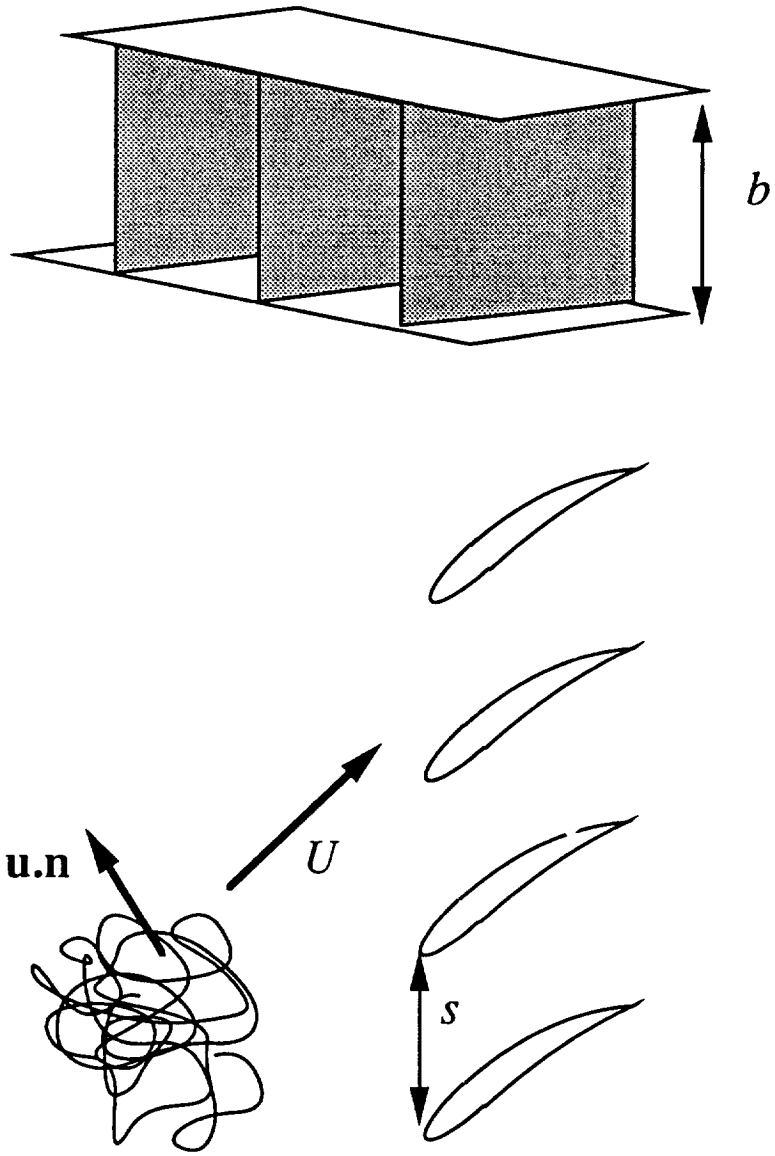

Figure 4.1 : The linear cascade model with rigid end walls

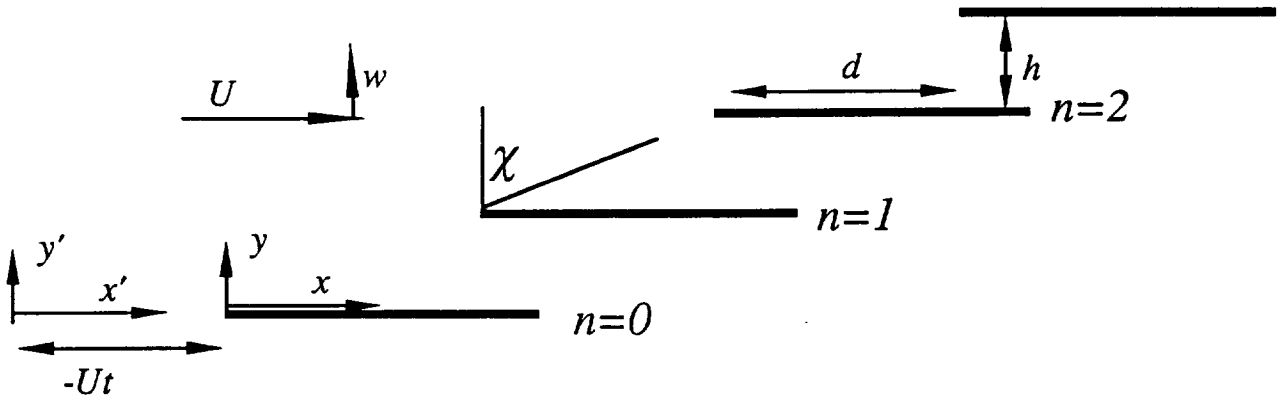

Figure 4.2: A linear cascade of blades in a uniform flow and an incident velocity perturbation given by *w*.

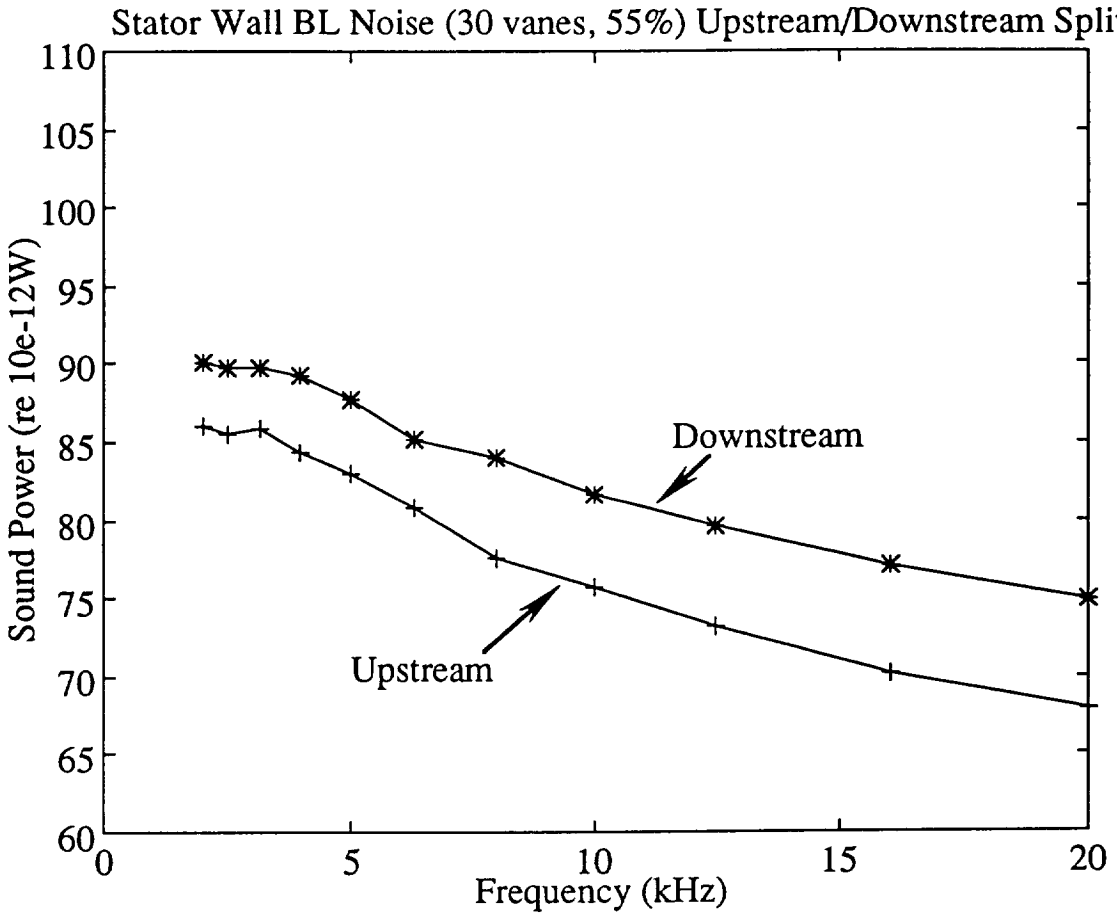

Figure 4.3: The sound power spectra for a set of 30 stator vanes showing the upstream and downstream radiated sound power. (*δ=14mm, L=8.7mm, 55% speed, VK spectrum, turbulence intensity=6%*)

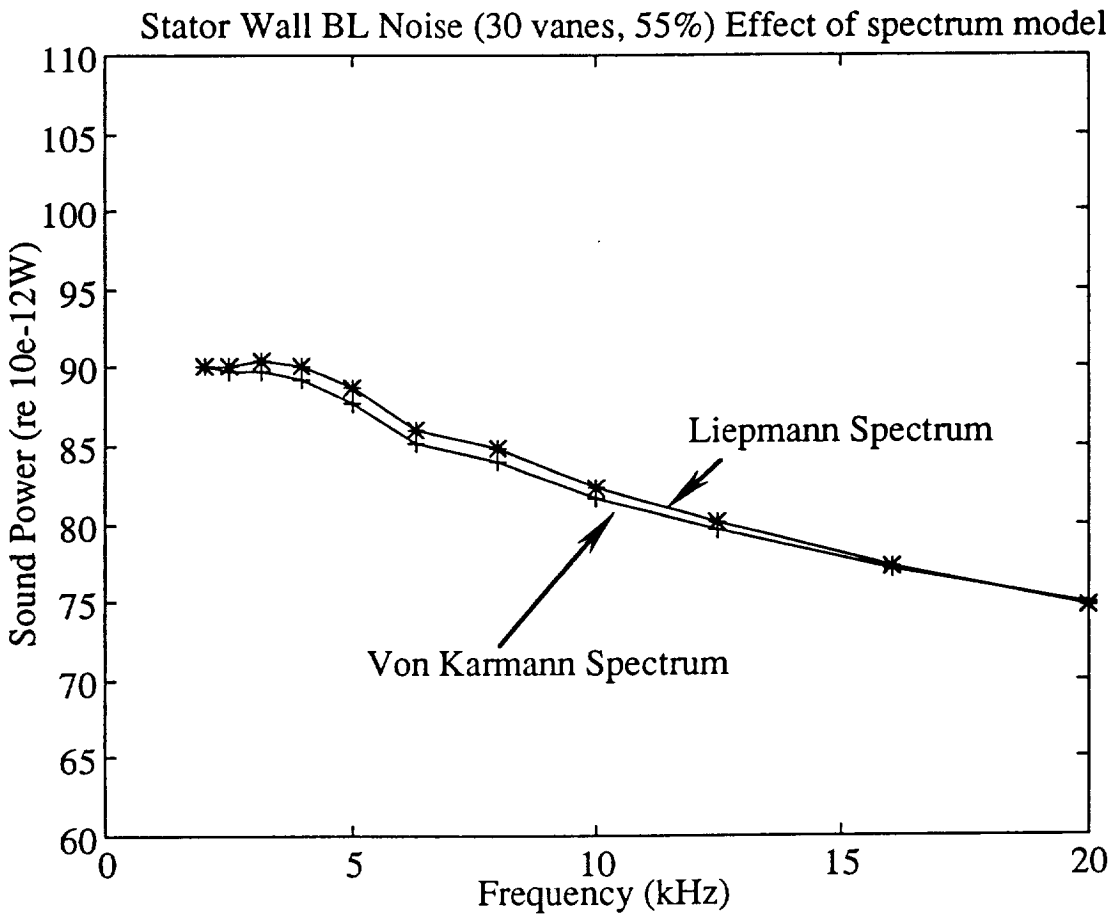

Figure 4.4: The sound power spectra for a set of 30 stator vanes showing the effect of the turbulence spectrum model. (*δ=14mm, L=8.7mm, 55% speed, downstream radiation, turbulence intensity=6%*)

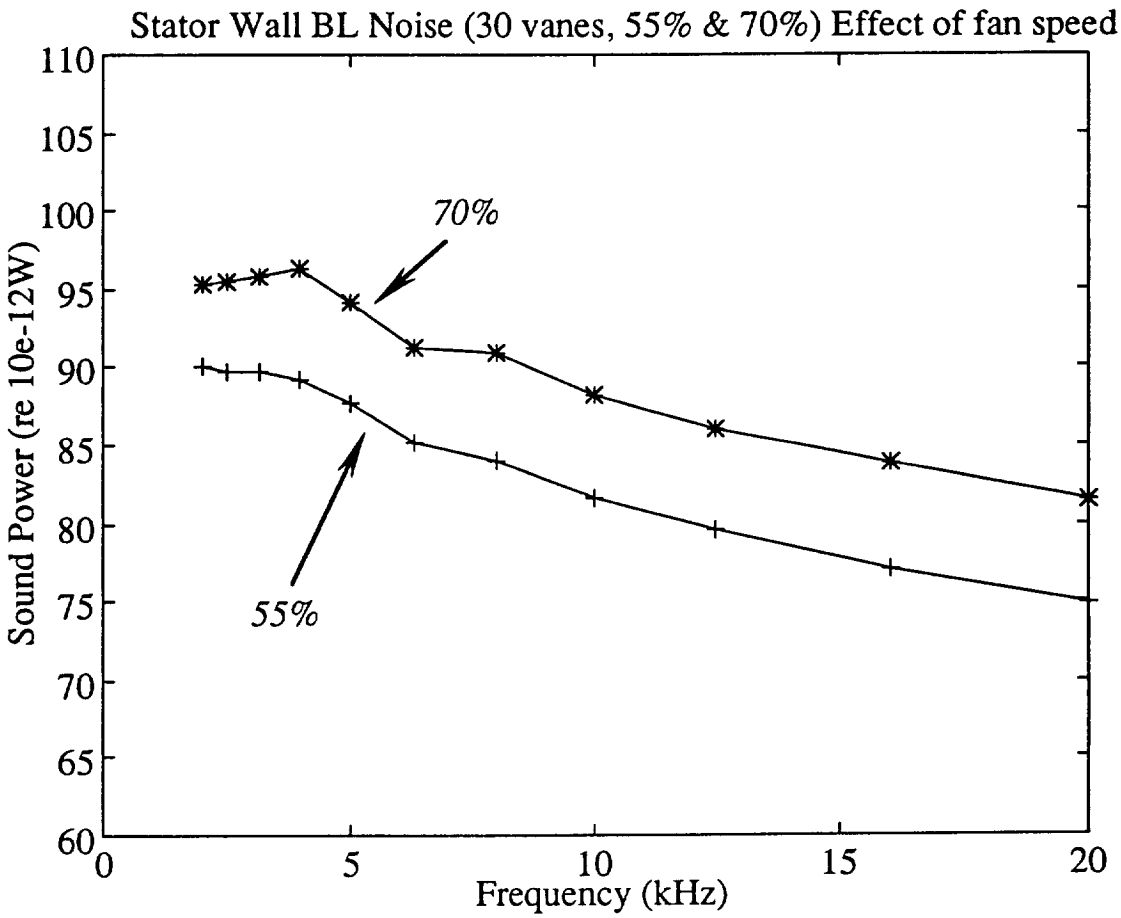

Figure 4.5: The sound power spectra for a set of 30 stator vanes showing the effect of the fan speed. (*δ=14mm, L=8.7mm, downstream radiation, turbulence intensity=6%*)

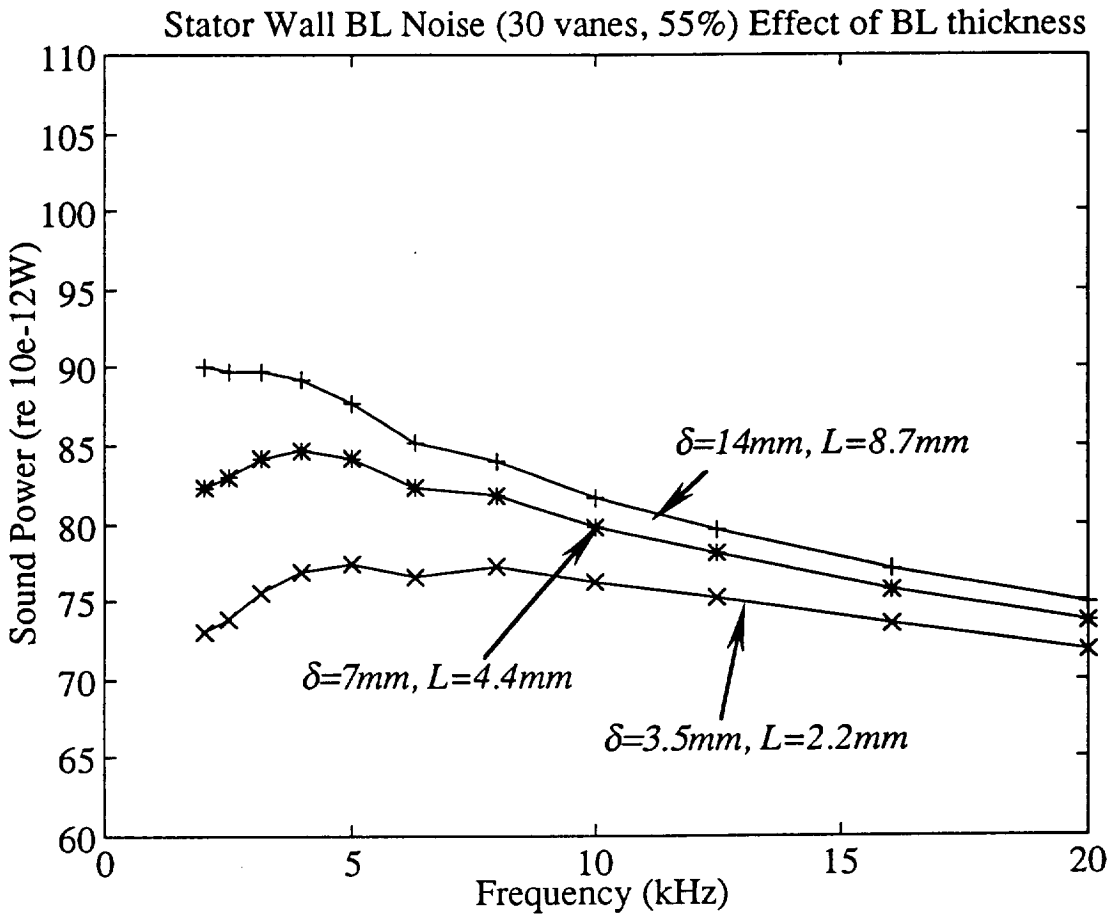

Figure 4.6: The sound power spectra for a set of 30 stator vanes showing the effect of the wall boundary layer thickness. (*L=3δ/4.8, 55% speed, downstream radiation, turbulence intensity=6%*)

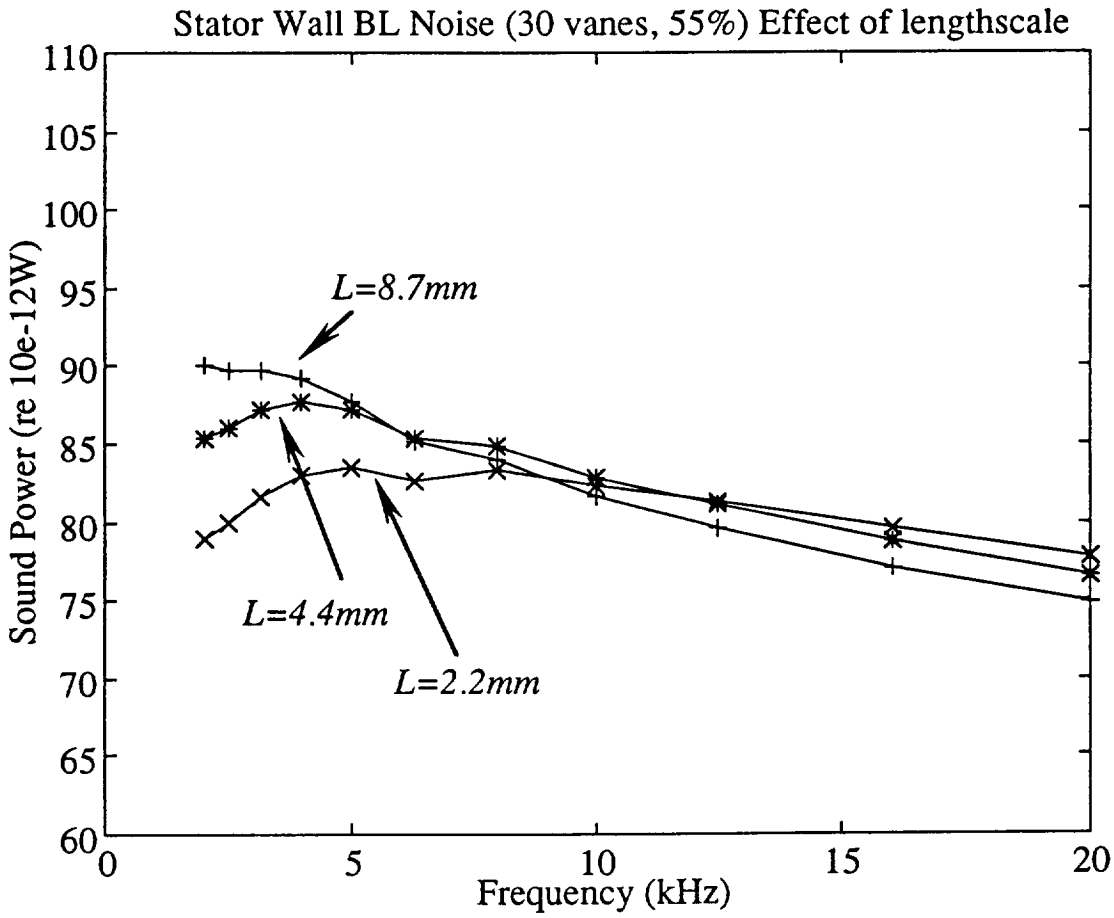

Figure 4.7: The sound power spectra for a set of 30 stator vanes showing the effect of the wall boundary layer turbulence lengthscale. (*δ=14mm, 55% speed, downstream radiation, turbulence intensity=6%*)

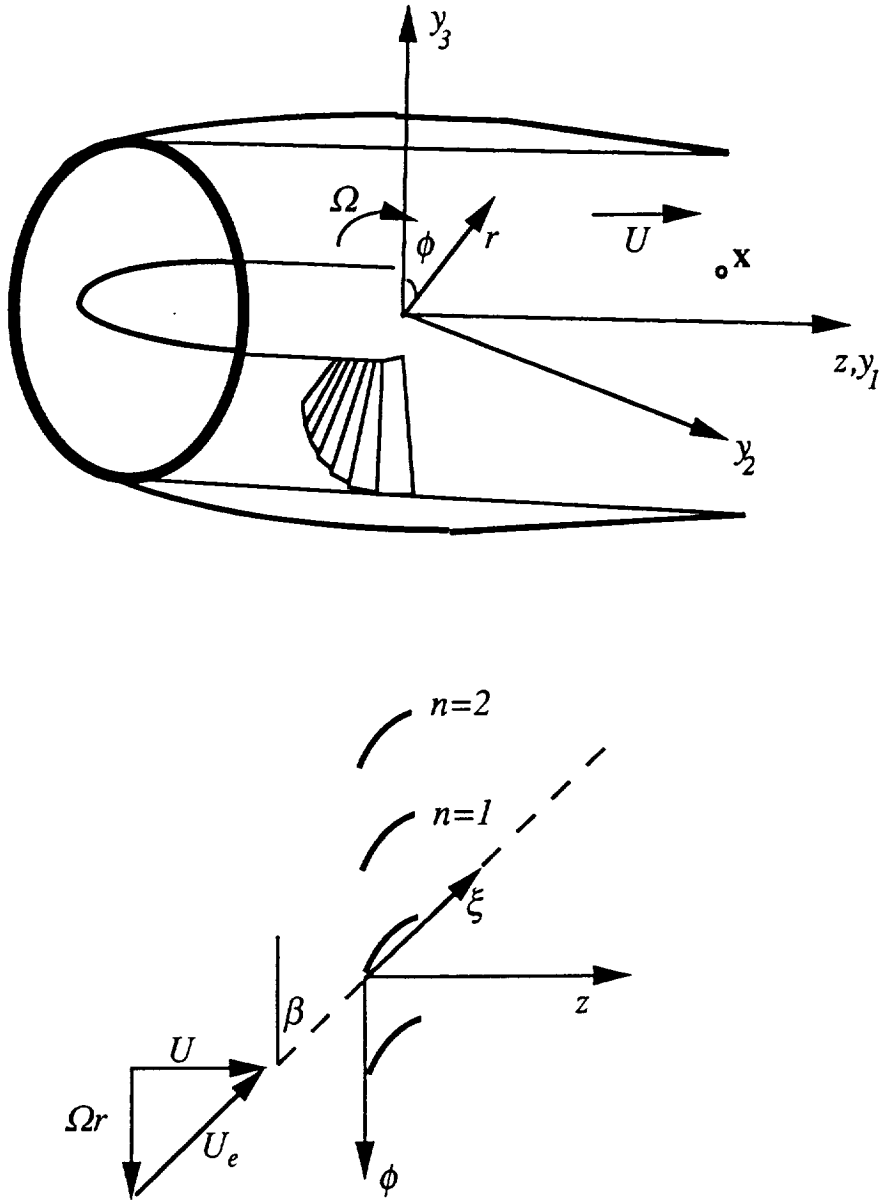

Figure 5.1: The co-ordinate systems used in the analysis

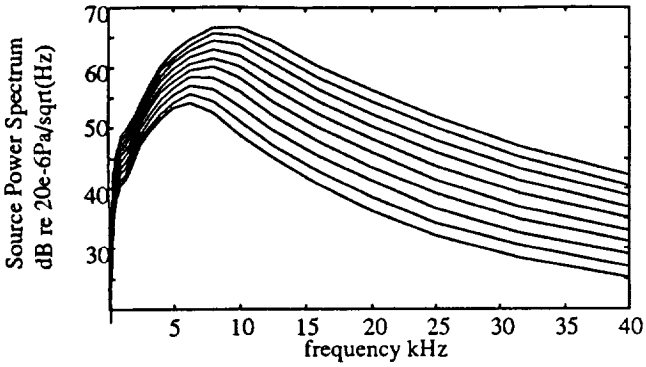

Figure 5.2: The source spectra for a rotating blade with a constant angle of attack of 7°.

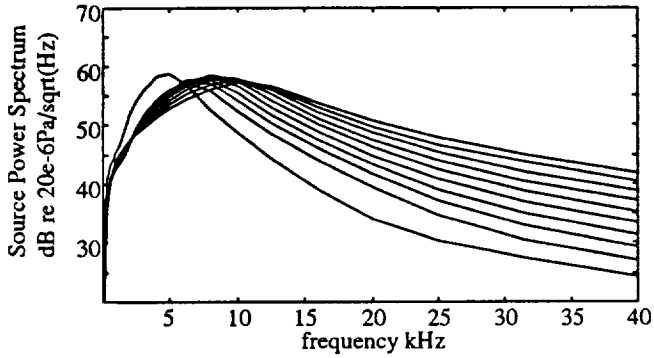

Figure 5.3: The source spectra for a rotating blade with a linearly varying angle of attack from 8° at the hub to 4° at the blade tip.

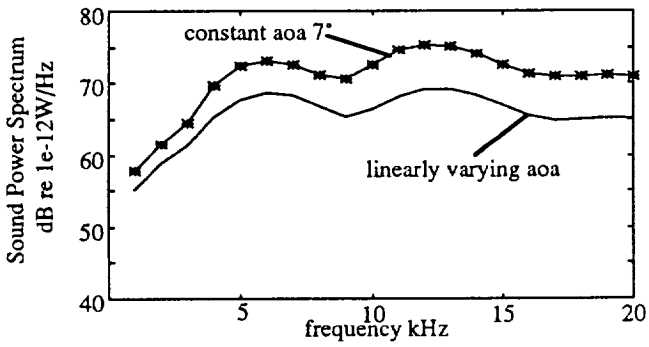

Figure 5.4: Downstream sound power for an angle of attack which is (a) constant across the span, and (b) linearly varying acoss the span.

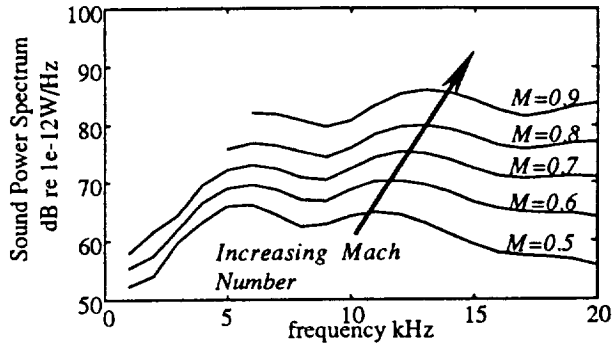

Figure 5.5: The effect of increasing the Mach number on the downstream sound power for case A.

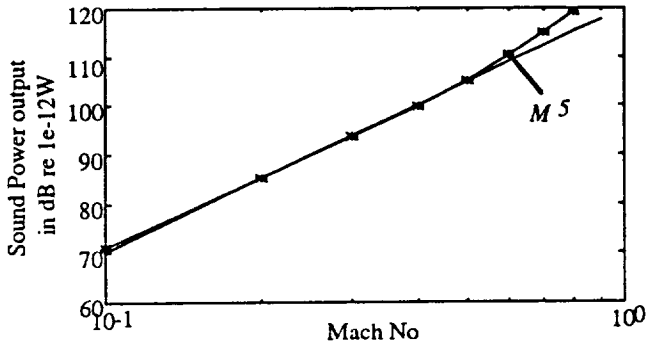

Figure 5.6: The overall sound power for case A as a function of blade tip relative Mach number. (note for Mach numbers >0.7 levels are underestimated)

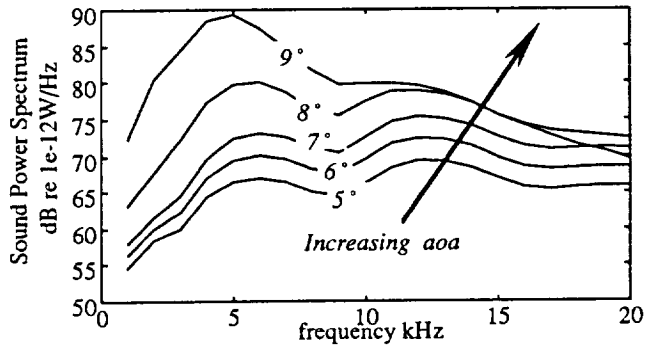

Figure 5.7: The effect of increasing the angle of attack on the downstream sound power for case A.

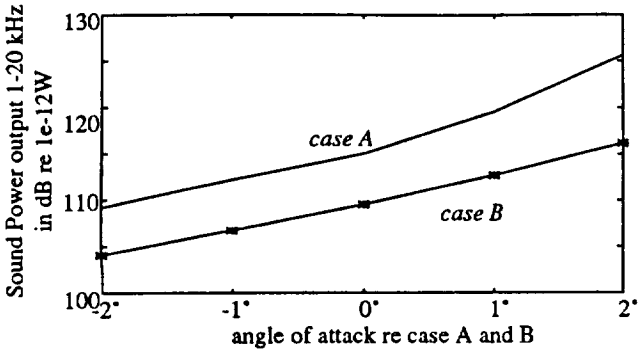

Figure 5.8: The effect of increasing the angle of attack on the downstream overall sound power for cases A and B.

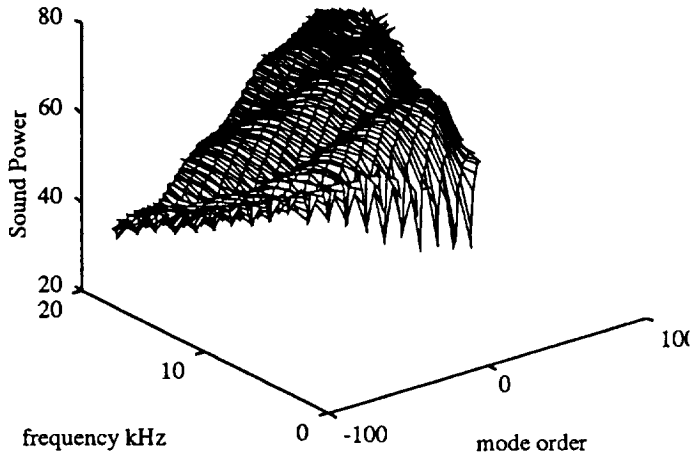

Figure 5.9: Modal Distribution of sound power as a function of frequency

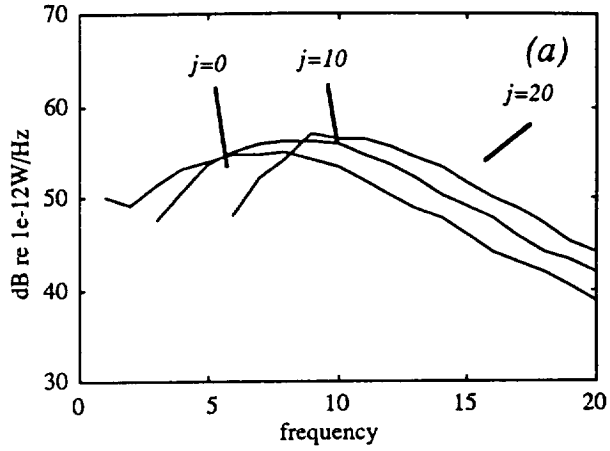

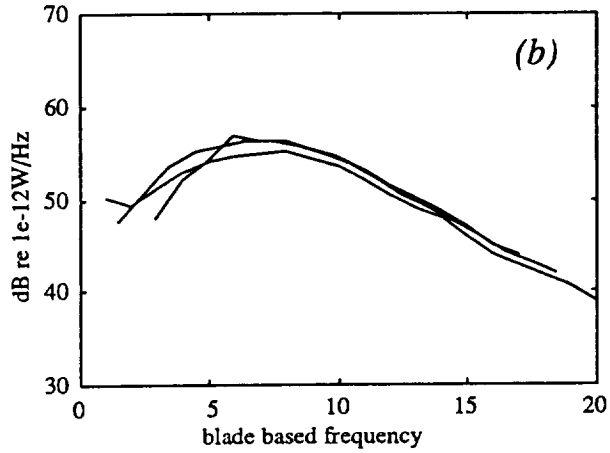

Figure 5.10: The modal sound power for case A as a function of frequency and blade based frequency for modes 0,10,20.

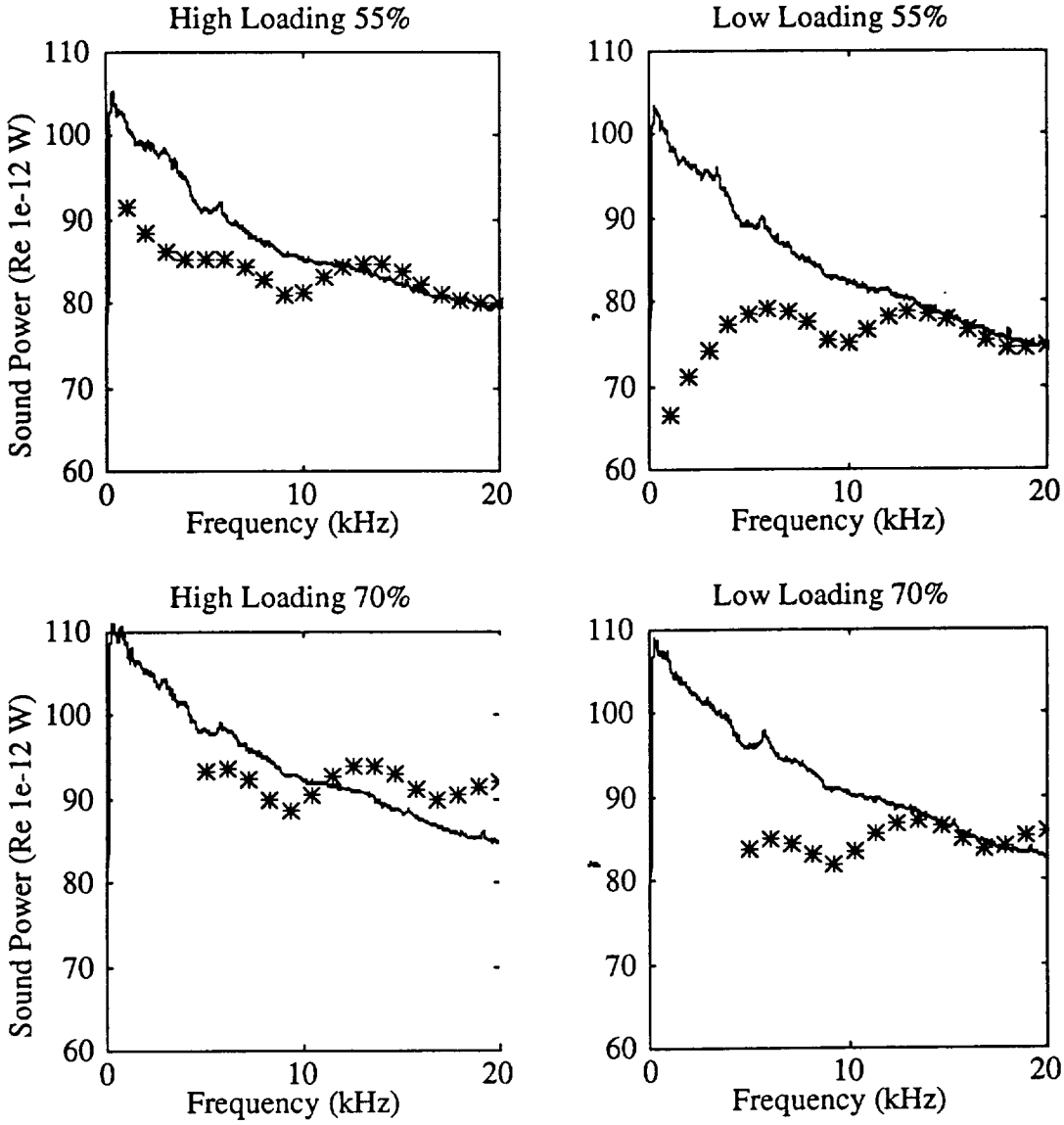

Figure 6.1 Self noise predictions and comparisons with measurements giving the downstream sound power for rotor alone cases with 100% bl bleed

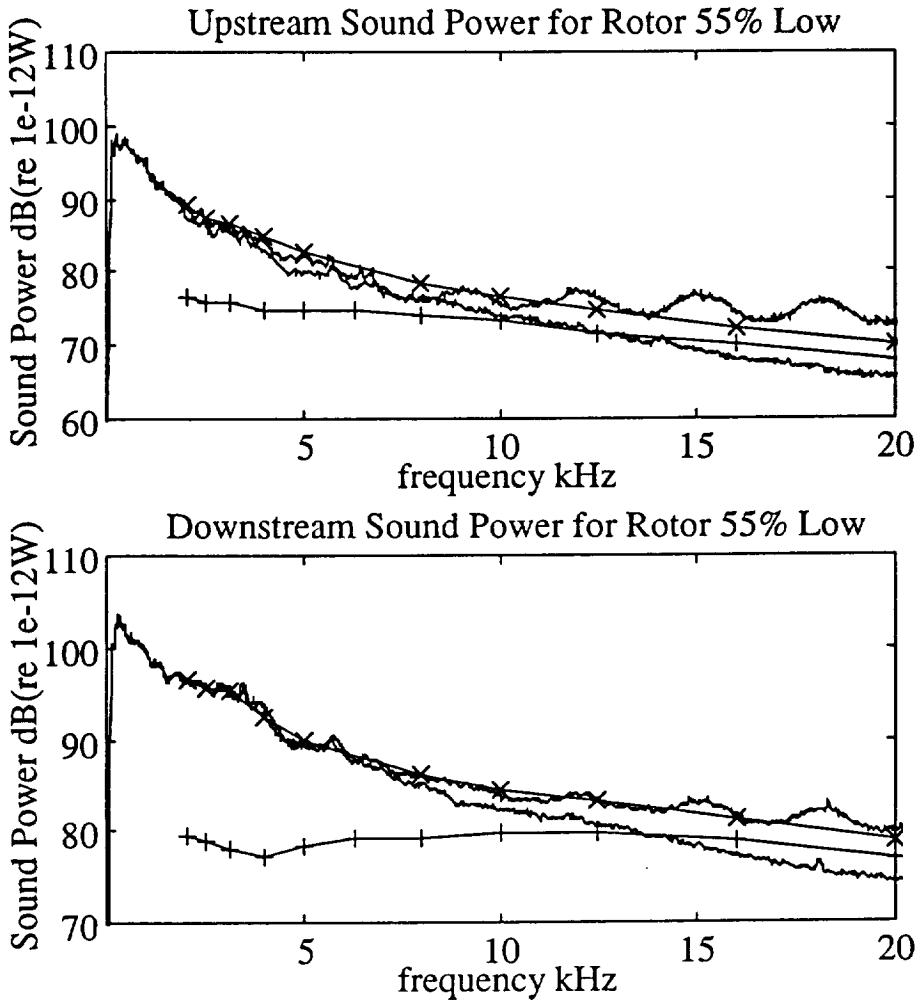

Figure 6.2: The measured and predicted upstream and downstream sound power at the 55% operating condition, low loading for rotor alone noise with no BL bleed. ----+---- predicted BL noise, ----x---- sum of predicted BL noise and measured level of rotor alone noise with 100% bleed.

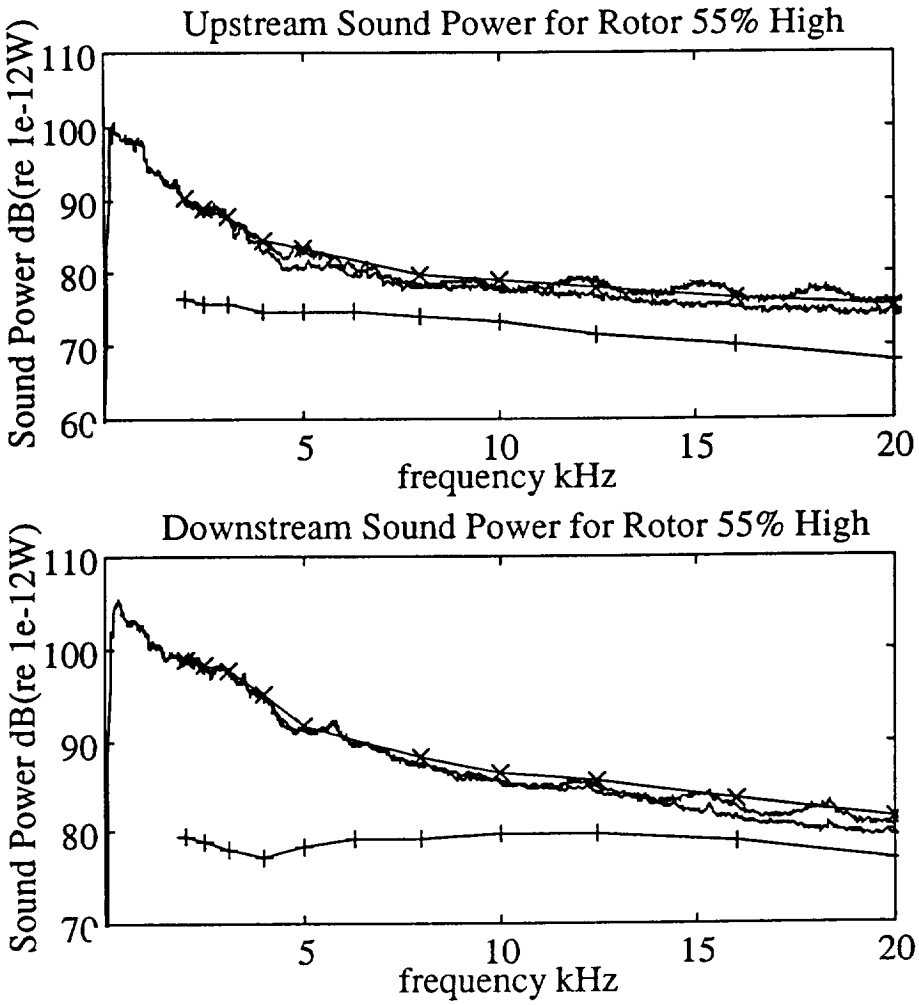

Figure 6.3: The measured and predicted upstream and downstream sound power at the 55% operating condition, high loading for rotor alone noise with no BL bleed. ----+---- predicted BL noise, ----x---- sum of predicted BL noise and measured level of rotor alone noise with 100% bleed.

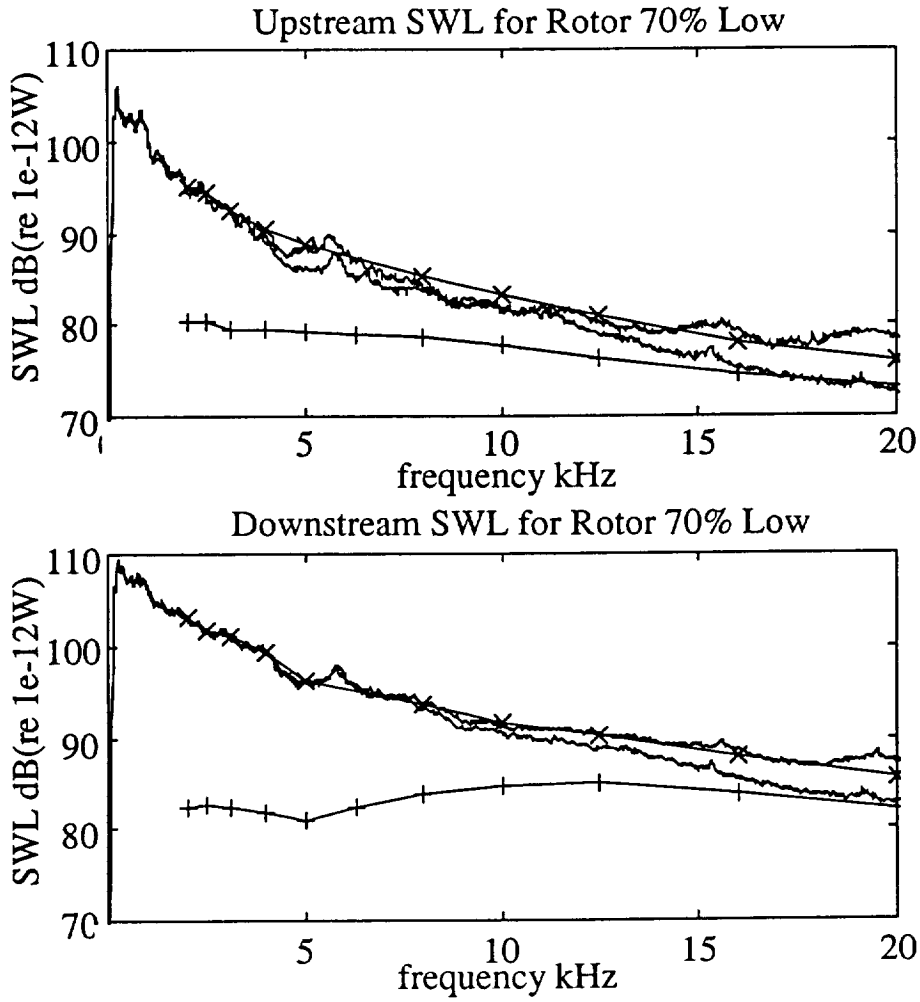

Figure 6.4: The measured and predicted upstream and downstream sound power at the 70% operating condition, low loading for rotor alone noise with no BL bleed. ----+---- predicted BL noise, ----x---- sum of predicted BL noise and measured level of rotor alone noise with 100% bleed.

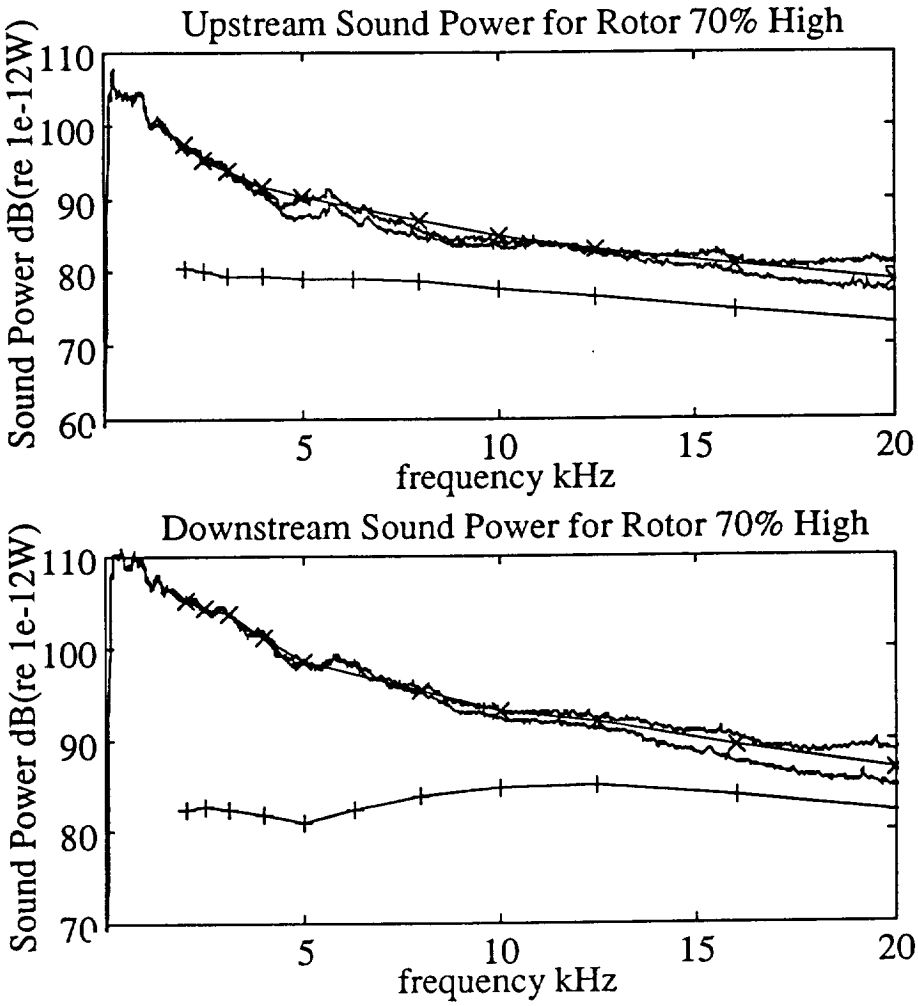

Figure 6.5: The measured and predicted upstream and downstream sound power at the 70% operating condition, high loading for rotor alone noise with no BL bleed. ----+---- predicted BL noise, ----x---- sum of predicted BL noise and measured level of rotor alone noise with 100% bleed.

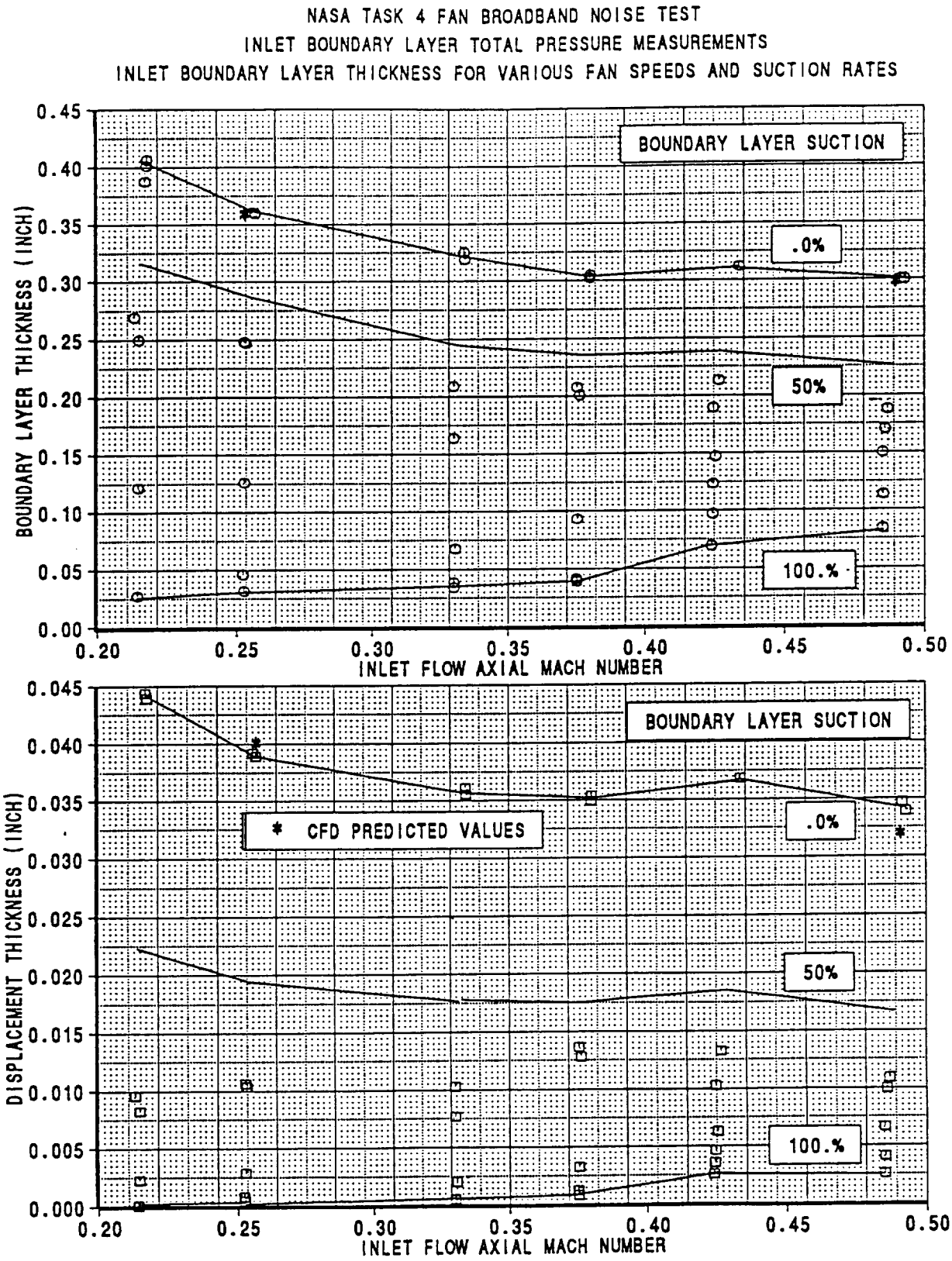

Figure 6.6: Calculations and measurements of the inlet boundary layer thickness.

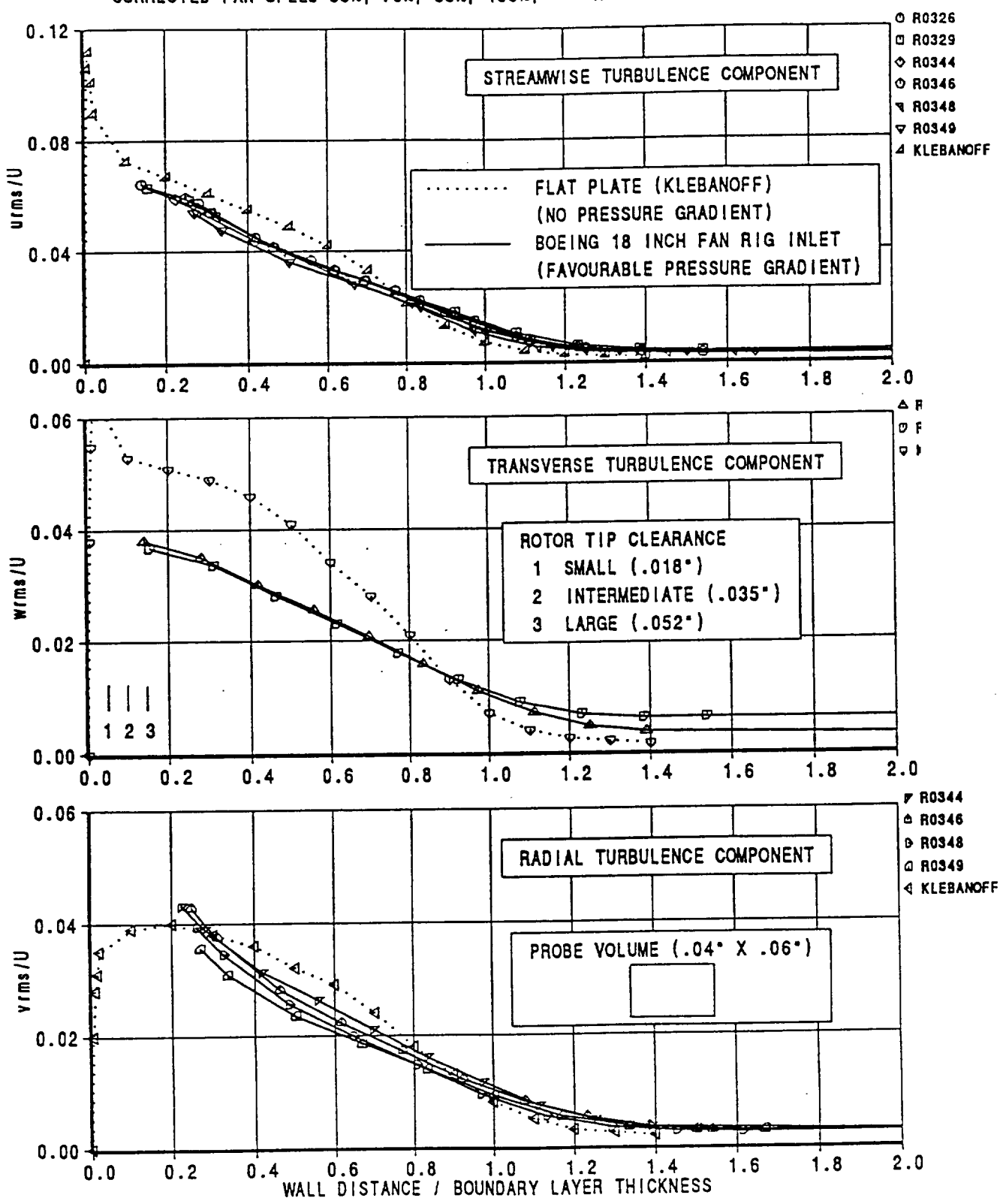

Figure 6.7: Turbulence intensities of the inlet boundary layer.

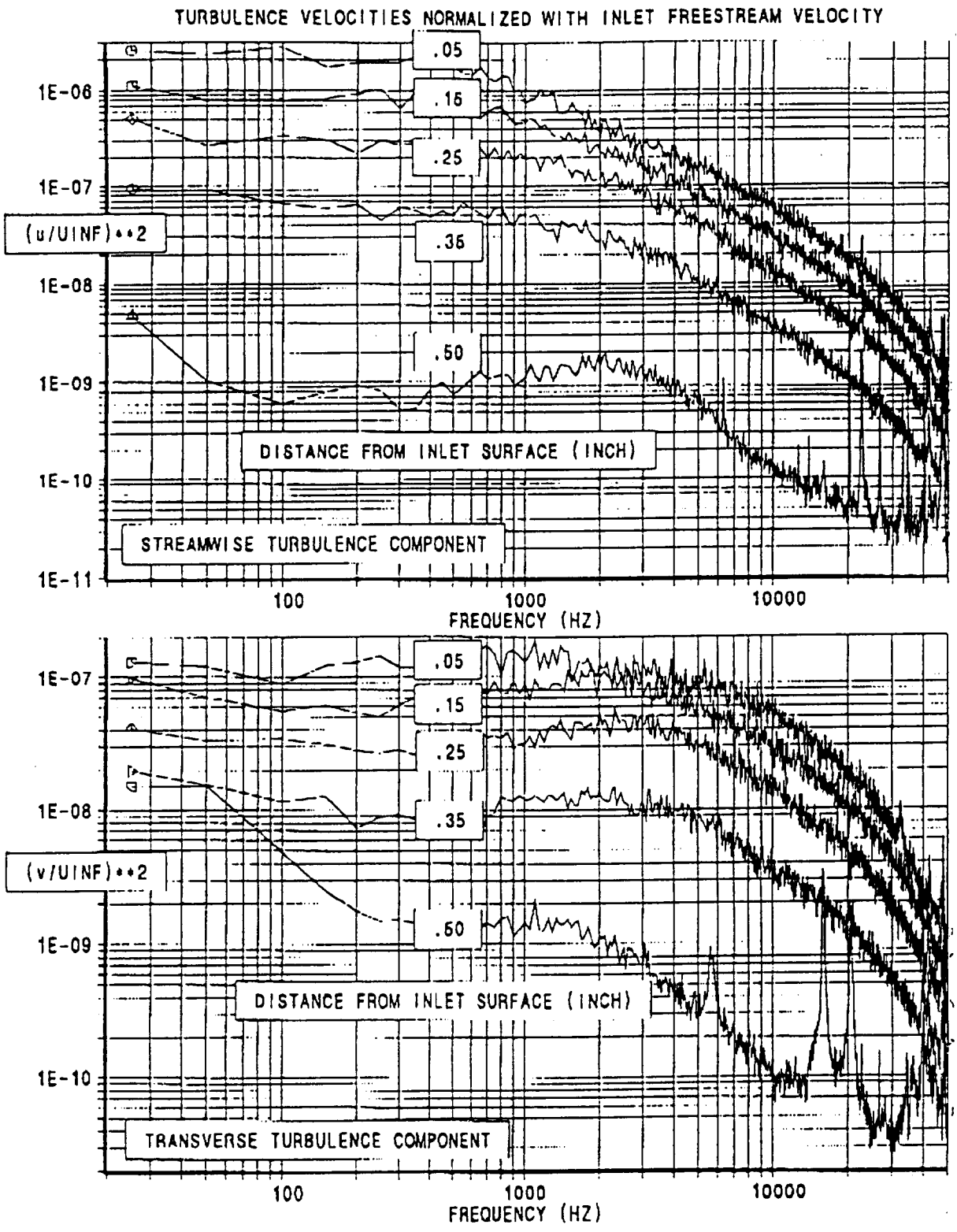

Figure 6.8: Inlet boundary layer turbulence spectra.

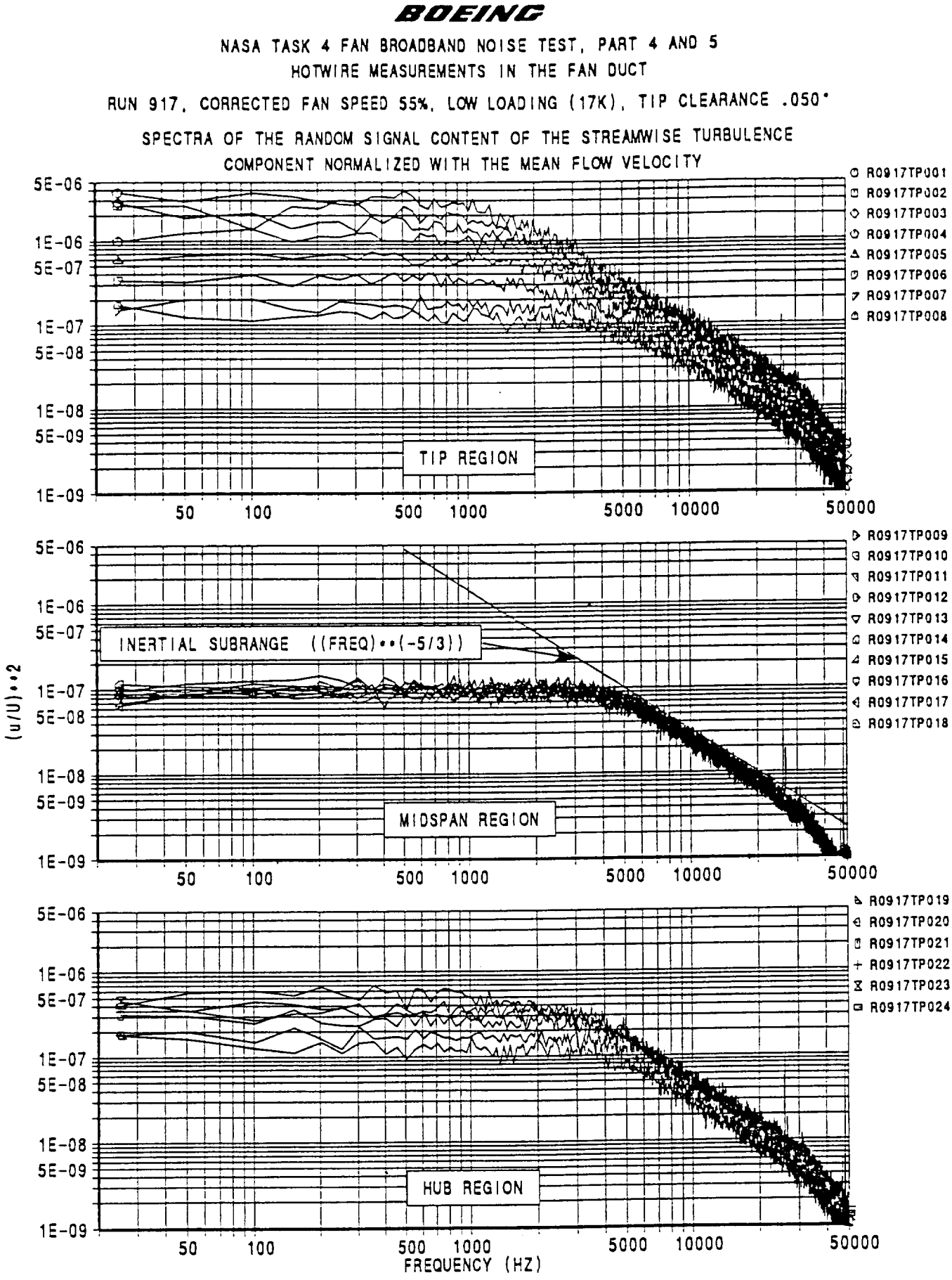

Figure 6.9: Rotor wake turbulence spectra

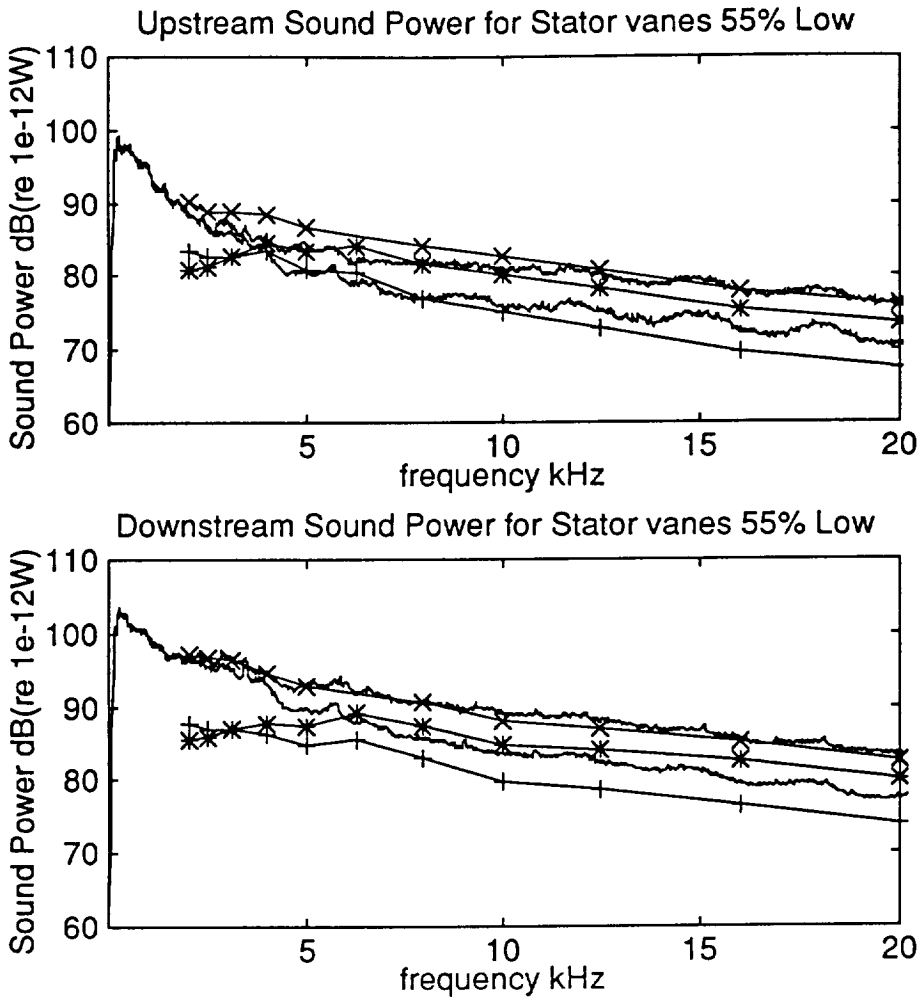

Figure 6.10: The measured and predicted upstream and downstream sound power at the 55% operating condition, low loading stator noise.
----+---- predicted BL noise, ----*---- predicted wake noise, ----x---- sum of predicted BL noise, predicted wake noise and measured level of rotor alone noise.